NOTICE

The quality of this microfiche is heavily dependent upon the quality of the original thesis submitted for microfilming. Every effort has been made to ensure the highest quality of reproduction possible.

If pages are missing, contact the university which granted the degree.

Some pages may have indistinct print especially if the original pages were typed with a poor typewriter ribbon or if the university sent us a poor photocopy.

Previously copyrighted materials (journal articles, published tests, etc.) are not filmed.

Reproduction in full or in part of this film is governed by the Canadian Copyright Act, R.S.C. 1970, c. C-30. Please read the authorization forms which accompany this thesis.

THIS DISSERTATION
HAS BEEN MICROFILMED
EXACTLY AS RECEIVED

AVIS

La qualité de cette microfiche dépend grandement de la qualité de la thèse soumise au microfilmage. Nous avons tout fait pour assurer une qualité supérieure de reproduction.

S'il manque des pages, veuillez communiquer avec l'université qui a conféré le grade.

La qualité d'impression de certaines pages peut laisser à désirer, surtout si les pages originales ont été dactylographiées à l'aide d'un ruban usé ou si l'université nous a fait parvenir une photocopie de mauvaise qualité.

Les documents qui font déjà l'objet d'un droit d'auteur (articles de revue, examens publiés, etc.) ne sont pas microfilmés.

La reproduction, même partielle, de ce microfilm est soumise à la Loi canadienne sur le droit d'auteur, SRC 1970, c. C-30. Veuillez prendre connaissance des formules d'autorisation qui accompagnent cette thèse.

LA THÈSE A ÉTÉ
MICROFILMÉE TELLE QUE
NOUS L'AVONS REÇUE

NUCLEAR EMULSION PROCESSING ON A SEMI-INDUSTRIAL SCALE

B. M. McLeod

Thesis submitted to the School of Graduate Studies in partial fulfilment of the requirements for the degree of Master of Science in Physics.

University of Ottawa
Ottawa, Canada, 1979

ABSTRACT

A synopsis of the mechanism of formation of the photographic latent image is presented. The role of delta-rays in latent image formation in nuclear track emulsion and their relationship to track grain density are discussed. Various sources of background and their qualitative effect upon the limit of detection of nuclear emulsion are discussed. Low temperature (5 to 7°C) processing of nuclear emulsion is described. The physical and chemical processes occuring in each of the processing stages are discussed. The design, construction and operation of a large scale nuclear emulsion processing system is included.

In high energy physics experiments using nuclear emulsion as a detector, it is concluded that minimization of fog background in order to optimize the limit of detectability of minimum tracks is of utmost importance. In processing, presoaking serves to swell the emulsion which increases the developer penetration rate during the development stage. Temperature control of ± 0.5°C is necessary during the developing stage of low temperature processing since the development rate is exponentially temperature dependent. The fixing rate is concluded to be a diffusion controlled because of the large thicknesses of nuclear emulsion pellicles. Consequently, the steady-state fixing rate is equal to the rate of discharge of silver-thiosulfate complex ion from the emulsion pellicles. Circulation in the

fixing bath increases the rate of fixing by increasing the aforementioned rate of discharge. It is found that after the final alcohol drying stage the emulsion thickness is greater than its final thickness by a factor of 2.3 ± 0.1 since it still contains excess absorbed water.

When designing a nuclear emulsion processing system, it is found that type 304 stainless steel, plexiglass, polyvinyl chloride and chlorinated polyvinyl chloride are staisfactory construction materials since they are capable of resisting corrosion by any of the processing solutions. Installing stainless steel processing vessels inside insulated polyethylene jacket tanks through which a continuous flow of temperature regulated coolant is passed provides the necessary temperature control.

ACKNOWLEDGEMENTS

The author wishes to take this opportunity to express his gratitude to his supervisor, Professor Jacques Hébert of the Physics Department of the University of Ottawa, for his faith and support during the design, construction and operation of the emulsion processing system.

A heart felt word of thanks must also go to all members of the University of Ottawa Physics Department workshop who participated in the construction of the processing system. Special mention must go to Mr. Nelson Goodchild, the workshop superintendent, for his invaluable assistance and suggestions during the design phase of the project. Special mention must also go to Mr. R. Lavigueur who built most of the processing equipment and also provided many invaluable suggestions during the design phase.

The author also wishes to express his gratitude to all members of the E-531 collaboration for their faith and support during this project.

CONTENTS

LIST OF ILLUSTRATIONS, DIAGRAMS AND DRAWINGS

LIST OF TABLES

STATEMENT OF OBJECTIVES.

The objectives in performing the work for and the writing of this thesis were:

i) To design and successfully operate of a large scale processing system for Fuji nuclear track emulsion. A 25 liter Fuji stack was processed with this system during the winter of 1979. The two basic processing procedures were supplied by Japanese emulsion physicists from Nagoya, Osaka City and Kobe Universities in Japan.

ii) To describe in detail the chemical and physical processes occuring during the various processing stages.

STATEMENT OF ORIGINALITY

To the best of the author's knowledge, the following are original contributions to the field of nuclear emulsion.

i) A system design for low temperature processing of nuclear emulsion on a large scale. At $5^{o}C$, the processing capacity for 330μ thick supported emulsion film is ∿7 liters per week. The capacity for 600μ thick support film is ∿2 liters per week at $7^{o}C$.

ii) A silver grain growth rate model. This model, equation 2-11, is derived from the principles of chemical kinetics, electrochemistry and chemical thermodynamics.

iii) A fixing rate model for low temperature fixing of thick emulsion films. The model is derived from the principles of unsteady-state mass transfer and chemical kinetics.

iv) An extension of the delta-ray explanation of the variation of track grain density with incident particle energy. The conventional delta-ray energy distribution, $N(E)\,dE = KE^{-2}\,dE$ is assumed but K is considered to be a parameter which varies as $1/v^2$, v being the incident particle velocity. A derivation of the aforementioned variation of K with incident particle velocity, equation 1.13, is presented and its effect upon the variation, with incident particle energy, of the number of latent

image producing delta-rays is discussed.

The author wishes to stress that the chemical reactions which appear in this thesis are standard known reactions and are consequently not part of the originality of the thesis.

INTRODUCTION

Experiment E-531 is a high energy neutrino physics experiment involving an international collaboration of physicists from Canada, Japan and the United States. This collaboration is searching for neutrino produced, charmed particle decays in nuclear emulsion. The Canadian universities involved are Ottawa, Toronto and McGill. The Japanese universities involved are Nagoya, Osaka City and Kobe. The American university involved is Ohio State. From mid-November 1978 to the end of January 1979, the E-531 collaboration exposed a 25 liter nuclear emulsion stack, consisting of approximately 4000 plates and pellicles, to a neutrino beam at Fermi National Accelerator Laboratory in Batavia, Illinois, U.S.A. This stack had been manufactured by Canadian and Japanese emulsion physicists, the author included, at the University of Ottawa during the late summer, 1978. Facilities for processing the exposed E-531 stack were designed by and built under the supervision of the author in the Physics Department of the University of Ottawa as the basis of his Master's thesis in nuclear emulsion physics, supervised by Professor J. Hébert.

This nuclear emulsion processing system is currently the largest of its kind in the world. It was used to process the E-531 stack during the six week period beginning in mid-February and running till the end of March, 1979.

CHAPTER 1. CHARACTERISTICS OF NUCLEAR EMULSION

1.1 Composition and Properties of Nuclear Emulsion

Nuclear emulsion is composed of animal gelatin, a plasticiser such as glycerin, sensitized silver halide crystals and water. << The halide crystals are mainly bromide with small admixtures of iodide. A fine layer of silver atoms and silver sulfide molecules on the surface of the crystals acts as a sensitizer.>>[1] The gelatin, a three dimensional organic network , acts as a support matrix for the crystals. The crystals are dispersed throughout this network which holds them firmly in place.

The gelatin is fabricated from the skin and bones of animals, in particular those of pigs and cattle. The essential components of the gelatin are collagen from the skin and osseine from the bones. The fabrication process is long, complicated and extremely specialized. It requires approximately four months to produce a batch of gelatin suitable for nuclear emulsion work. << Osseine and collagen are transformed into gelatin by a slow, cold hydrolysis process in the presence of lime or, less often hydrochloric, phosphoric or sulfuric acid.>>[2] Many of the details of the various nuclear emulsion manufacturing processes are industrial secrets and as such are unavailable. For further details see reference 1.

1. Ref. 2, pg. 4
2. Ref. 1, pg. 31.

1.2 Track Formation and the Latent Image

The trajectories of charged particles traversing nuclear emulsion are registered by the emulsion. A charged particle traversing a medium transfers some of its energy to the medium consequently losing energy itself due to the various electromagnetic interactions it undergoes. Thus, a charged particle such as a proton traversing nuclear emulsion transfers some of its energy to the silver bromide crystals along its path, activating them in the process. Some of these activated crystals acquire a "latent image".

During the developing stage of processing, silver bromide crystals possessing a "latent image" are reduced to grains of solid silver. Most of those crystals which do not posses a "latent image" are left intact, being unaffected during the developing stage. The undeveloped crystals are then removed from the gelatin support during the fixing stage, the developed grains being unaffected during fixing. Thus, a track of silver grains which can be viewed under a microscope remains in the gelatin network. Complete processing details, including reagents and reactions involved, are discussed in detail in Chapter 2.

The fine sensitizing layer of silver atoms on the surfaces of the crystals plays a crucial role in the formation of the latent image. << The arrangement of atoms in a perfect silver halide crystal

is equivalent to two interpenetrating face-centered cubic lattices, one made up of silver and the other of halide ions.>>[3] The sensitizing layer is dispersed over the surface of the crystal. The "sub-latent image" is due to aggregation of the surface silver atoms into groups of two or three. The mechanism of formation of these surface aggregates is still subject to theoretical speculation. The mechanism to be discussed here is mainly due to Mitchell and his co-workers (1953, 1954, 1955, 1957 and 1958).[3a]

A silver bromide crystal becomes photoconducting if light is shone on it and an electric field is applied. This photoelectric current is believed to be due to the deionization of bromine ions in the crystal lattice by the photons of light. In the body of the crystal, each bromine ion is negatively charged and is surrounded by six positively charged silver ions. When a bromine ion is ionized by a photon of light, the electron is pumped into the conduction band of the silver lattice where it effectively neutralizes a silver atom. This electron is not free to move as in the conduction band of an ordinary metal. The ionized bromine ion becomes a neutral bromine atom surrounded by six positively charged silver atoms. This results in a center of positive charge or "positive hole". If an electric field is applied, the electrons migrate in a direction opposite to that of the field, jumping from one atomic sight to another and the holes migrate

[3] Ref. 2, pg. 1.

[3a] Ref. 14, 15, 16, 17, 18, 19, 20

in the direction of the field. The migration of the positive holes can be thought of as electrons jumping into the holes from neighbouring bromine ions. If no electric field is applied, the holes and electrons diffuse rapidly through the crystal.

These positive holes and associated electrons eventually recombine but it is the mechanism of recombination which is critical to the formation of the sub-latent image. The holes diffuse to "kink sites" at the surface of the crystal and become trapped since the electrical potential at the kink sites is minimum. This can be understood by considering the fact that at surface "kink" sites a neutral bromine atom will be surrounded by a minimum number of positive silver ions rather than the maximum number of six as in the body of the crystal. A hole trapped at a kink site can now be neutralized by one of the silver atoms of the sensitizing layer. A silver atom donates an electron to a hole. The donating silver atom thus becomes a silver cation. <<It has been suggested by Mitchell (1954) that immediate recombination of the electron in the conduction band with the silver ion is prevented by the operation of the Frank-Condon principle. The radius of a silver ion is about 1.1 $\mathring{A}$ and of an atom 1.4 $\mathring{A}$. If the ion is to capture the electron, its nucleus must therefore move out from neighbouring surface atoms through a distance of approximately $\sim$0.3 $\mathring{A}$. The process of capture is thus rendered very improbable.>>[4] The surface silver ion,

[4] Ref. 2, pg. 5.

though, is free to migrate on the surface of the crystal. It is attracted to other silver atoms of the surface layer by Van Der Waals forces. The ion forms an aggregate with one or two silver atoms, the positive charge being shared between them. The charged aggregate then neutralizes itself by capturing the electron from the conduction band. This neutral aggregate forms what is called a "latent" sub-image speck. These specks grow into latent images by capturing electrons from the conduction band and interstitial silver ions from the body of the crystal. Latent sub-image specks can also be produced by surface silver ions and mobile interstitial silver ions in the immediate neighbourhood. In conventional photography, the latent image is produced by photon absorption whereas in nuclear emulsion it results from delta-rays produced by the ionizing effect of charged particles traversing the crystal.

1.3 Grain Density and The Role of the Delta-Ray

One of the most important properties of processed nuclear emulsion is the track grain density, conventionally defined as the number of grains per hundred microns. In nuclear emulsion physics, it is generally accepted that those crystals acquiring a latent image along the trajectory of a charged incident particle do so because of the action of delta-rays produced by the incident particle. Delta-rays are freed electrons produced by the ionizing effect of the incident particle. The average rate of energy loss of the incident particle can only account for the observed grain density as a function of incident particle energy if a halide crystal sensitivity distribution identical to the measured distribution in developed grain size

is assumed. Unfortunately, experiments with light indicate that no such sensitivity distribution exists. If each crystal acquiring a latent image is assumed to do so because of the action of a single delta-ray produced in and arrested in the crystal itself, the observed variation in grain density with incident particle energy can be explained satisfactorily.

Consider a heavy, charged, incident particle of charge ze and velocity v traversing a medium. Consider a collision with an individual electron in the medium. The electron is assumed to be free and at rest and the incident particle velocity great enough that the electron's position changes negligibly during the collision. The particle passes within a perpendicular distance b, the impact parameter, of the electron. The incident particle is travelling in the x-direction and is moving with sufficient momentum that its direction changes negligibly during the collision. The situation is shown schematically in Fig. 1.1. ε is the electric field intensity of the incident particle at the position of the electron and $\varepsilon_\perp$ is the component of its electric field perpendicular to its trajectory.

The average ionization energy loss of the incident particle per unit path length, $-dE_I/dx$, is conventionally given by the Bethe-Block formula

Fig. 1.1 - Illustration of The Collision of a Charged Incident Particle And an Electron

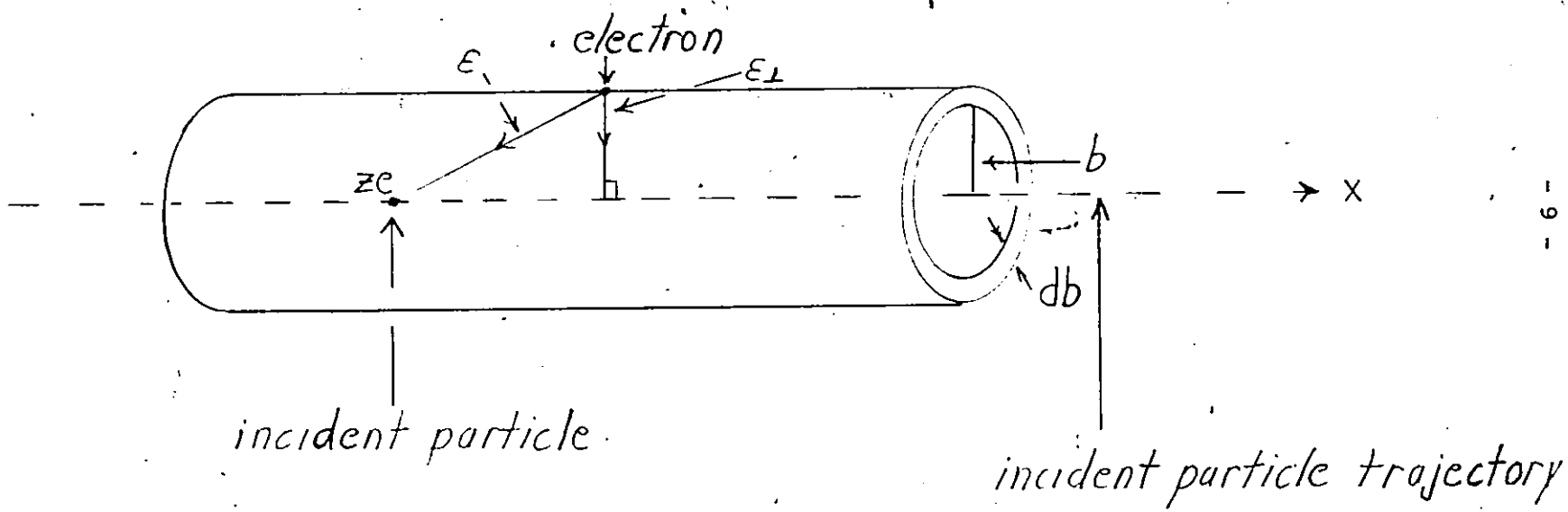

$$-dE_I/dx = \frac{4\pi z^2 e^4}{mv^2} n \left[\log \frac{2\gamma^2 mv^2}{I} - B^2 \right] \qquad (1.1)^5$$

where

m - rest mass of an electron

n - electron density of the medium

B - relativistic speed of the incident particle

(B = v/c)

c - speed of light

I - average ionization energy of the medium.

The average ionization energy is an average of the atomic ionization potentials of the medium. It is found to be approximately proportional to the atomic number, Z, of the medium. The impact parameter in a single collision is probabilistic, the energy transfer to the electron being given by

$$E = \frac{2}{m} \left(\frac{ze^2}{bv}\right)^2 = \frac{(\Delta\rho)^2}{2m} , \qquad (1.2)^6$$

where $\Delta\rho$ is the momentum transfer

The maximum impact, b_{max}, is

$$b_{max} = \frac{v\gamma}{\langle\nu\rangle} \qquad (1.3)^7$$

5 Ref. 3, pg. 31.

6 Ref. 3, pg. 29.

7 Ref. 3, pg. 30.

where

$\langle \nu \rangle$ - is an average of the atomic orbital frequencies

$\gamma = (1 - B^2)^{-\frac{1}{2}}$ is the relativistic factor.

The minimum distance of approach occurs in a head-on elastic collision. In the frame of reference of the incident particle, the electron is moving with initial speed v and initial momentum γmv directly towards the incident particle. After the collision, it is moving directly away from the incident particle with momentum γmv if recoil is neglected. Therefore,

$$\Delta p \simeq 2\gamma mv \qquad (1\text{-}4)$$

Combining equations 1-2 and 1-4, the minimum classical distance of approach b_{min}, is

$$b_{min} = \frac{ze^2}{\gamma mv^2} \qquad (1\text{-}5)$$

Equations 1-1, 1-2, and 1-3 are standard formulae employed to describe ionization energy losses of charged particles in matter and thus a rigorous development is not presented. These formulae are included here because they are useful in explaining the delta-ray energy distribution and observed track grain densities in nuclear emulsion physics.

Useful expressions for maximum and minimum energy transfer to electrons in individual collisions can now be determined . Since the electron in Fig. 1.1 was assumed to be free and at rest, the maximum energy transferred is equal to maximum delta-ray energy produced by the incident particle. Combining equations 1.2 and 1.3, the minimum energy transfer, E_{min}, is

$$E_{min} = \frac{2}{m} \left(\frac{\langle \nu \rangle z e^2}{B^2 c^2 \gamma}\right)^2 \tag{1.6}$$

The minimum energy transfer occurs at maximum impact parameter. Combining equations 1.2 and 1.4, the maximum energy transfer, E_{max}, is

$$E_{max} = 2\gamma^2 B^2 mc^2$$

$$= \frac{2mv^2}{1 - B^2} \tag{1.7}$$

This is the maximum kinematically allowed energy transfer and occurs at minimum approach distance. This expression concurs with the expression found in the reference literature (Ref. 9, pg. 25).

If one examines equations 1.3, 1.4, 1.6 and 1.7, it is evident that the energy transfer to electrons and consequent delta-ray energy distribution is statistical in nature.. The upper limit

of the spectrum depends upon the incident particle energy since both the minimum and maximum energy transferred depend upon the incident particle speed. As the incident energy increases, the minimum energy transferred decreases due to an increase in the maximum impact parameter and the maximum energy transferred increases due to a decrease in the minimum approach distance. Thus, the delta-ray energy spectrum broadens with increasing incident particle energy.

As previously mentioned, a "latent" image is produced in a crystal in which a delta-ray is produced and recaptured. If the delta-ray escapes from the parent crystal, there is high probability that no latent image is produced and consequently a corresponding grain of elemental silver does not usually appear in the developed track. << It has been previously stated that it is delta-rays of energy less than $\sim$ 5 keV which are particularly effective in the formation of the latent image in crystals along a track, for they are frequently arrested within the crystal in which they originate.>>[8] Those delta-rays of energy $\sim\geq$ 5 keV escape from the parent crystals which consequently do not usually acquire a latent image. A low energy delta-ray follows a path which is both short in length and extremely contorted since it has a small relativistic mass and thus undergoes a large amount of scattering. Correspondingly, there is a high probability of it being captured in the parent crystal. As the delta-ray energy

[8] Ref. 2, pg. 46.

increases, the path length and relativistic mass both increase. It acts more and more like a heavy fast moving particle. The scattering is reduced, thereby reducing the path contortion. Thus, the probability of escaping the parent crystal increases.

The grain density in nuclear emulsion is proportional to the degree of ionization squared, z^2, of the incident particle. Since the average rate of ionization energy loss of the incident particle, expressed quantitatively by equation 1.1, is also proportional to z^2, the grain density is proportional to the average rate of ionization energy loss. The average rate of ionization energy loss, the energy loss per unit path length, of the incident particle is the product of the average delta-ray energy and number of delta rays per unit path length, plus a constant term. As will be discussed later, for fixed incident particle energy, the average delta-ray energy is constant. Thus, the grain density is proportional to the number of delta-rays produced. Consequently, the production of a latent image can be attributed to the action of single delta-rays rather than the joint action of two or more delta-rays.

Since the track grain density is proportional to the average rate of ionization energy loss given by equation 1.1, the grain density curve as a function of incident particle energy has the same shape as the energy loss curve. The two shapes are identical up to minimum ionization energy loss. Minimum ionization energy loss in emulsion

Fig. 1.2 - Illustration of the Energy Loss and Grain Density Curves

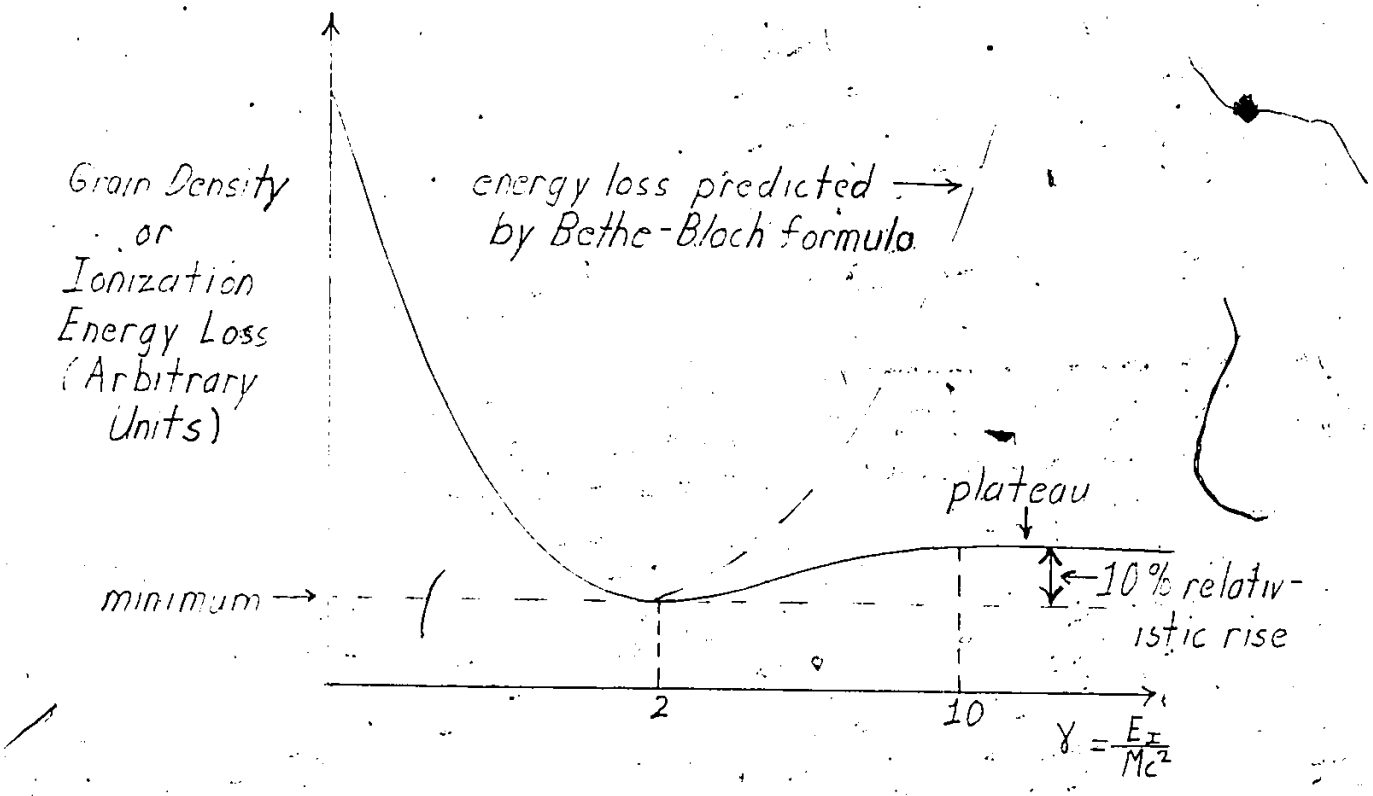

Fig. 1.3 - Heavy Incident Particle Passing a Distance b to b+db From a Given Electron

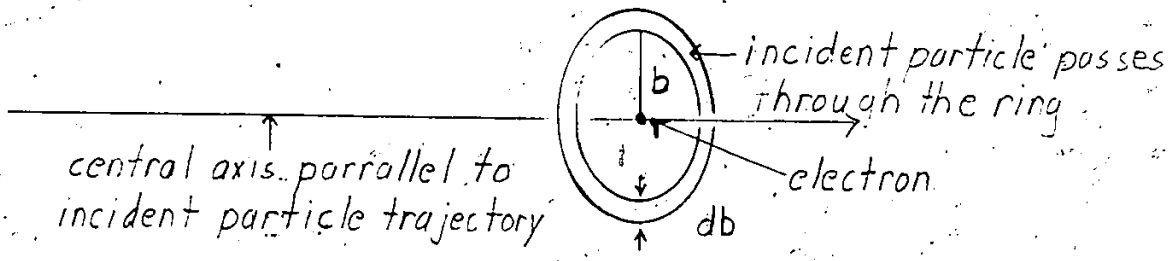

occurs at incident particle energy of $\sim 2Mc^2$ where M is the rest mass of the incident particle. Thus, $\gamma = 2$ at minimum ionization. Beyond minimum ionization loss, the observed grain density differs from the predicted value. This is shown schematically in Fig. 1.2. At low incident particle energy, the average rate of energy loss (equation 1.1) varies as $1/v^2$, the first term in the equation being dominant. The more slowly varying second term increases logarithmically as $\gamma^2 v^2$ and consequently contributes negligibly. Thus, the rate of energy loss decreases with increasing incident particle energy. For extremely relativistic particles, v^2 increases slowly with increasing incident energy but γ^2 rapidly approaches infinity. The second term becomes dominant and the average rate of energy loss increases rapidly with increasing incident particle energy. The grain density curve, though, no longer follows the rate of energy loss curve. It increases very slowly from minimum at minimum ionization energy loss at $\gamma = 2$ up to a constant plateau value at $\gamma = 10$, the plateau grain density being about 10% higher than the minimum.

An alternative approach in explaining the observed grain density as a function of incident particle energy is to consider both the mechanism of latent image formation and the energy distribution of the delta-rays. One assumes a delta-ray energy distribution to explain the observed grain density. << For delta-rays of higher energy the distribution in energy is commonly assumed to be

$$N(E)dE = KE^{-2}dE \qquad (1.7)$$

the spectrum extending up to a value of E_{max}, which is defined by the need to conserve energy and momentum in a collision.>>[9] N(E) is the number of delta rays of energy E per unit path length. The maximum possible energy transfer has already been discussed. K is assumed to be a constant of proportionality.

The author proposes that this energy distribution assumption is unnecessary since it is a natural consequence of the laws of probability and the physics involved. The proportionality constant, K, is actually constant only for fixed incident particle energy. It changes with changing incident particle energy. This is easily seen if one considers the statistical nature of the impact parameter in a single collision. The probability, p(b)db, of an incident particle passing within a distance b to b + db of a given electron is proportional to $2\pi bdb$. This is shown schematically in Fig. 1.3. Thus,

$$p(b)db \propto 2\pi bdb \qquad (1.8)$$

The energy transferred in the collision is given by equation 1.2. If one rearranges this equation to isolate b^2, it becomes.

$$b^2 = \frac{2(ze^2)^2}{mv^2} \frac{1}{E} \qquad (1.9)$$

9 Ref. 2, pg. 48.

If one now takes the derivative for fixed incident particle energy (constant v), one finds that

$$bdb = - \frac{(ze^2)^2}{mv^2} \frac{1}{E^2} dE \qquad (1.10)$$

If one combines equations 1.10 and 1.8 and absorbs the negative sign into the constant of proportionality, one can say that

$$p(b)db \propto \frac{2(ze^2)^2}{mv^2} \frac{1}{E^2} dE \qquad (1.11)$$

The number of electrons per unit path length acquiring energy E to E + dE is proportional to the probability of an electron acquiring this energy in an individual collision. Consequently,

$$N(E)dE \propto \frac{2(ze^2)^2}{mv^2} \cdot E^{-2} dE \qquad (1.12)$$

If one now compares equations 1.12 and 1.7, one finds that

$$K \propto \frac{2(ze^2)^2}{mv^2} \qquad (1.13)$$

Recalling the fact that v is the incident particle speed, equation 1.13 indicates that K is actually a parameter which depends upon the incident particle energy since K varies as $1/v^2$. Consequently, both the upper limit and the shape of the delta-ray energy distribution depend upon the incident particle energy and the variation of the parameter K is

identical to the variation of the rate of incident particle energy loss.

The delta-ray energy distribution is useful in calculating the average delta-ray energy. The total energy, E_{12}, per unit path length, of the delta-rays between limits E_1 and E_2 for fixed incident particle energy is

$$E_{12} = \int_{E_1}^{E_2} EN(E)\,dE = \int_{E_1}^{E_2} EKE^{-2}\,dE$$

$$= K \ln E_2/E_1 \qquad (1.14)$$

The number of delta-rays, N_{12}, per unit path length between the limits E_1 and E_2 is

$$N_{12} = \int_{E_1}^{E_2} N(E)\,dE$$

$$= K \left(\frac{1}{E_1} - \frac{1}{E_2}\right) \qquad (1.15)$$

The average delta-ray energy between these limits is

$$E_{AV} = \frac{E_{12}}{N_{12}} = \frac{\ln E_2/E_1}{\frac{1}{E_1} - \frac{1}{E_2}} \qquad (1.16a)$$

If $E_2 >> E_1$

$$E_{AV} \simeq E_1 \ln E_2/E_1 \tag{1.16b}$$

The delta-ray energy distribution is assumed to be valid from the average, latent image forming delta ray energy, E'_{min}, determined experimentally to be $\sim$ 200 eV, to the maximum delta-ray energy as given by equation 1.7. If one now recalls that delta-rays of energy $\geq$ 5 keV, E'_{max}, are unlikely to produce latent images, then the fraction, F_L, of the total delta-ray energy of delta-rays of energy $\geq E'_{min}$ which produces latent images is approximately

$$F_L = \frac{\ln E'_{max}/E'_{min}}{\ln E_{max}/E'_{min}} \tag{1.17}$$

Recall that E_{max} is the maximum possible energy transfer in a collision.

This energy distribution has several important features. Firstly, the average delta-ray energy of those delta-rays producing latent images is

$$E_{AVL} = \frac{\ln E'_{max}/E'_{min}}{\frac{1}{E'_{min}} - \frac{1}{E'_{max}}} \tag{1.18}$$

Since E_{AVL} is independent of K, the distribution parameter, and both E'_{min} and E'_{max} are fixed average values, the average energy of latent image producing delta-rays is independent of the incident particle energy. This is extremely important in explaining the observed grain density variation with incident particle energy. On the other hand, the approximate number of latent image forming delta-rays, N_L, is not independent of the incident particle energy since

$$N_L = K \left(\frac{1}{E'_{min}} - \frac{1}{E'_{max}}\right) \tag{1.20}$$

Thus, the number of latent images per unit path length and consequently the observed grain density depend upon the distribution parameter K which varies as $1/v^2$. The rate of energy loss of the incident particle also varies as $1/v^2$ up to minimum ionization energy loss (Fig. 1.2). Thus the energy loss and grain density curves must be identical in shape up to this point. They are identical due to the nature of the variation of the distribution parameter, this variation being a fundamental manifestation of the physical and statistical nature of the electron collisions of the ionizing particle.

Secondly, the distribution indicates that the total number, N_T, of delta-rays of energy $\geq E_{min}$ also depends upon the incident particle energy but in a manner slightly different from that of the total number of latent image producing delta-rays since

$$N_T = K \left(\frac{1}{E'_{min}} - \frac{1}{E_{max}} \right) \tag{1.21}$$

where E_{max} and K are functions of the incident particle energy. Thirdly, the fraction of the total delta-ray energy of delta-rays $\geq E'_{min}$ which produces latent images, equation (1.17), decreases as the incident energy increases since the maximum energy transfer increases.

One can estimate the fraction of the total delta-ray energy and thus the fraction of the ionization energy loss producing "latent images" in emulsion at minimum ionization energy loss. It has been stated that γ has a value of two at this point. Thus, from equation 1.7, the maximum energy transfer, E_{max}, is

$$E_{max} = 2\gamma^2\beta^2 mc^2 \tag{1.7}$$
$$= 2 \times 2^2 \times 0.75 \times 0.511 \text{ MeV}$$
$$= 3.06 \text{ MeV}.$$

This is in accord with the value found in the literature. <<The average rate of energy loss of a particle of mass M, charge $|e|$ and energy $2Mc^2$ is about 650 KeV/mm of which about 500 keV is lost in the halide. The maximum possible energy transfer by such a particle to an electron, if M >> m, is $\sim$3 MeV.[10] >> The average maximum and minimum

[10] Ref. 2, pg. 48.

energy of latent image forming delta-rays is 5 keV and 200 eV, respectively. Thus, from equation 1.17, the fraction of the total delta-ray energy of delta-rays of energy $\geq$ 200 eV which produces latent images is

$$F_L = \frac{\ell n \ E'_{max}/E'_{min}}{\ell n \ E_{max}/E'_{min}} \qquad (1.17)$$

$$= \frac{\ell n \ (5000/200)}{\ell n \ (3 \times 10^6/200)}$$

$$= 0.335$$

Thus, at minimum ionization, less than 35% of the ionization energy loss forms latent images. The percentage decreases as the incident particle becomes more and more relativistic.

Beyond minimum ionization, $\gamma > 2$, the grain density increases slowly to a constant plateau value at $\gamma = 10$. It remains constant and equal to the plateau value in the extreme relativistic region, the plateau grain density being about 10% higher than the minimum value. The rate of energy loss, though, increases quite rapidly since it increases logarithmically with γ which rapidly approaches infinity. Thus, the grain density and energy loss curves no longer correspond. There are two reasons for this. As equation 1.6 indicates, the maximum transferable energy varies as γ^2 and thus becomes very

large whereas the fraction, equation 1.17, of the total delta-ray energy of delta-rays $\geq E'_{min}$ which produces latent images becomes very small since E_{max} becomes very large. Thus, most of the incident particle energy loss appears as very rare, extremely energetic, delta-rays that escape from the parent crystals which thus do not acquire latent images. These crystals do not appear as grains of silver in the track after processing. The slight 10% rise to the plateau grain density is attributed to an increase in the number of low energy delta-rays since the minimum energy transfer varies as $1/\gamma^2$ (equation 1.6) and the number of low energy delta-rays depends on E_{min}. It was stated previously that the average minimum delta-ray energy required for latent image production was $\sim$ 200 eV. This is necessarily statistical in nature since in order to produce a latent image holes must be trapped at a "kink" site at the surface of a crystal and the electrons must be retained in the conduction band. A hole resulting from a low energy delta-ray produced near the surface of the crystal obviously has more chance of reaching the surface and being trapped instead of recombining with the electron than a hole from a delta-ray of equivalent energy produced near the center of the crystal. If there is a significant increase in the number of low energy delta-rays , there is a corresponding increase in the number of low energy delta-rays produced near the surface of some crystals and thus an increase in the number of low energy delta-rays producing latent images. This decreases the average minimum energy of latent image producing delta-rays. Since K, which varies as $1/v^2$, is nearly constant, there is an increase in the number

of latent image forming delta-rays per unit path length, as equation 1.20 indicates. Consequently, there is a slight increase in grain density, corresponding to the 10% rise to the plateau.

The plateau is attributed to polarization of the medium, which limits the maximum impact parameter. The polarization is attributed to the relativistic elongation of the perpendicular component of the incident particle electric field

$$\varepsilon_{\perp}' = \gamma\varepsilon_{\perp} \qquad (1.21)$$

$\varepsilon_{\perp}$ is the perpendicular component of the incident particle electric field in the incident particle rest frame whereas $\varepsilon_{\perp}'$ is the perpendicular component in the medium rest frame. In effect, the electrons in the medium see ε' rather than ε. When the perpendicular component becomes elongated to the point where it has a significant intensity at a distance from the incident particle of the order of the average interatomic distance of the medium, polarization of the medium occurs. As a result, distant electrons are shielded by the reverse electric field produced by the polarization. The maximum impact parameter reaches a constant maximum value. The minimum energy transfer and consequently the number of latent image producing delta-rays become constant which results in a constant plateau grain density.

The onset of polarization obviously depends on the density of the medium. As the density decreases, the average interatomic distance increases proportionaly, as does the value of the maximum impact parameter. Thus, the beginning of the plateau occurs at higher values of γ. Consequently, the relativistic rise is increased. It can be as much as 60% in gases when considering only local ionization energy loses.

1.4 Classification of Tracks.

In nuclear emulsion physics, there are several classifications of tracks. The tracks are conventionally classified according to their grain density, the grain density being the number of grains per hundred microns.

a) Minimum Tracks

Minimum tracks are produced by incident particles of minimum ionization energy loss, particles with $\gamma \simeq 2$. Thus, minimum tracks are tracks of minimum grain density, g_o.

b) Shower Tracks

Shower tracks are conventionally classified as tracks with a grain density less than or equal to 1.4 times the minimum grain density. Thus,

$$g_o \leq g \leq 1.4\, g_o \qquad (1.22)$$

where g is the grain density. Thus, minimum tracks are included in the larger set of shower tracks.

c) Grey Tracks

Grey tracks are tracks of grain density $1.4\ g_o \leq g \leq 80$. They are called grey tracks because they appear greyish under the microscope. The grain density is still low enough that individual grains can be distinguished and counted.

d) Black Tracks.

Black tracks appear black under the microscope. The grain density becomes so high that individual grains can no longer be distinguished with any degree of certainty. The track appears as almost solid black lines of silver. Black tracks are produced by low energy particles since they have a high rate of energy loss and a correspondingly high grain density.

1.5 Background

Once Fuji emulsion gel is melted and poured into sheets it becomes active. It begins to accumulate background. Emulsion registers several different types of background . Fog, cosmic rays and slow electrons are some examples.

a) Fog

During the developing stage of processing, a small percentage of the halide crystals in the emulsion, either not possessing a latent image or acquiring one randomly, are reduced to grains of silver. These background grains, commonly called "fog", seem to develop randomly but at a much slower rate than crystals possessing latent images along tracks. In emulsion physics, it is extremely important to minimize the fog density so that minimum tracks can be distinguished. If the fog density becomes too great, minimum tracks can be either partially or completely masked. If this occurs in high energy experimentation, it can be fatal to an entire experiment since one is dealing with interactions by relativistic particles and, consequently, minimum tracks. Fog and methods of minimizing it will be discussed in more detail in Chapter 2 which describes nuclear emulsion processing in detail.

b) Cosmic Rays and Natural Radiation

Nuclear emulsion registers the tracks of all charged particles, such as, muons, pions and protons produced by cosmic rays. Cosmic ray pions are created by high energy collisions between cosmic rays and nuclei of the atmosphere. A muon is created when a pion subsequently decays to a muon and a neutrino. This charged secondary radiation which results from primary cosmic radiation leaves background tracks in the emulsion.

Naturally radioactive materials such as thorium and radon are actually contained in the emulsion. They leave small radioactive stars in the emulsion when they decay. Slow electrons are produced by "Compton" scattering or absorption of high energy electromagnetic radiation. Gamma-rays are particularily harmful as they can result in both Compton scattering and pair production. If an electron absorbs sufficient energy during "Compton" scattering or absorption of a gamma-ray it can become a delta-ray which either escapes from the parent grain producing a short contorted track called a slow electron track or is recaptured by the parent crystal which consequently acquires a latent image and thus contributes to the fog background. Pairs also leave background tracks.

Concrete can be extremely harmful to emulsion plates. Concrete contains potassium fourty, K^{40}. K^{40} is radioactive. It can decay to excited argon forty by electron capture. The excited argon forty nuclei then each emit a 1.461 MeV gamma-ray as they decay to the ground state. These gamma-rays are sufficiently energetic to produce unwanted tracks of pairs and slow electrons in the emulsion. Unshielded emulsion stacks should be kept as far away from concrete walls, floors, etc as possible. One should take great pains to properly shield emulsion stacks prior to and during exposure. Non-radioactive lead is particularly effective.

1.6 Idiosyncrasies of Emulsion

A particularily interesting characteristic of emulsion, a property which is extremely important in emulsion physics, is the hygroscopic nature of the gelatin. Gelatin immersed in an aqueous solution absorbs water. It also absorbs water from the water vapor in the air until equilibrium is reached at which point the rate of absorption from the air equals the rate of desorption into the air. The equilibrium water content depends upon the relative himidity of the air. If the relative humidity of the air decreases, the rate of desorption becomes greater than the rate of absorption. There is a net desorption of water until the two rates again become equal. As a consequence, the emulsion "shrinks". The reverse effect occurs if the relative himidity is increased. This causes the emulsion to swell. Dimensional changes occur as the emulsion "shrinks" or "swells" due to a net desorption or absorption of water. Thus spatial and grain density track measurements change with changing temperature and humidity conditions. If consistent, unbiased data is to be obtained, the necessary steps must be taken to ensure that measurements are always performed in a controlled, consistent environment.

A controlled storage environment is also essential for processed emulsion due to the hygroscopic nature of the gelatin. It is common practice to stick emulsion pellicles to a glass or plastic

support just prior to processing. The pellicles remain stuck to the support during and after processing. If the processed emulsion loses to much water in an uncontrolled environment, enormous tensional forces are created in the gelatin network as the emulsion dries out. Such forces can become large enough to break or even tear the glass support, rendering the emulsion worthless for any further quantitative measurements. Optimum storage conditions depend upon the type of emulsion. The processed Fuji emulsion used in experiment E-531 must be stored at relative humidity $\geq$ 70% and a temperature range of 20 to 25°C.

The non-elastic and hygroscopic nature of gelatin are two extremely important factors in nuclear emulsion processing. The gelatin support network behaves somewhat like a plastic material. During the processing, the emulsion absorbs large amounts of water and can thus swell to several times its initial size. During the alcohol drying stages at the end of processing (Diagrams 1 & 2), the absorbed water is removed at a controlled rate. As the absorbed water is removed, the network shrinks but not being completely elastic in nature significant distortion can occur if this swelling and subsequent shrinkage is not carefully controlled. Distortion produces unnatural bending in the silver grain tracks and thus the true trajectory of the ionizing incident particle is not properly registered. Minimization or complete elimination of this distortion is one of the major goals of nuclear emulsion processing. Swelling, being one of the primordial causes of distortion, must be minimized and the rate of swelling must be carefully

controlled. Also the shrinkage rate, controlled by the drying rate, must be carefully controlled.

Several techniques and combinations there of, are available for minimizing the swelling and controlling its rate during processing. One of the most effective, a technique perfected by the Japanese and employed here in Ottawa in developing the 25 liter E-531 emulsion stack, is low temperature processing. Careful control of fixing solution pH is also extremely important. These techniques will be discussed in detail during the discussion of emulsion processing in Chapter 2.

A plasticiser, usually glycerin, is added to the emulsion to reduce the brittleness. The plasticiser promotes plastic flow under stress. If insufficient plasticiser is added, the thick pellicles used in nuclear emulsion work can become extremely brittle and break as they shrink.

CHAPTER 2 NUCLEAR EMULSION PROCESSING

2.1 General Description of the Processing of the E-531 Emulsion Stack.

A detailed description of nuclear emulsion processing will now be presented. The various processing stages are described in chronological order. A discussion of the various chemical and physical processes occuring in each stage is included. The chemical reagents along with their functions and reactions are discussed. The chemical solutions used in the various stages, including the concentration of each component, are tabulated in Tables I and II.

Two processes are depicted schematically in Process Flow Diagrams 1 and 2. These processes are low temperature techniques used for processing Fuji emulsion. The original process was developed by G. Marguin - C.R. Ac. Sci. Paris. The process was modified slightly by the Japanese emulsion groups at Nayoga, Kobe and Osaka City Universities in Japan headed by Professors Nui, Fujioka and Kusumoto, respectively. A 25 liter emulsion stack consisting of approximately four thousand plates was processed at the University of Ottawa during during a two-month period in the winter of 1979. The emulsion had been exposed to a neutrino beam for two and one-half months at Fermilab as part of experiment E-531. This neutrino beam was produced by the interaction of a 350 GeV proton beam with a beryllium target. The resulting pions and kaons decayed in flight via the modes $\pi^+ \rightarrow \mu^+ + \nu$ and $K^+ \rightarrow \mu^+ + \nu$. The resulting neutrino beam contained of the order of

10^9 neutrinos per pulse. The emulsion processing system was designed and built at Ottawa. A detailed description of the system is presented in Chapter 3.

Both vertical and horizontal emulsion plates were processed. Vertical plates were exposed vertically to the neutrino beam whereas the horizontal plates were exposed horizontally. The two cases are depicted schematically in Diagrams 3a and b. The vertical plates, 12 cm x 9.5 cm x 730 μ, consisted of a layer of emulsion 330 microns thick stuck to each side of a 70 μ thick polystyrene support. The emulsion was poured directly onto the plastic support prior to exposure. The horizontal plates were emulsion pellicles, 14 cm x 5 cm x 614 μ, mounted on lucite plates of dimensions 16 cm x 7 cm x 2 mm. The horizontal pellicles were stuck to the lucite supports just prior to processing.

The processing data for both the vertical and horizontal emulsion is tabulated in Tables VIA and B, respectively. The vertical emulsion, 15.3 liters in total, was processed in batches of approximately 1.06 liters with each batch containing approximately 140 plates. Parallel processing was used. The batches were processed two at a time with a fifty minute delay between the two batches. A total of fifteen days was required to process the fourteen and one-half batches since two new batches were begun every second day. The processing time per batch was approximately 3 days.

The horizontal emulsion, 9.8 liters in total, was processed in batches of approximately 1.14 liters, each batch containing approximately 264 plates. The eight and one-half batches were processed in approximately six weeks. Staggered parallel processing was used. The batches were processed two at a time with a one day delay between the two batches. A new set of two batches was begun every six days. The processing time per batch was approximately 12 days.

The horizontal processing time was much longer than that of the vertical emulsion since the horizontal pellicles were twice as thick as the vertical pellicles. The processing time is generally proportional to the square of the pellicle thickness. All stages prior to drying were done at $5^{\circ}C$ for the vertical emulsion. All stages prior to washing were done at $7^{\circ}C$ for the horizontal emulsion. The washing was done at $\leq 10^{\circ}C$ in the horizontal case. Circulation was employed in the fixing and washing stages of both types of emulsion.

Concentrations symbols, [ ], will be used in all chemical equilibrium and rate expressions with the understanding that, at ionic strengths ≥ 0.01 gmoles/L, they imply activities rather than concentrations. Activity accounts for the non-ideality of aqueous solutions at ionic strengths above 0.01 gmole/L. The hydronium ion, H_3O^+, rather than the hydrogen ion, H^+, will be used throughout to denote acidity.

DIAGRAM 1 - PROCESS FLOW DIAGRAM FOR VERTICAL FUJI EMULSION PLATES (330 μ THICKNESS)

NOTE : 1/3 FIX MEANS 1/3 STRENGTH FIXER. ETC.

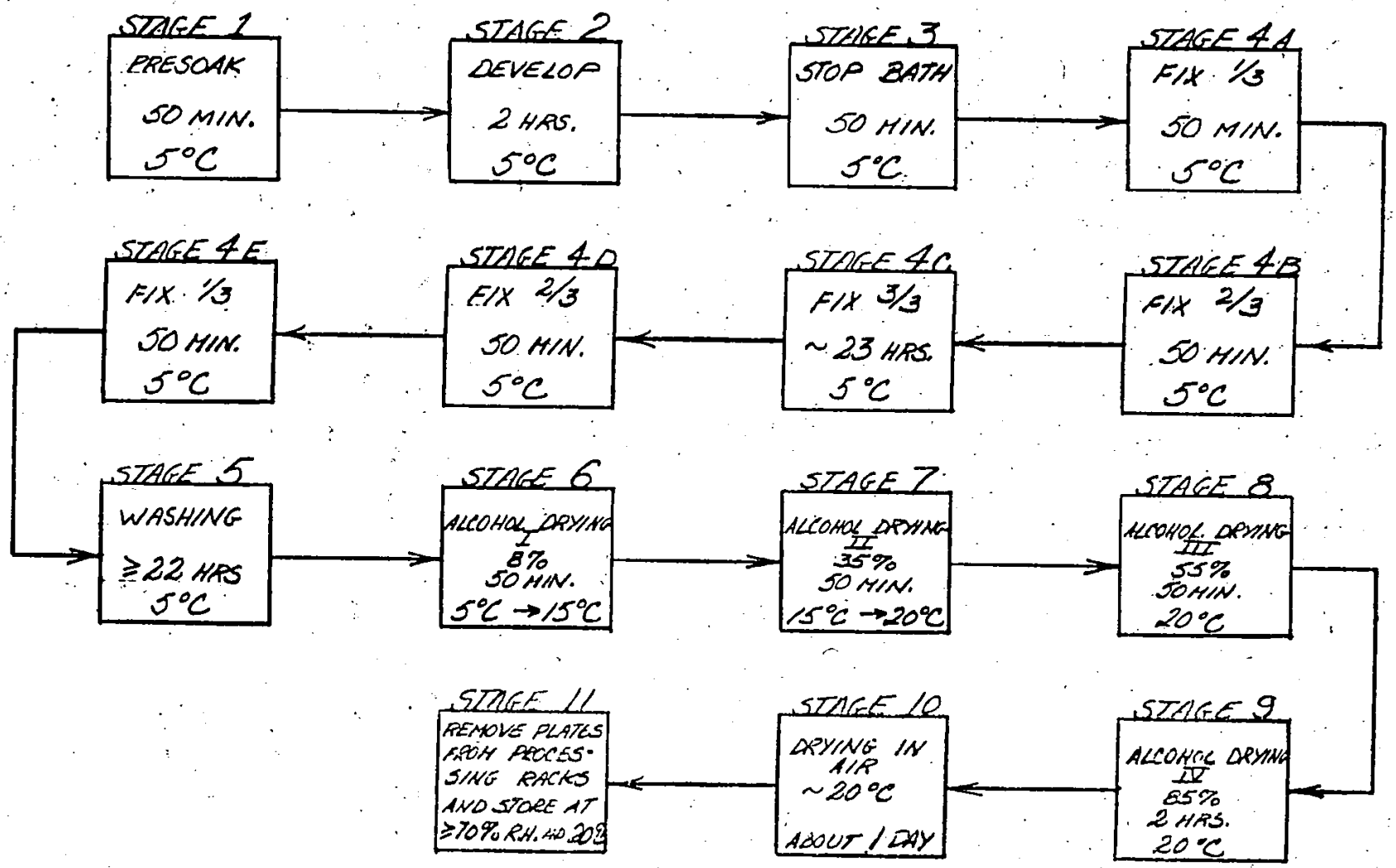

DIAGRAM 2 - PROCESS FLOW DIAGRAM FOR HORIZONTAL FUJI EMULSION PLATES (614μ THICKNESS)

NOTE : ½ FIX MEANS ½ STRENGTH FIXER, ETC.

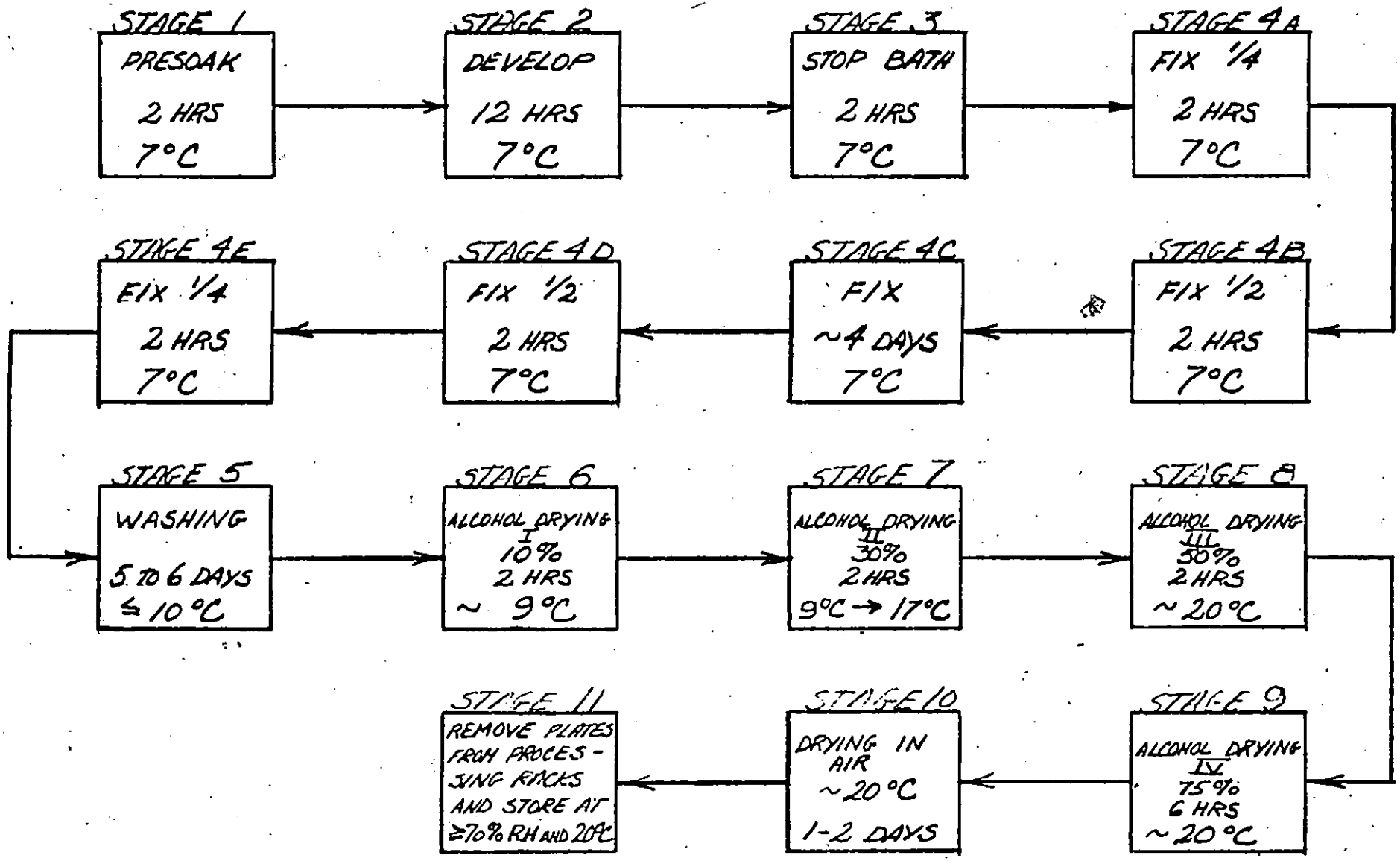

DIAGRAM 2 - PROCESS FLOW DIAGRAM FOR HORIZONTAL FUJI EMULSION PLATES (6¼ THICKNESS)

NOTE : ½ FIX MEANS ½ STRENGTH FIXER, ETC.

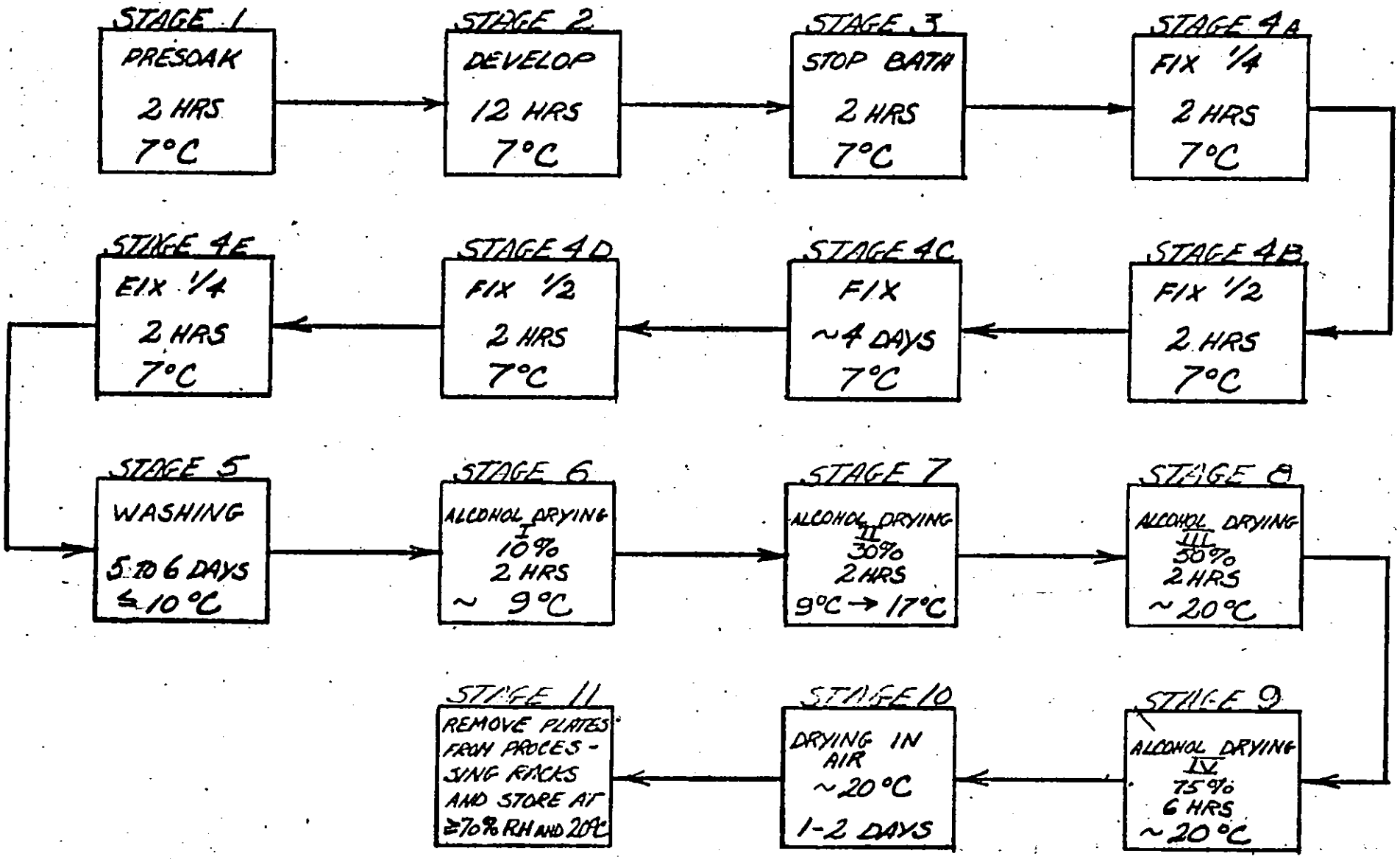

DRAWING 3A - VERTICAL EMULSION PLATE

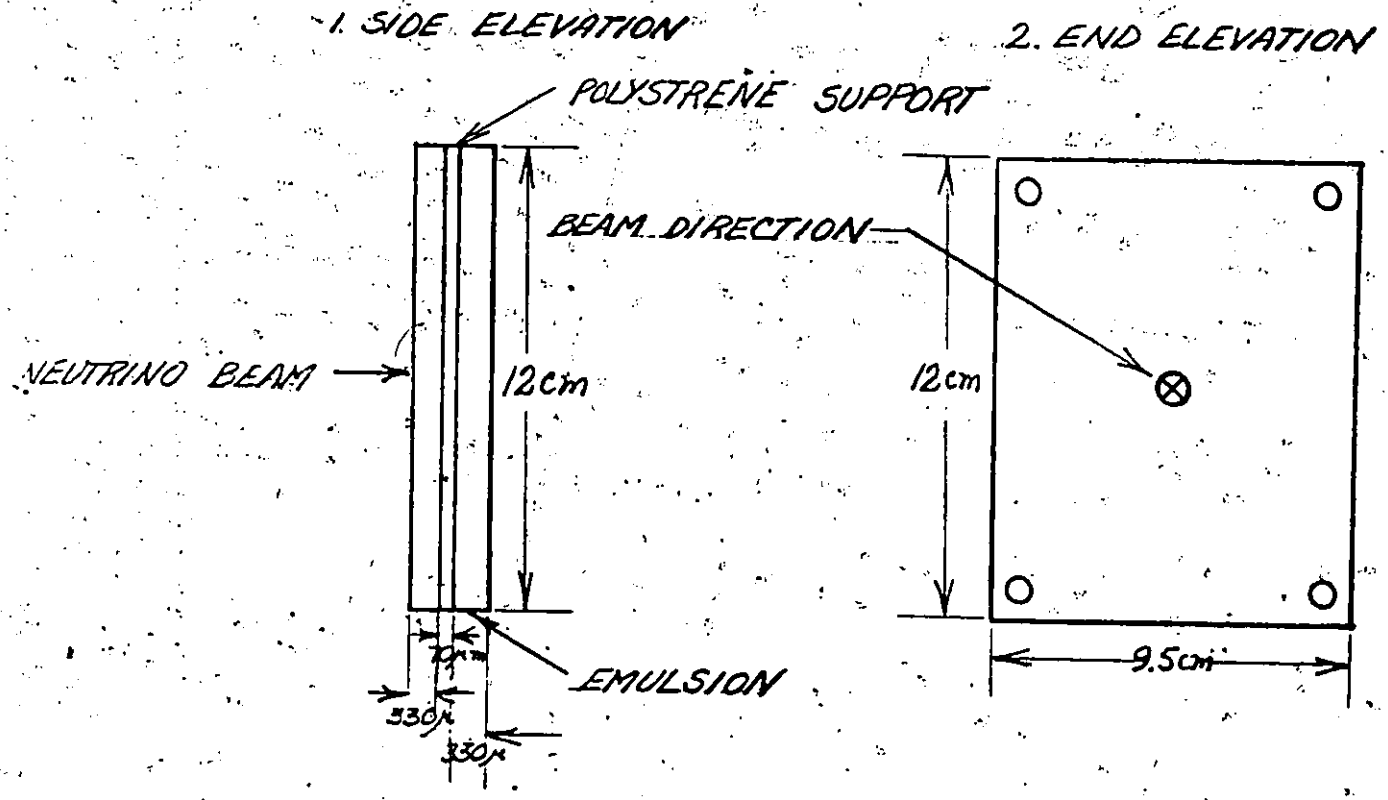

DRAWING 3B - UNMOUNTED HORIZONTAL PELLICLE.

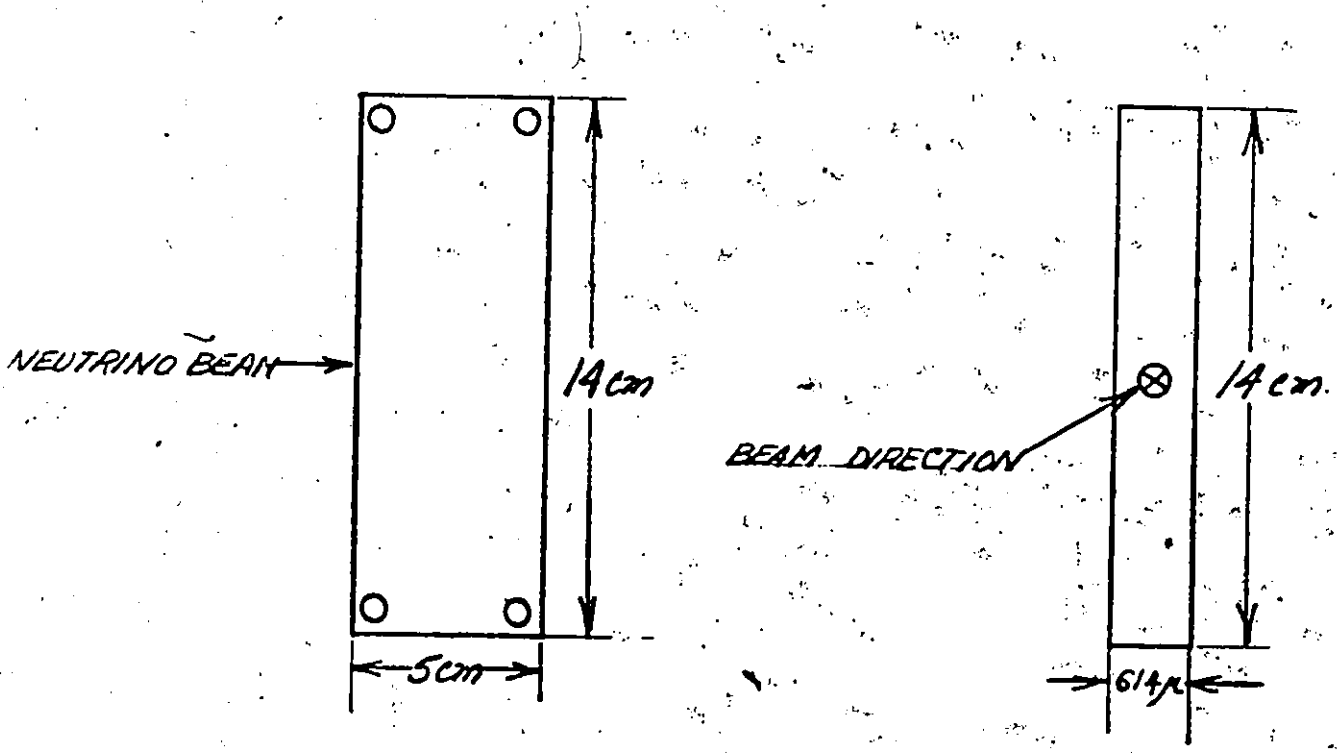

2.2 Stage 1 - Presoak

The horizontal emulsion plates were soaked in a deionized cold water bath at 7°C for two hours. The vertical emulsion plates were soaked in a 0.035 molar solution of sodium sulfate and deionized water at 5°C for fifty minutes.

The major process occuring during the presoak is a physical one, since no significant chemical reactions occur. The emulsion gelatin, being hygroscopic, absorbs water and consequently swells to approximately twice its initial thickness. This swelling expedites the developing solution penetration of the gelatin support matrix during the second stage of processing by increasing the developer diffusion rate, the coefficient of diffusion being dependent on the amount of swelling.

Sodium sulfate, Na_2SO_4, is a salt of sulfuric acid, H_2SO_4. It dissociates completely in aqueous solution. Since it is the salt of a strong acid, the sulfate anion undergoes only a very slight hydrolysis reaction of the nature

$$\underset{\text{base 1}}{SO_4^{2-}}\ (aq) + \underset{\text{acid 2}}{H_2O} \rightleftharpoons \underset{\text{acid 1}}{HSO_4^-}\ (aq) + \underset{\text{base 2}}{OH^-}\ (aq) \qquad (2\text{-}R1)$$

Acids and bases are defined according to the Lowry-Bronsted definitions

of acids being proton donators and bases being proton acceptors in aqueous solution. The symbol (aq) implies aqueous solution. The hydrolysis equilibrium constant, K_h, is

$$K_h = \frac{[HSO_4^-]_e[OH^-]_e}{[SO_4^{2-}]_e} = \frac{K_w}{K_{a2}} \qquad (2\text{-}1)$$

where K_w is the equilibrium constant for the acid-base reaction of water with iself

$$\underset{\text{acid 1}}{H_2O} + \underset{\text{base 2}}{H_2O} \rightleftharpoons \underset{\text{acid 2}}{H_3O^+} + \underset{\text{base 1}}{OH^-} \qquad (2R\text{-}2)$$

$$K_w = [H_3O^+]_e [OH^-]_e \qquad (2\text{-}2)$$

$$= 10^{-14} \text{gmoles}^2 - L^{-2} \text{ @ } 25^oC$$

K_{a2} is the second dissociation constant of sulfuric acid

$$K_{a2} = \frac{[H_3O^+]_e[SO_4^{2-}]_e}{[HSO_4^-]_e} \qquad (2\text{-}3)$$

$$= 1.2 \times 10^{-2} \text{gmoles} - L^{-1} \text{ @ } 25^oC.$$

Thus, from equation 2-1,

$$K_h = \frac{10^{-14}}{1.2 \times 10^{-2}} = 8.3 \times 10^{-13} \text{gmoles} - L^{-1} \text{ @ } 25^oC.$$

This extremely small value for the hydrolysis constant indicates that reaction 2-R1 is very far to the left at equilibrium. Thus, insignificant amounts of HSO_4^- and OH^- are formed during the hydrolysis of the sulfate anion. Consequently, the pH of the vertical emulsion presoak solution is essentially identical to that of pure deionized water. This was verified experimentaly and is tabulated in Table III.

In the sulfate anion, the sulfur atom exists in its highest oxidation state, having an oxidation number of +6. Since the sulfur is in its highest oxidation state, the sulfate anion will not undergo further oxidation. As a result, it does not react with and remove oxygen dissolved in the presoak water. From this, one can conclude that dissolved oxygen is not a problem during presoak since it is not removed chemically prior to the commencement of processing. This is in direct contrast to the developing stage where removal of dissolved oxygen, prior to the addition of the developing agent to developing solution, is absolutely essential.

2.3. Stage 2 - Developing

The developing stage is the most crucial stage of nuclear emulsion processing. The developer is an aqueous solution of amidol, sodium sulfite and sodium metabisulfite. In the horizontal case, potassium bromide is added. It acts as a "restrainer". The sodium

sulfite and sodium metabisulfite form a "buffer", controlling the pH at about 6.6. The sulfite anion also removes dissolved oxygen in the deionized water. The salts are added before amidol, the developing agent. The horizontal plates were developed at 7°C for twelve hours whereas the vertical plates were developed at 5°C for four and one-half hours. The horizontal plates were developed for a longer time because they were thicker. Precise control of temperature and developing time is of paramount importance. The standard Bristol developing solution was used.

The processes occuring during the developing stage are both physical and chemical in nature. Initially, the developing solution must penetrate the gelatin support matrix by the physical process of diffusion. The developing agent, amidol (2, 4-diaminophenol dihydrochloride), is a powerful reducing agent. Its molecular structure is shown in Fig. 2.1. Silver bromide crystals possessing a "latent image" are reduced to grains of elemental silver by the diaminophenol. The diaminophenol is oxidized during the development reaction. The development reaction is thus a redox (oxidation-reduction) reaction. Silver bromide crystals which do not posses a latent image are much less susceptible to reduction than those possessing a latent image although some do develop randomly but at a much slower rate. This random development of non-latent image carrying halide crystals produces background grains, called "fog", in the emulsion. As will be discussed in more detail later, a "restrainer" suppresses this random development and thereby reduces the fog density.

Fig. 2.1 - Molecular Structure of Amidol

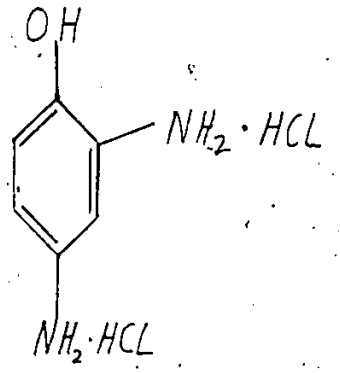

Fig. 2.2 - Molecular Structure of the Doubly Charged Cation of 2,4 - Diaminophenol

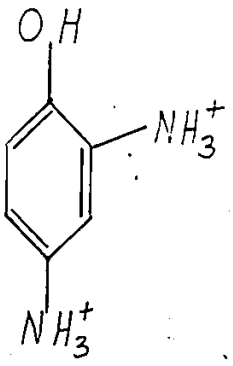

Uniform development with respect to depth from the pellicle surface is one of the major criteria for a successful development in nuclear emulsion physics. The degree of uniformity can be calibrated by determining the grain density of minimum tracks at various depths in the emulsion. If the developer penetration rate, a diffusion process, is slow in comparison to the development rate, a chemical process, a significant degree of development will occur near the upper surface of the pellicles before the developer has diffused to the base, the unfavourable result being highly non-uniform development. This is not a major problem in conventional photography since the emulsion thickness is only of the order of ten microns.

In nuclear emulsion processing, several techniques can be combined to minimize the non-uniformity of development with respect to depth. Presoaking swells the gelatin support network. This increases the rate of developer diffusion into the emulsion and through the support matrix. Thus, developer can penetrate to the base of the pellicles more rapidly. The development rate, being an exponential function of temperature, is extremely temperature sensitive. The development rate is approximately an order of magnitude lower at $7^{\circ}C$ than in more conventional hot-stage development performed at $24^{\circ}C$. Combining low temperature development with presoaking permits developer to diffuse rapidly to the base of the pellicles before a significant amount of development can occur near the upper surface, the highly favourable result being more uniform development.

As previously indicated, the development rate is extremely temperature dependent. In the E-531 development, six hundred and fourteen micron thick emulsion pellicles stuck to lucite supports were developed for twelve hours at 7°C. In a separate test development, six hundred micron thick pellicles stuck to glass supports were developed successfully using a combined cold soak and immersed hot-stage development. These plates were cold soaked in full-strength developer at 5°C for two and one-half hours and then transferred to warm half-strength developer at 24°C for about one hour. This amounts to approximately a tenfold increase in development rate when one considers the half-strength factor. This is an example of the extreme temperature dependence of the development rate. This cold soaking followed by immersed hot-stage is another example of the techniques available for improving uniformity of development in nuclear emulsion work. The relative merits of the two techniques which have been described will be discussed later. As will be discussed shortly, the development rate temperature dependence can be partially attributed to the temperature dependence of the development reaction redox potential.

The 2, 4-diaminophenol development reaction and its mechanism are not well understood. A reaction and mechanism are proposed and discussed in detail in Appendix B. The overall development reaction is proposed to be

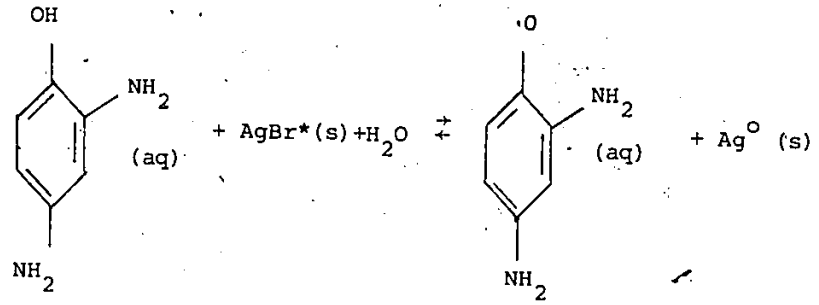

(2-4-diaminophenol) (aq) + Br^- (aq) + H_3O^+ (aq). (Bc-R5)

note: * Signifies an AgBr crystal possessing a latent image with the redox reaction being the following single electron transfer reaction

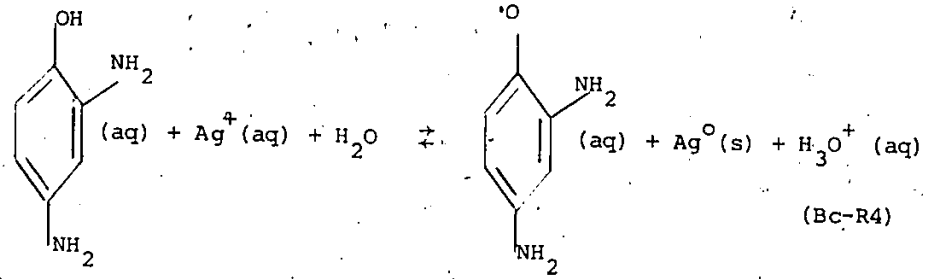

(Bc-R4)

in which silver cations are reduced to solid elemental silver and diaminophenol is oxidized. For convenience sake, the 2, 4-diaminophenol and the oxidized 2, 4-diaminophenol in reaction Bc-R4 will be abbreviated as DAP and DAPOx, respectively. The redox potential of this reaction, as given by the standard Nernst equation, is

$$\Delta\varepsilon = \Delta\varepsilon^{\circ} + 2.303 \frac{RT}{nF} \log \frac{[DAP]\,[Ag^+]}{[DAPOx]\,[H_3O^+]} \qquad \text{(Bc-1)}$$

where

$\Delta\varepsilon^{o}$ - standard potential in volts when reactants are in their standard states (unit activity @ 25°C)

T - absolute temperature in °K

R - ideal gas constant (1.98 cal-gmoles^{-1} - °K^{-1})

F - Faraday (the charge on a gmole of electrons = 96489 coul. = 23060 cal - volts^{-1})

As this equation indicates, the redox potential is a function of the reaction temperature, the activities of the reactants and products and the nature of the reacting species. The effect of the nature of the reacting species is manifested by the standard potential, $\Delta\varepsilon^{o}$.

Latent images are known to be due to aggregates of silver atoms on the surface of latent image carrying silver bromide crystals. As discussed in detail in Appendix A, it is suggested that latent images form developing sites since they behave as microcrystals of metallic silver. According to the free electron model of metallic crystals, valence electrons behave as free electrons confined to a box or potential well. Such metals are capable of accepting electrons since these electrons fall into the potential well and consequently lower their energy states. Latent images are thus able to capture electrons from the reducing agent, diaminophenol, which is consequently oxidized. As a result, the latent images become negatively charged. A negatively charged latent image will attract local free silver cations which become attached to the surface and consequently neutralized. This process will

cause the latent image to grow into a silver grain and the corresponding silver bromide crystal to disappear since it dissociates due to the local consumption of free silver cations.

The growth rate of a developing grain is related to the redox potential, $\Delta\varepsilon$, and the surface area of a developing grain. The rate of deposition of silver on the surface of the grain will be proportional to grain surface area, the local free silver cation activity and diaminophenol activity. Since the redox reaction is reversible, corrosion of the developing grain will simultaneously occur, the corrosion rate being proportional to the grain surface area, the hydromium ion activity and the oxidized diaminophenol activity. The net growth rate, R_G, will be equal to the difference between the deposition and corrosion rates. Thus,

$$R_G = A(t) \{ k_f [DAP] [Ag^+] - k_i [H_3O^+] [DAPOx] \} \quad (2.4)$$

where k_f is the deposition rate constant and k_i is the corrosion rate constant. These rate constants have units $gmoles^{-1}\text{-}cm^{-2}\text{-}s^{-1}$. A(t) is the grain surface area in cm^2. The surface area is a function of time while the grain is growing. At equilibrium, the net growth rate will be zero, the deposition and corrosion rates will be equal and the surface area constant. Thus, from equation 2.4,

$$\frac{k_f}{k_i} = \frac{[H_3O^+]_e \ [DAPOx]_e}{[Ag^+]_e \ [DAP]_e} \quad (2.5)$$

The subscript e denotes equilibrium. The equilibrium constant, K_R, of the redox reaction Bc-R4 is

$$K_R = \frac{[H_3O^+]_e \; [\text{DAPOx}]_e}{[Ag^+]_e \; [\text{DAP}]_e} \qquad (2\text{-}6)$$

Combining 2-5 and 2-6.

$$K_R = \frac{k_f}{k_i} \qquad (2\text{-}7)$$

One can rearrange the Nernst equation, Bc-1 , to yield

$$[\text{DAPOx}][H_3O^+] = [Ag^+][\text{DAP}] \exp\{ - \frac{(\Delta\varepsilon - \Delta\varepsilon^o)nF}{RT} \} \qquad (2\text{-}8)$$

Combining 2-4, 2-7 and 2-8, the growth rate expression becomes

$$R_G = k_f A(t) \; [\text{DAP}][Ag^+]\{ 1 - \frac{1}{K_R} \exp\{ - \frac{(\Delta\varepsilon - \Delta\varepsilon^o)nF}{RT} \}\} \qquad (2\text{-}9)$$

The relationship between the standard Gibbs free energy of reaction, ΔG_r^o, and the equilibrium constant, as given by equation A-10 in Appendix A, is

$$K_R = \exp\{ - \Delta G_r^o/RT\} \qquad (A\text{-}10)$$

The Gibbs free energy and the standard redox potential are related as follows:

$$\Delta G_r^{o\prime} = -nF\,\Delta\varepsilon^{o} \qquad (2\text{-}10)$$

Combining equations, 2-9, 2-10 and A-10, the growth rate expression becomes

$$R_G = k_f A(t)\ [DAP][Ag^+]\ \{1 - \exp\{-\frac{\Delta\varepsilon nF}{RT}\}\} \qquad (2\text{-}11a)$$

The temperature dependence of the rate constant is given by the standard Arrhenius equation. Thus,

$$k_f = A \exp\{-E_a/RT\} \qquad (2\text{-}11b)$$

where E_a is the activation energy and A is the pre-exponential factor.

As equation 2-11 indicates, the silver grain growth rate is an exponential function of both temperature and redox potential, the temperature dependence being dominated by the temperature dependence of the rate constant. The development rate is closely related to this growth rate. As the temperature decreases, the growth rate decreases exponentially. When the redox potential becomes zero the growth rate and consequently the development rate become zero. Since the redox potential is extremely sensitive to pH, the development rate is also extremely pH sensitive. As discussed in detail in appendix B, the diaminophenol activity is also pH sensitive, decreasing as the H_3O^+ activity increases, since an increasing portion of it is tied up as the doubly charged cation of diaminophenol. The molecular structure of this cation is shown in Fig. 2-2. Thus, lowering the pH reduces the development rate. The development can be stopped if the pH is lowered to the point where the redox potential is zero.

Equation 2-11a also indicates that the silver grain growth rate is dependent on the local activity of the free silver cation. This expression contains both an explicit and implicit dependence. Explicitly, the growth rate is dependent on the Ag^+ activity to first order. The implicit rate dependence results from the logarithmic dependence of the redox potential on the Ag^+ activity. As the silver cation activity decreases, the growth rate and consequently the development rate decrease .

In Appendix B, it is proposed that one of the steps in the development reaction mechanism is the local dissociation of latent image carrying silver bromide crystals in aqueous solution via the reaction

$$AgBr^*(s) \rightleftharpoons Ag^+(aq) + Br^-(aq) \qquad \text{(Bc-R1)}$$

The solubility product, K_{sp}, of crystals with no latent image is

$$K_{sp} = [Ag^+]_e [Br^-]_e \qquad (2\text{-}12)$$

$$= 5.2 \times 10^{-13} \text{ gmoles}^2\text{-L}^{-2} \text{ @ } 25^oC$$

If silver bromide is the only source of bromine anions, the equilibrium silver cation and bromine anion activities will be equal and equal to

7.2×10^{-7} gmoles-L^{-1}. The value of this solubility product at 7°C can be calculated from its value at 25°C and the enthalpy of dissociation, ΔH_D^o, using equation A-12, the thermodynamic relationship in Appendix A. The enthalpy of dissociation at 18°C is calculated to be 20100 cal-gmole^{-1} using the heat of formation data in Table VIIa. The dissociation is endothermic and will consequently be suppressed as the temperature is lowered. Thus, from equation A-12

$$K_{sp}' = K_{sp} \exp\left\{ - \frac{\Delta H_D^o}{R} \left(\frac{1}{T'} - \frac{1}{T} \right) \right\}^{11} \qquad (2\text{-}13)$$

$$= 5.9 \times 10^{-14} \text{ gmoles}^2 \text{ L}^{-2} \text{ @ } 7^oC$$

As a result, the free silver cation and bromine anion activities are reduced by a factor 3.13 to 2.3×10^{-7} gmoles-L^{-1}.

Similar arguments apply to latent image carrying crystals although the local free ionic activities will be larger since these crystals will have a greater tendency to dissociate than those not possessing a latent image. This can be understood by considering the mechanism of latent image formation. A latent image grows on the surface by trapping interstitial silver cations from the body of the crystal. This will increase the number of vacancies at ionic sites in the crystal. As a result, the average bond energy will be reduced which will increase the crystal's tendency to dissociate. Thus, the formation of a latent image weakens the internal structure of the

11 Ref. 5, pg. 301.

crystal. Nevertheless, reducing the temperature will also reduce the dissociation tendency of latent image carrying crystals, thereby reducing the local free silver cation activity which will reduce the development rate.

Since the silver grain growth rate and consequently the development rate are exponentially temperature sensitive, extreme care is required in designing a developing vessel to process on a large scale. Over or under development will occur if the temperature and developing times are not precisely controlled. The vessel and accompanying temperature control system must be designed to prevent the creation of both horizontal and vertical temperature gradients in the developing solution since non-uniform development from plate to plate will occur if such gradients exist.

The necessary models are now at hand to adequately discuss the relative merits of prolonged low temperature development versus the more conventional immersed hot-stage. Since the development rate is an exponential function of temperature, the rate of change of the development rate with respect to temperature is also exponential. Since the development rate decreases exponentially with temperature, the rate of change of the development rate also decreases exponentially with temperature. As a result, the variation of development rate caused by temperature fluctuations in the developing solution will be smaller for low temperature development, than for immersed hot-stage development.

Thus, developing time and temperature must be controlled more precisely with immersed hot-stage development in order to prevent over or under development. The maximum recommended temperature fluctuation is $\pm 0.1^{\circ}C$ with immersed hot-stage whereas, in the recent E-531 development, satisfactory results were obtained with temperature fluctuations as large as $\pm 0.5^{\circ}C$ using the prolonged low temperature development technique ($5-7^{\circ}C$). The plate-to-plate non-uniformity, caused by minor vertical and horizontal temperature gradients, is also less severe using cold development.

The major advantage of immersed hot-stage development is the reduction in developing time but this produces only a small reduction in overall processing time since the fixing and washing stages are very long compared to the developing stage. This is immediately evident if one examines Tables VIa and b in which the processing data of the recent E-531 development are tabulated. On the other hand, the emulsion is subjected to thermal shock when it is transferred from the cold soak. It swells rapidly as it warms up in the hot-stage. This rapid swelling and subsequent shrinking upon transfer to the cold stop bath may contribute significantly to distortion in the processed plates. It would also be much more expensive to design and build an adequate control system and vessel for immersed hot-stage development than for prolonged low temperature development since more precise temperature control is required for the former.

Adding a "restrainer", such as potassium bromide, to the developing solution is another useful technique used to slow the development rate and reduce fog. At this point, it is useful to recall that in emulsion physics one wishes to slow the development rate to improve the uniformity of development with respect to depth and minimize fog in order to be able to distinguish minimum tracks. Potassium bromide is an extremely soluble salt which totally dissociates in aqueous solution at concentrations $\sim \leq 4.5$ gmoles-L^{-1} at 7°C. The solubility product, as estimated from the data in Table VIIa, is 23.5 gmoles ^{2}-L^{-2} at 7°C. <<The presence of an alkaline bromide, such as potassium bromide, lowers the degree of ionization of silver bromide and, by reducing the concentration of silver cations, restrains the development. The addition of potassium bromide, however, is ordinarily for the purpose of preventing "fog" because the restraining effect is greater on fog than on the latent image.>>[12] The local silver cation concentration is reduced by the common ion effect and, as a result, the developing rate slows. Since the dissociation of halide crystals not possessing latent images is suppressed more than those having latent images, the fog developing rate is reduced more than the developing rate of tracks. With a restrainer present, one can increase the developing time in order to have the same degree of track development as occurs with no restrainer but the fog density is reduced,

12 Ref. 6, p. 35.

allowing minimum tracks to be distinguished more easily or, conversely, decreasing the minimum grain density or track length required for them to be distinguished.

As equations Bc-1 and 2-9 indicate, the developing rate is extremely sensitive to the pH of the developing solution, decreasing as the pH decreases. Amidol developer is highly acidic in aqueous solution. Reference to figure 2-1 indicates that each molecule of amidol contains two molecules of hydrated hydrogen chloride which form hydrochloric acid in aqueous solution. Table IV shows that a solution of deionized water and amidol of the same concentration as the developing solution has a pH of 2.8 ± 0.1. At this pH amidol will not develop since the redox potential is negative. A buffer is required to set and maintain the developer pH at approximately 6.6 ± 0.1, as indicated in Table I, so that development can occur. The buffer must be present in sufficient concentration to maintain a stable pH during the development since the redox reaction, reaction Bc-R4, produces hydronium ions. If sufficient buffer is not present, the developing solution acidity will increase as development proceeds consequently slowing and eventually stopping the reaction before the development is complete.

A conventional "buffer" is a solution of a weak acid and its sodium salt. In aqueous solution, the sodium salt completely dissociates whereas the weak acid remains almost entirely as

undissociated molecules. The hydronium ion activity is

$$[H_3O^+]_e \simeq K_a \frac{[\text{weak acid}]_e}{[\text{salt anion}]_e} \qquad (2\text{-}14)$$

where

$[\text{weak acid}]_e$ - activity of the undissociated weak acid

$[\text{salt anion}]_e$ - activity of the salt anion

K_a - acid dissociation constant

The pH is dependent upon the ratio of the undissociated acid to the salt anion activities. When the solution is diluted, the activities of the acid and salt anions change but the ratio remains constant. Consequently, the pH remains constant. The pH is also relatively insensitive to the addition of small amounts of strong acid since the hydrogen ions from the strong acid combine with anions from the salt to form undissociated weak acid molecules. If the amount of weak acid and salt is much greater than amount of hydrogen ion added, the percentage change in their activities is small. Thus, the ratio remains almost constant and the pH of the solution changes negligibly. The classic example of a buffer solution is a solution of acetic acid and its salt, sodium acetate.

In the developing solutions (Tables I and II) used for the E-531 development, the formation of the buffer is somewhat more complex. The buffer is formed by the combined action of the salts sodium sulfite,

Na_2SO_3, and sodium metabuisulfite, $Na_2S_2O_5$. Due to its complexity, this is discussed in detail in Appendix B. Briefly, sodium meta-bisulfite and the acid salt sodium bisulfite, $NaHSO_3$, are functionally equivalent in aqueous solution due to the equilibrium

$$S_2O_5^{2-}\ (aq) + H_2O \rightleftarrows 2HSO_3^-\ (aq) \qquad \text{(Ba-R2)}$$

Either salt can be used since the equilibrium state of Ba-R2 is independent of the direction of approach. Thus, either one will provide a source of bisulfite anions, HSO_3^-. HSO_3^- is a weak acid whose corresponding sodium salt is sodium sulfite. This weak acid and its salt form the buffer in the developing solution. The molecular weights of sodium metabisulfite and sodium bisulfite are, respectively, 190 and 104 but since each mole of $S_2O_5^{2-}$ which reacts with water will produce two moles of bisulfite ion, HSO_3^-, addition of 0.91 grams of sodium metabisulfite to aqueous solution is equivalent to the addition of 1.0 gram of sodium bisulfite.

Sodium sulfite has one additional function. It removes dissolved oxygen from the water. Diaminophenol which acts as a powerful reducing agent in the development redox reaction is very easily oxidized. The supply can be completely or partially depleted due to oxidation by oxygen dissolved in the water used to make the developing solution. Fortunately, the anion $SO_3^=$ is easily oxidized in basic solution. It reacts with and removes the dissolved oxygen via the reaction.

$$2SO_3^{=}\ (aq) + O_2\ (aq) \rightleftarrows 2SO_4^{=}\ (aq) \qquad (2\text{-}R3)$$

The sulfur atom in the sulfite anion has oxidation number +4. It is oxidized to a higher oxidation state in the sulfate anion in which it has an oxidation number +6. Sodium sulfite is the first component added when preparing a developing solution. As Table IV indicates and as discussed in detail in Appendix B, the solution of deionized water and sodium sulfite is basic, having a pH of 9.8 ± 0.1 due to the hydrolysis of the sulfite anion. This provides the necessary alkalinity for removal of dissolved oxygen and is the reason why sodium sulfite must be the first compound dissolved when preparing the developer.

2.4 Stage 3 - Stop Bath

As mentioned previously, the development rate is extremely pH sensitive. The development can be stopped and even reversed by lowering the pH. Reversal of the development reaction, resulting from the net redox reaction, Bc - R4, being in the reverse direction, would result in corrosion of developed grains of silver. This is highly undesirable since one wishes to maximize the grain density of minimum tracks in order to distinguish them from background "fog". Lowering the pH by adding a large amount of strong acid directly to the developer would stop the development but at the same time cause corrosion.

The problem of stopping the reaction and simultaneously minimizing any possible corrosion is solved by transfering the plates directly into a weak (0.5%) acetic acid solution. Only a small amount of developing agent and buffer, that absorbed in the pellicles and the thin film adhered to the support plate and pellicle surfaces, is transferred. The acetic acid, being a weak acid, does not lower the pH to a point where corrosion becomes serious and its action is not inhibited by a large amount of buffer. Upon transfer, the acetic acid immediately begins to diffuse into the emulsion whereas the developer and buffer diffuse out. Consequently, the developer and buffer are diluted, the overall dilution factor being of the order of two orders of magnitude. Once again, it is important that the acetic acid diffuse rapidly to the base of the emulsion since development at the base does not stop until the acid has completely penetrated the pellicles.

Since the stopper must completely penetrate the pellicles, the length of time in the stop bath depends upon the thickness of the pellicles. For the E-531 development, the 614μ thick horizontal plates were left in the stopper for 2 hours at 7°C whereas the 330μ thick vertical plates were left in stopper for only fifty minutes at 5°C.

In photography in general, a weak rather than a strong acid is used as a stopper since it is desirable just to stop the reaction. Transfering to a bath of strong acid of low pH would not only stop the reaction but also cause serious corrosion problems due to the resulting large negative redox potential, equation Bc-1. This would seriously reduce the quality of developed negatives, since it would reduce the contrast between exposed and unexposed areas.

Stage 4 - Fixing

During fixing, the undeveloped silver bromide crystals are removed from the emulsion. The plates are immersed in a strong solution - 1.9 molar for vertical and 2.5 molar for horizontal - of sodium thiosulfate, $Na_2S_2O_3$. The fixing solution also contains sodium metabisulfite to a concentration of 1.44×10^{-1} molar. The metabisulfite acts as a buffer, setting and maintaining the pH at 4.5 and at the same time inhibiting the decomposition of thiosulfate anion. Potassium aluminum sulfate is added to a concentration of 1.9×10^{-2} molar to the solution for vertical plates. It acts as a hardener and thus reduces the swelling. In the E-531 development, the vertical plates were fixed at $5^{\circ}C$ whereas the horizontal plates were fixed at $7^{\circ}C$.

Minor temperature fluctuations are less serious during fixing than during developing. For low temperature fixing, a control of $\pm 1.0^{\circ}C$ is satisfactory. Low temperature fixing is very slow but helps to minimize swelling, thereby reducing the problem of distortion. It also reduces the risk of bubble formation and subsequent growth since the emulsion stays relatively hard.

For both the horizontal and vertical emulsion plates, the fixing is divided into the five substages shown in Diagrams 1 and 2. In the horizontal case, the plates are transferred from the stop bath to substage 1, a bath of 1/4-strength fixer, where they remain for 2 hours whereas in the vertical case they are transferred to a bath of 1/3-strength fixer where they remain for fifty minutes. Substage 2 is a bath of 1/2-strength fixer in the horizontal case and 2/3-strength fixer in the vertical case, the respective processing times being identical to those of substage 1. Substages 1 and 2 reduce the risk of corrosion of developed grains of silver. During substage 3, the plates are immersed in full-strength fixer for approximately four days in the horizontal case and approximately twenty hours in the vertical case. The plates clear during this substage, indicating that all but the final traces of silver bromide have been dissolved. Substages 4 and 5 are respectively identical to substages 2 and 1, the 1/2- and 1/4-strength substages. They are the dilution substages.

The role of each compound in the fixing solution will now be discussed individually and in detail.

i) The Role of Sodium Thiosulfate

The silver bromide crystals are dissolved by sodium thiosulfate. They react chemically with the thiosulfate anions to form silver-thiosulfate complex ions. The overall fixing reaction is

$$AgBr\ (s) + 2S_2O_3^{=}\ (aq) \rightleftarrows Ag(S_2O_3)_2^{3-}\ (aq) + Br^-\ (aq) \quad (2\text{-}R4)$$

The developed grains of elemental silver are not attacked by the fixer. Consequently, they are left intact and in place in the gelatin network. The gelatin is also inert to the chemical action of the fixer. After all but the final traces of the silver bromide have been dissolved, the emulsion becomes transparent, the time required being called the "clearing time".

The plates are not removed from full-strength fixer immediately after clearing. Cleared plates are commonly left in full-strength fixer for a length of time equal to a least two-thirds of the clearing time. This provides time for the final traces of silver bromide to be dissolved and the concentration of silver-thiosulfate complex ion to minimize in the gelatin network via diffusion out of the emulsion.

Fig. 2.3 - Schematic Illustration of Physical and Chemical Processes Occurring During Fixing

Step 1 - Diffusion of Reagent $S_2O_3^=$ into the Emulsion

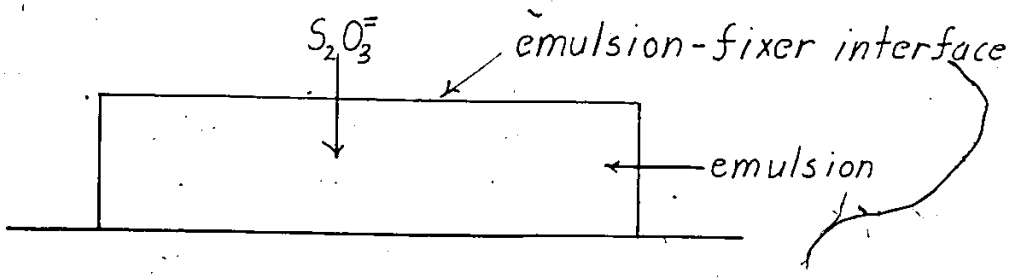

Step 2 - Reaction of $S_2O_3^=$ with AgBr Crystals

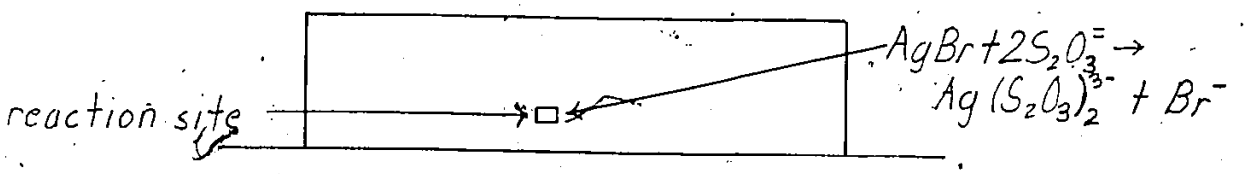

Step 3 - Diffusion of $Ag(S_2O_3)_2^{3-}$ and Br^- to the Emulsion-Fixer Interface

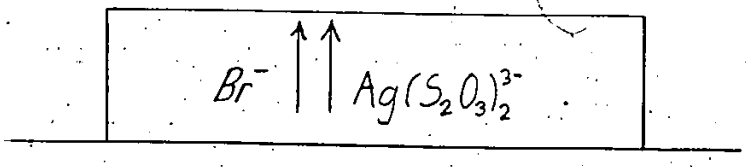

Fig. 2.3 - Continued

Step 4 - Diffusion of $Ag(S_2O_3)_2^{3-}$ and Br^- Across the Interface

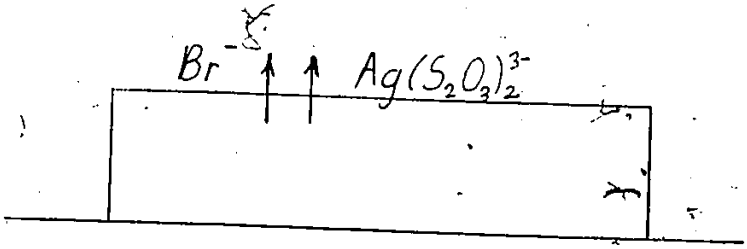

Step 5 - Transport of $Ag(S_2O_3)_2^{3-}$ and Br^- Away from the Interface

a) No Circulation

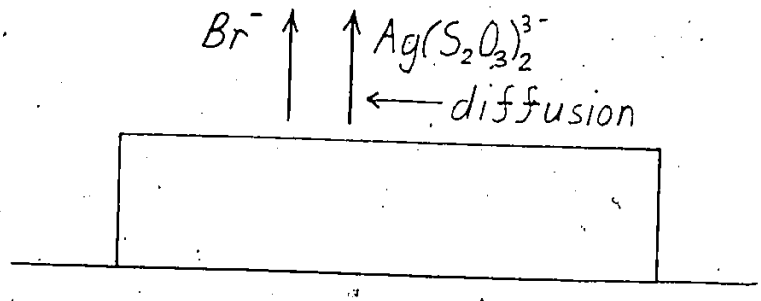

b) Circulation

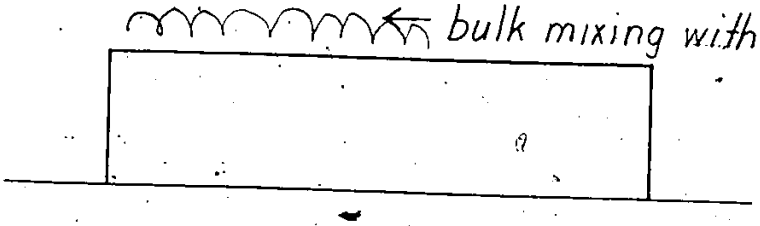

A further reduction occurs during the two dilution substages. In the next stage, the washing stage, the problem of reformation of silver bromide via the reverse reaction of 2-R4 is considerably reduced because the $Ag(S_2O_3)_2^{3-}$ and Br^- concentrations are at their minima when the plates are transferred.

The fixing process is a combination of the physical and chemical processes depicted schematically in Fig. 2-3. Initially, thiosulfate anions, $S_2O_3^=$, must diffuse into the emulsion support network to reaction sites. These anions then react chemically with silver bromide crystals producing silver-thiosulfate complex ions, $Ag(S_2O_3)_2^{3-}$ and bromine anions, Br^-, according to reaction 2-R4. The silver complexes and the bromine anions must then diffuse out through the network to emulsion-fixer interface. They must then diffuse across the interface. If no agitation or circulation is included in the fixing bath, they must then diffuse away from the interface and into the bulk of the fixer.

The reaction mechanism of the fixing reaction is not well understood. A logical approach, though, is to consider it to be a two step reaction consisting of dissociation of silver bromide crystals followed by an elementary termolecular process of two thiosulfate anions complexing with a silver cation. Thus, 2-R4 can be broken into the following two steps

$$AgBr\ (s) \underset{\text{reverse}}{\overset{\text{forward}}{\rightleftarrows}} Ag^+\ (aq) + Br^-\ (aq) \qquad \text{(Bc-R1)}$$

step 1 - dissociation

and

$$Ag^{+}\ (aq) + 2S_2O_3^{=}\ (aq) \underset{\text{reverse}}{\overset{\text{forward}}{\rightleftarrows}} Ag(S_2O_3)_2^{3-}\ (aq) \qquad (2\text{-R5})$$

step 2 - complexing.

It is possible to further subdivide the complexing reaction, 2-R5, into two bimolecular elementary reactions of the nature

$$Ag^{+}\ (aq) + S_2O_3^{=}\ (aq) \rightleftarrows AgS_2O_3^{-}\ (aq) \qquad (2\text{-R6})$$

followed by

$$AgS_2O_3^{-}\ (aq) + S_2O_3^{=}\ (aq) \rightleftarrows Ag(S_2O_3)_2^{3-}\ (aq) \qquad (2\text{-R7})$$

but, as will be shown, the fixing rate in nuclear emulsion physics is a diffusion controlled process due to the large thickness of the emulsion pellicles. Since the arguments which will follow concerning the fixing rate are identical in both cases, the simplified two step mechanism is chosen as the model.

Firstly, consider the silver bromide dissociation. At equilibrium, the rate of dissociation of the crystals is equal to the rate of association of bromine and silver ions. Recall that

$$K_{sp} = [Ag^{+}]_e [Br^{-}]_e \qquad (2\text{-}12)$$

$$= 5.2 \times 10^{-13}\ \text{gmoles}^{2}\text{-L}^{-2}\ @\ 25^{\circ}C$$

$$= 5.9 \times 10^{-14}\ \text{gmoles}^{2}\text{-L}^{-2}\ @\ 7^{\circ}C$$

The net dissociation rate, R_{DS}, in gmoles-cm^{-3}-s^{-1}, is

$$R_{DS} = \text{Dissociation Rate} - \text{Association Rate}$$
$$= k_D [AgBr\ (s)] - k_A [Ag^+][Br^-] \qquad (2\text{-}15)$$

where k_D is the rate constant for dissociation and k_A is the rate constant for association. The concentration of silver bromide crystals is constant since it is in the solid phase. The rate constants are functions of temperature. Also,

$$\frac{k_D}{k_A} = \frac{K_{SP}}{[AgBr\ (s)]} \qquad (2\text{-}16)$$
$$= 1.5 \times 10^{-14} \text{ gmoles-L}^{-1} @ 25^\circ C$$
$$= 1.7 \times 10^{-15} \text{ gmoles-L}^{-1} @ 7^\circ C$$

since the density of silver bromide is 6.47 g/cc. This indicates that the rate of association is inherently much more rapid than the rate of dissociation since the rate constant for association is much larger than for dissociation. Thus, at equilibrium almost all of the silver and bromine exists as undissociated solid phase crystals because it is extremely insoluble in water.

Consider now the kinetics of the complexing reaction, 2-R5, in detail. The equilibrium constant is

$$K_e = \frac{[Ag(S_2O_3)_2^{3-}]_e}{[Ag^+]_e[S_2O_3^{=}]_e^2} \qquad (2\text{-}17)$$

$$= 2.4 \times 10^{14} \text{ gmoles}^{-2}\text{-L}^2 \text{ @ } 25^\circ\text{C}$$

$$= 2.1 \times 10^{15} \text{ gmoles}^{-2}\text{-L}^2 \text{ @ } 7^\circ\text{C}$$

The equilibrium constant at 7°C was calculated from its value at 25°C and the enthalpy of reaction, using equation A-12 in Appendix A. The enthalpy of reaction is -19800 cal/gmole. It was calculated from the data in Table VIIa. This large equilibrium constant indicates that the silver-thiosulfate complex ion is an extremely stable chemical species in aqueous solution. It renders the silver bromide extremely soluble since the silver ions are immediately tied up as complexes by the thiosulfate anions. Only an extremely small proportion of ionic silver will exist as aqueous silver cations at equilibrium. The net complexing rate, R_c, in gmoles-cm^{-3}-s^{-1}, is

$$R_c = \text{foward rate} - \text{reverse rate}$$

$$= k_c [Ag^+][S_2O_3^{=}]^2 - k_{-c} [Ag(S_2O_3)_2^{3-}] \qquad (2\text{-}18)$$

where

k_c is the complexing rate constant

k_{-c} is the decomplexing rate constant

and

$$K_e = \frac{k_c}{k_{-c}} = 2.4 \times 10^{14} \text{ gmoles}^{-2}\text{-L}^2 \text{ @ } 25^\circ\text{C} \qquad (2\text{-}19)$$

This indicates that the complexing reaction rate is inherently much more rapid than the decomplexing rate because it has a much larger rate constant.

If one compares the dissociation reaction with the complexing reaction, it is immediately obvious that the complexing of silver cations by thiosulfate anions is inherently much more rapid than the dissociation of silver bromide since the former is inherently very rapid whereas the latter is inherently very slow. In a well agitated reaction vessel containing thiosulfate anions and "free" silver bromide crystals, the reaction products will be rapidly removed from the reaction sites. Therefore, the reverse reaction rates will be extremely small. Consequently, the dissociation of silver bromide will be the rate determining step of the fixing reaction. The fixing rate will thus be equal to the net rate of dissociation of the silver bromide.

In nuclear emulsion, the situation is quite different due to the fact that the silver bromide crystals are embedded in the gelatin support network and because of the large thicknesses involved. The reaction products, silver-thiosulfate complex ions and bromine anions, must diffuse out through the gelatin in order to get away from the reaction sites. The diffusion of the $Ag(S_2O_3)_2^{3-}$ complex is undoubtedly extremely slow because of its large size. Since this diffusion is very slow, a rapid build up of $Ag(S_2O_3)_2^{3-}$ will occur at reaction sites in the

gelatin. $Ag(S_2O_3)_2^{3-}$ will consequently have a large steady-state concentration. The net complexing rate will slow tremendously, due to the increase in the rate of the reverse complexing (decomplexing) reaction. The net complexing rate will be controlled by the steady-state concentrations which are controlled by the rates of diffusion. The average net dissociation rate of silver bromide will never exceed the net complexing rate since, on its own, it is extremely insoluble. The diffusion coefficient of bromine anions will be larger than that of silver-thiosulfate complex ions since the complex is much larger. Consequently, the build up of bromine anion at reaction sites will be less severe. As a result, its steady-state concentration will be lower than that of the silver-thiosulfate complex ions. Thus, the average net dissociation rate of silver bromide, which is equal to the fixing rate, will be equal to and controlled by the net complexing rate, equation 2-18, which is diffusion controlled. Consequently, at steady-state, the differential fixing rate , R_F, in gmoles-cm^{-3}-s^{-1}, is

$$R_F = R_C = k_C [Ag^+]_s [S_2O_3^=]_s^2 - k_{-C} [Ag(S_2O_3)_2^{3-}]_s$$

$$= k_D [AgBr\ (s)] - k_A [Ag^+]_s [Br^-]_s \qquad (2\text{-}20)$$

where the subscript s signifies steady-state values, steady-state signifying time independence.

The process of liquid phase diffusion of silver-thiosulfate

Fig 2.4 - Coordinate System for Horizontal Emulsion Plate in Fixer

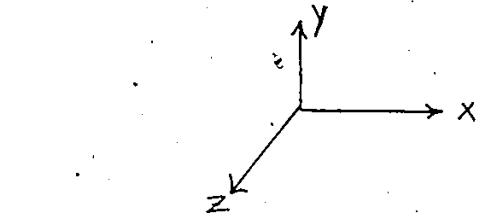

i) xy projection

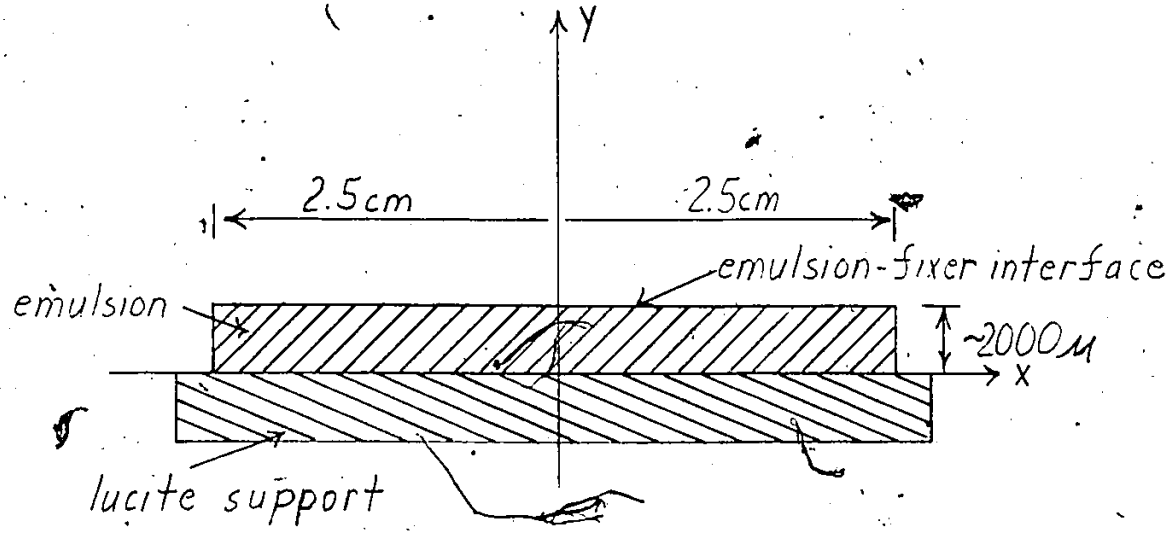

ii) yz projection

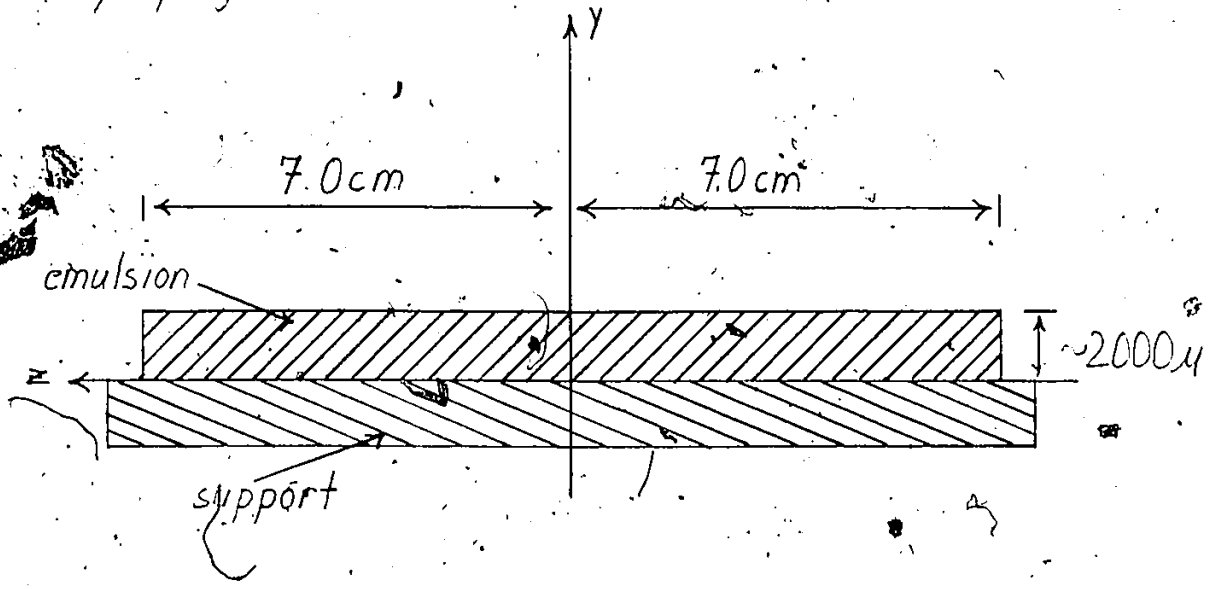

complex ion , thiosulfate anion and bromine anion will now be considered in detail. Consider a horizontal emulsion pellicle placed in a cartesian co-ordinate system as shown in Fig. 2-4. To a good first approximation, the diffusion of reactants into and products out of the emulsion can be considered to be unidirectional in the y-direction since the thickness at this stage is of the order of 2000 microns compared to a width of 5 cm and a length of 14 cm for a horizontal pellicle. Under unsteady-state conditions, concentrations, net reaction rates, fluxes and diffusivities are both time and position dependent. The unsteady-state differential equations governing the physical and chemical processes which occur are developed and discussed in detail in Appendix C. Only their steady-state analogues will be discussed here, steady-state signifying time independence of concentrations and, consequently, fluxes, net reaction rates and diffusivities.

In the following discussion, silver-thiosulfate complexes ions, bromine anions and thiosulfate anions will be labelled components A, B and C, respectively.

In Appendix C, a unidirectional material balance is performed on a strip of emulsion of infinitessimal thickness dy and surface area A', equal to the surface area of the pellicle. The steady-state fluxes of components A, B and C are

$$N_A(y) = -D_A(y) \frac{dC_A(y)}{dy} \qquad (2\text{-}21a)$$

$$N_B(y) = -D_B(y) \frac{dC_B(y)}{dy} \qquad (2\text{-}21b)$$

$$N_C(y) = -D_C(y) \frac{dC_C(y)}{dy} \qquad (2\text{-}21c)$$

where D is the diffusivity in $cm^2 - s^{-1}$ and C is the concentration in gmoles-cm^{-3}. In liquid phase diffusional processes, the diffusivity is in general a function of the diffusing species, the concentration of the species and the temperature. At low concentrations, the diffusivities are often independent of concentration. The net steady-state reaction rates, as derived from the law of diffusion and a material balance, are

$$R_A(y) = \frac{dN_A(y)}{dy} \qquad (2\text{-}22a)$$

$$R_B(y) = \frac{dN_B(y)}{dy} \qquad (2\text{-}22b)$$

$$R_C(y) = \frac{dN_C(y)}{dy} \qquad (2\text{-}22c)$$

where $R_A(y)$ and $R_B(y)$ are, respectively, the net differential rates of production of silver-thiosulfate complex ion and bromine anion and $R_C(y)$ is the rate of consumption of thiosulfate anion, the units being gmoles-cm^3-s^{-1}. From the stoichiometry of the fixing reactions, the differential fixing rate is related to the rates of production of A and B and consumption of C as follows

$$R_F(y) = R_A(y) = R_B(y) = \frac{1}{2} R_C(y) \qquad (2\text{-}23)$$

The factor one-half arises from the fact that two moles of thiosulfate anion are consumed for each moles of silver bromide dissolved, the fixing rate being equal to the rate of dissolution of silver bromide.

An expression for the total fixing rate can be found by summing the differential fixing rate over the thickness of the pellicle. Thus, from equations 2-22 and 2-23

$$R_{FT} = A' \int_{y=0}^{y=h} R_F(y)\, dy = A' \int_{y=0}^{y=h} \frac{dN_A(y)}{dy}\, dy$$

$$= A' \{N_A(h) - N_A(0)\} \qquad (2\text{-}24)$$

where R_{FT} is the total fixing rate in gmoles-s^{-1}. Steady-state conditions demand that the concentration of silver-thiosulfate complex ion be time independent. Thus, its total net production rate, R_{FT}, cannot be less than its rate of discharge, $A'N_A(h)$, from the emulsion pellicle. If the net production rate were less than its rate of discharge, there would be a net depletion of these complex ions in the emulsion and, as a consequence, its concentration would decrease with time and thus not be time independent. As a result, one is forced to conclude that, at steady-state, the flux, $N_A(0)$, at the base of the pellicle is zero and equation 2-24 simplifies to

$$R_{FT} = A' \; N_A(h) \tag{2-25a}$$

$$= A' \; D_A(h) \left(\frac{dC_A(y)}{dy}\right)_{y=h} \tag{2-25b}$$

Analogously,

$$R_{FT} = A' \; N_B(h) \tag{2-26a}$$

$$= A' \; D_B(h) \left(\frac{dC_B(y)}{dy}\right)_{y=h} \tag{2-26b}$$

$$R_{FT} = \frac{A'}{2} \; N_C(h) \tag{2-27a}$$

$$= \frac{A'}{2} \; D_C(h) \left(\frac{dC_C(y)}{dy}\right)_{y=h} \tag{2-27b}$$

Also,

$$N_A(0) = N_B(0) = N_C(0) = 0 \tag{2-28}$$

and thus from equation 2-21

$$\left(\frac{dC_A(y)}{dy}\right)_{y=0} = \left(\frac{dC_B(y)}{dy}\right)_{y=0} = \left(\frac{dC_C(y)}{dy}\right)_{y=0} = 0 \tag{2-29}$$

Equations 2-25a, 2-26a and 2-27a indicate that the rates of discharge of complex ion and bromine anion from the emulsion are equal and equal to the fixing rate and that the rate of entry of thiosulfate anion is double the fixing rate. Equations 2-25b, 2-26b and 2-27b indicate that the fixing rate is proportional to the slopes of the

Fig. 2.5 - Steady-State Concentration Profile of Silver-Thiosulfate Complex Ion

Note: Profile only valid prior to commencement of clearing

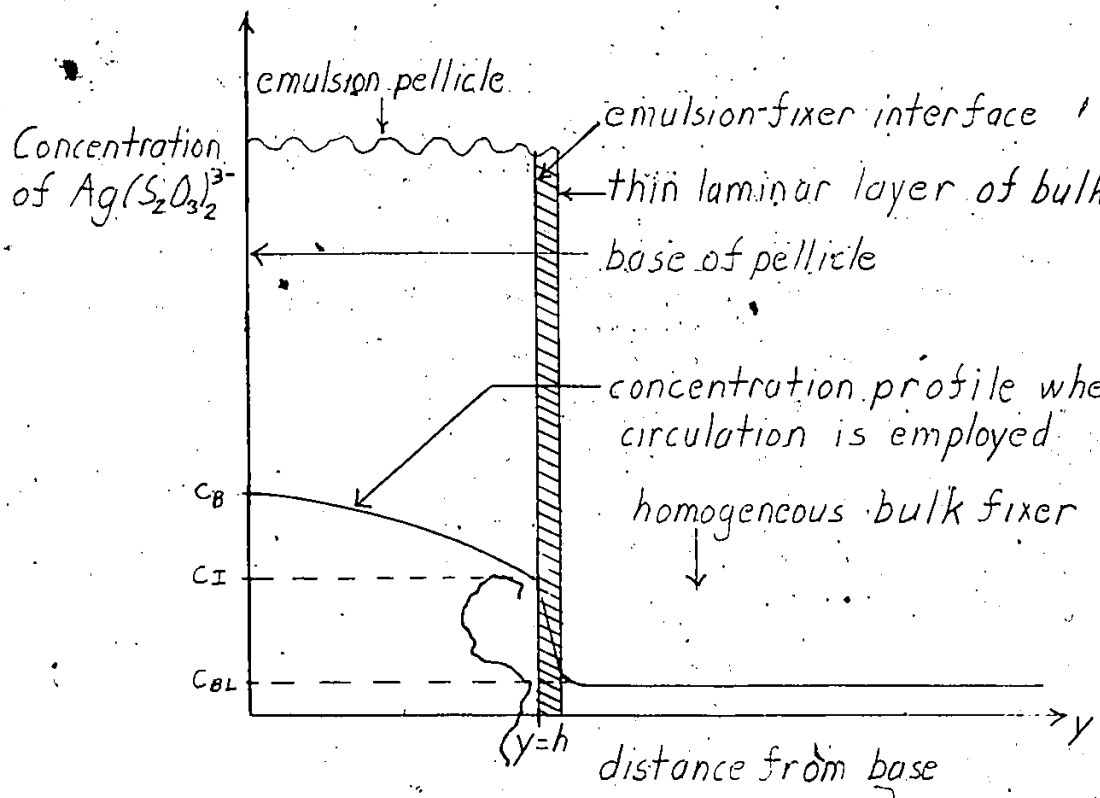

Fig. 2.6 - Pellicle Cleared to Depth d

Note: Clearing begins approximately 40 hrs after the start of fixing when circulation is present. Clearing occurs rapidly (in ~2 to 3 hrs) in infinitesimal.

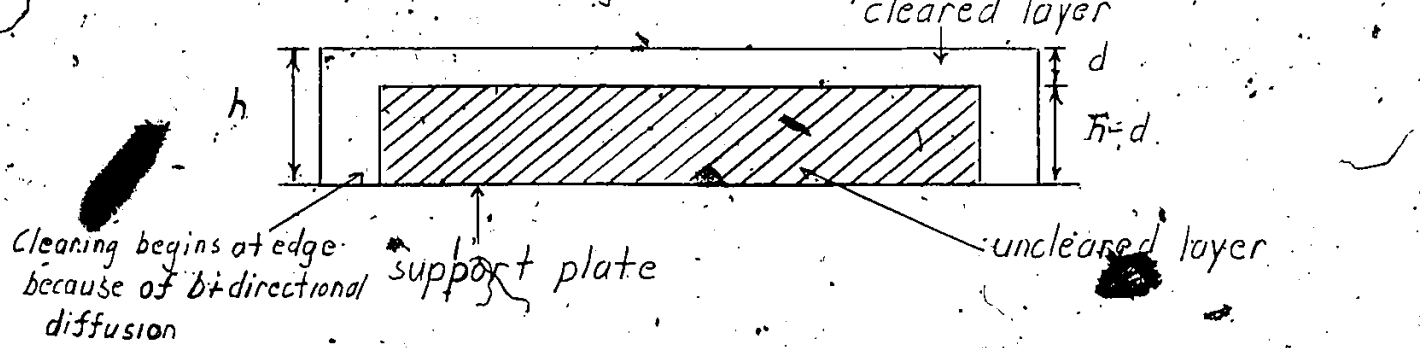

concentration profiles of A, B, and C at the emulsion-fixer interface. Equation 2-29 indicates that the slopes of the concentration profiles are zero at the bases of the pellicles. A sketch of a reaction product concentration profile is shown in Fig. 2-5. Furthermore, since the fixing rate is equal to rate of diffusion of reactants out of the emulsion, the fixing process is diffusion controlled.

As equation 2-28 indicates, the fluxes of A, B and C are zero at the bases of the pellicles. Thus, the corresponding flux gradients, dN/dy, are also zero, indicating that the net differential reaction rates, as given by equations 2-22a, b and c are zero. Since at the base there is no net conversion of reactants to products, the reacting species are in chemical equilibrium. As a result, the absolute concentrations at the base are determined by the equilibrium expressions, equations 2-12 and 2-17. The equilibrium expressions consequently provide one set of boundary conditions for the steady-state differential equations governing the physical and chemical processes. The differential fixing rate given by equation 2-20 varies from zero at the base to a maximum value at the emulsion-fixer interface. Consequently, the departure from chemical equilibrium varies from zero at the base to a maximum at the interface since the differential fixing rate is a measure of the departure from equilibrium of the reacting species.

The preceding discussion neglected the fact that significant two and three-directional diffusion occurs at the edges and corners,

respectively, of the pellicles. The equations which have been derived are thus approximations. If fixing is in fact diffusion controlled, the rate will be faster at the corners and edges of a pellicle than at its centre. Therefore, they should clear at the corners and edges first. It is well known in nuclear emulsion processing that pellicles do in fact clear at the corners and edges before they clear at the center. This provides considerable support for the hypothesis of fixing rate being controlled by diffusion rather than the inherent chemical kinetics of the reacting species.

Consider a fixing vessel in which there is no circulation or agitation. Recall that the steady-state fixing rate is equal to the diffusion rates of bromine anion and thiosulfate complex ion and one-half the diffusion rate of thiosulfate anion across the emulsion-fixer interface. The fixing rate is controlled by these interface diffusion rates. These interface diffusion rates are themselves controlled by their corresponding rates of diffusion through the bulk of the fixer near the interface. If circulation is included in the fixing stage, there will be a thin laminar layer of fixer outside the interface (see Fig. 2-5). Beyond this layer forced diffusion will occur due to the bulk mixing provided by the circulation. The rates of diffusion will increase since upon leaving or approaching the emulsion, the ionic species must now only diffusion through this thin layer. As a result, the fixing rate should increase when circulation is added if it is indeed diffusion controlled.

Circulation was incorporated into the fixing stage of the large scale processing system described in detail in Chapter 3. More conventional small scale systems usually do not use circulation or agitation. A considerable decrease in clearing time was obtained with the circulation system. As Table VIb indicates, the 614 micron thick horizontal pellicles cleared in approximately 42 hours at 7°C whereas at this temperature 600 micron thick pellicles usually require about 3 days to clear when there is no circulation. This reduction in clearing time can only be due to an increase in the fixing rate. This provides further support for the hypothesis of the fixing rate being diffusion controlled.

As previously discussed, the differential fixing rate varies from zero at the base of the pellicles to a maximum value at the emulsion-fixer interface. Consequently, the infinitessimal layer at the interface will be the first to clear, disregarding for the moment, edge effects, since the dissolution rate of silver bromide is the most rapid in this layer. No clearing occurs at the edges until 2 or 3 hours before the pellicle completely clears. Therefore, during the initial forty hours of fixing, no clearing occurs anywhere in the pellicle. Consequently, once clearing begins a pellicle will clear rapidly in successive layers from the interface to the base. Once the base has cleared, the emulsion is completely cleared and becomes transparent. The concentration profile, Fig. 2-5, and the fixing rate expression, equation 2-25, are valid only while there is still silver bromide throughout the entire depth of the pellicle. When the silver bromide has been consumed to a depth d - see Fig. 2-6, the instananeous unsteady-stage fixing rate is, from equation C-11

$$R_F(t) = A' \int_0^{h-d} \left\{ \frac{\partial C_A(y,t)}{\partial t} \right\} dy + A' \{ N(h-d,t) - N(0,t) \} \qquad (2\text{-}30)$$

When $d = h$ all but the final traces of silver bromide have been dissolved and the pellicle becomes transparent. In the cleared portion, negligible net reactions are occurring and the differential fixing rate is approximately zero. The flux gradients, equations 22-2a, b and c, are also approximately zero which means that all fluxes are, to a good approximation, constant. Thus,

$$N_A = -D_A(y) \left(\frac{dC_A(y)}{dy} \right) = \text{constant}, \quad h-d \leq y \leq h \qquad (2\text{-}31)$$

The expressions for the fluxes of B and C are similar. The concentration gradients would only be constant for the simplified case of the diffusivity being concentration independent.

ii) The Role of Sodium Bisulfite or Metabisulfite

In the fixing solution, sodium metabisulfite has several functions. It inhibits the decomposition of thiosulfate anion in acidic solution, forms a buffer with sodium thiosulfate and minimizes the emulsion swelling by setting and maintaining the pH at 4.5 ± 0.1 during

the five fixing substages. As in the developing solution, the bisulfite anion is the critical ionic species.

In aqueous acid solution, thiosulfate anion can undergo decomposition to elemental sulfur and bisulfite anion via the reaction

$$S_2O_3^{=}\ (aq) + H_3O^+\ (aq) \rightleftarrows HSO_3^-\ (aq) + S\ (s) + H_2O \qquad (2\text{-R8})$$

The equilibrium constant can be calculated from the thermodynamic data in Tables VII and VIII. Using equation A-7, the standard Gibbs free energy of this reaction is

$$\Delta G_r^o = \Delta G_f^o\ (\text{products}) - \Delta G_f^o\ (\text{reactants}) \qquad (A\text{-}7)$$

$$= \Delta G_f^o\ (HSO_3^-) - \Delta G_f^o\ (S_2O_3^{=})$$

$$= 1180\ \text{cal-gmoles}^{-1} \quad @\ 25^oC$$

Using equation A-10, the equilibrium constant is

$$K_{eq} = \exp\left\{ - \frac{\Delta G_r^o}{RT} \right\} \qquad (A\text{-}10)$$

$$= 0.135\ \text{gmoles}^{-1}\text{-L}\ @\ 25^oC$$

The standard enthalpy of reaction, calculated using equation A-11a, is

$$\Delta H_r^o = \Delta H_f^o \text{ (products)} - \Delta H_f^o \text{ (reactants)}$$

$$= \Delta H_f^o (HSO_3^-) - \Delta H_f^o (S_2O_3^{=})$$

$$= -6524 \text{ cal-gmoles}^{-1} \quad @ \ 18^oC$$

This indicates that the decomposition reaction is exothermic. Therefore, its equilibrium constant will increase as the temperature decreases. The equilibrium constant at 7°C, calculated from its value at 25°C using equation A-12, is

$$K_{eq}' = K_{eq} \exp \{ - \frac{\Delta H_r^o}{R} (\frac{1}{T'} - \frac{1}{T}) \} \qquad \text{(A-12)}$$

$$= 0.273 \text{ gmoles}^{-1}\text{-L} \quad @ \ 7^oC$$

Thus, lowering the temperature from 25°C to 7°C increases the equilibrium constant of the thiosulfate anion decomposition reaction by a factor of 2.02.

The thiosulfate anion decomposition reaction has an equilibrium expression of the nature

$$K_{eq} = \frac{[HSO_3^-]_e}{[S_2O_3^{=}]_e [H_3O^+]_e} \qquad \text{(2-32a)}$$

$$= 0.135 \text{ gmoles}^{-1}\text{-L} \quad @ \ 25^oC$$

$$= 0.273 \text{ gmoles}^{-1}\text{-L} \quad @ \ 7^oC$$

An expression for the hydronium ion activity can be found by rearranging equation 2-32a to give

$$[H_3O^+]_e = \frac{1}{K_{eq}} \quad \frac{[HSO_3^-]_e}{[S_2O_3^=]_e} \qquad (2\text{-}32b)$$

Thus, the presence of the bisulfite anion simultaneously inhibits the decomposition of thiosulfate anion and sets the fixer pH at the optimum value of 4.5 ± 0.1. As Table V indicates, the two salts form a buffer solution since the fixer pH remains constant when it is diluted to one-half and one-quarter strength . The pH is also constant over the 25°C to 7°C temperature range. Since less than one percent of the thiosulfate anion is consumed during fixing, the pH will remain essentially constant throughout this stage.

Sodium metabisulfite minimizes swelling by setting the fixer pH at its optimum value of 4.5. <<Minimum swelling is obtained at a pH of 4.5 for gelatin manufactured by a lime hydrolysis process and 8.5 for gelatin from an acid hydrolysis. >>[13] One can thus conclude that the Fuji emulsion of experiment E-531 was manufactured using a lime hydrolysis process. As explained in Chapter 1, minimizing swelling during processing reduces distortion in the tracks of processed emulsion. Either sodium metabisulfite or sodium bisulfite has the advantage of lowering the pH to its optimum value while simultaneously inhibiting

[13] Ref. 2, pg. 32.

the decomposition of the thiosulfate anion.

An expression for the bisulfite anion activity can be found by re-arranging equation 2-32a. Thus,

$$[HSO_3^-]_e = K_{eq} [S_2O_3^{=}]_e [H_3O^+]_e \qquad (2\text{-}33)$$

The concentration of thiosulfate anion is 2.5 gmoles-L^{-1} and the hydronium ion activity can be calculated from the measured ph. Unfortunately, fixer is a solution of extremely high ionic strength. It was calculated to be 7.5 molar using equation A-13 in Appendix A. The activity of the thiosulfate anion can not be calculated analytically from the known concentration by calculating the activity coefficient from the extended Debye-Hückel equation, equation A-14, since this equation is of questionable validity for solutions of ionic strength $\sim$ >0.1 molar. For solutions of ionic strength $\sim$ 7.5 molar, one is strictly into the realm of empiricism where activities must be measured experimentally since no reliable analytical models exists for calculating activities from concentrations. Activity coefficients have been measured for $Na_2S_2O_3$ at this ionic strength (see Table IIC ; data taken from 12) but only at 25°C. Since low temperature fixing is carried out at 7°C, these empirically measured values cannot be used at these low processing temperatures because activities are temperature dependent.

The sodium metabisulfite also produces dissolved sulfur dioxide via the reverse reaction of reaction Ba-R6 in Appendix B.

$$SO_2\ (aq) + 2H_2O \rightleftharpoons HSO_3^-\ (aq) + H_3O^+\ (aq) \qquad (Ba\text{-}R6)$$

for which the equilibrium expression is:

$$K_{al} = \frac{[HSO_3^-]_e \; [H_3O^+]_e}{[SO_2\,(aq)]_e} \qquad \text{(Ba-5)}$$

$$= 1.2 \times 10^{-2} \text{ gmoles-L}^{-1} \text{ @ } 25^oC$$

$$= 1.7 \times 10^{-2} \text{ gmoles-L}^{-1} \text{ @ } 7^oC$$

The 7^oC value of K_{al}, the first dissociation constant of sulfurous acid, was calculated from its value at 25^oC and the standard enthalpy of reaction (-2400 cal-gmole^{-1}-exothermic), using equation A-12. The enthalpy of reaction was calculated from the enthalpy of formation data in Table VII. An expression for the activity of dissolved sulfur dioxide can be found by re-arranging Ba-5. Thus,

$$[SO_2\,(aq)]_e = \frac{1}{K_{al}} \; [HSO_3^-]_e [\,H_3O^+]_e \qquad \text{(2-34)}$$

Qualitatively, the activity of the dissolved sulfur dioxide will increase with decreasing temperature since the solubility of gases increases as the solute temperature decreases.

iii) Silver Recovery From Used Fixer

The used fixer contains ionic silver, almost all of which is tied up as silver-thiosulfate complex ions. Ths silver can be recovered electrolytically. Silver is an extremely valuable metal. The current price of pure silver is of the order of $325. per kilogram. Nuclear

track emulsion contains a large amount of silver ($\sim$ 1.82 Kg/L), the weight of silver bromide per cc of emulsion being greater than in conventional photographic emulsion by a factor of approximately eight. During the developing stage, up to 5 to 10% of the silver is reduced to the grains of elemental silver which form the tracks and fog background. Thus, approximately 90% or more is removed by the fixer. When processing on a large scale like that of the recent development where 25 liters of emulsion were processed, it became desirable, from both an eoncomic and antipollution point of view, to recover the silver. The used fixer contained about 40 kg of recoverable silver. This amount has a current market value of the order of $12,000.

In processing the E-531 emulsion stack, approximately 2.15 liters of fixer were used per cc of emulsion. Thus, the used fixer had an $Ag(S_2O_3)_2^{3-}$ concentration of approximately 7.8×10^{-3} gmoles/L.

The silver can be recovered electrochemically. The redox reaction in fixer is

$$4Ag(S_2O_3)_2^{3-}\ (aq) + 5H_2O \rightleftarrows 4Ag^{o}(s) + 7S_2O_3^{2-}\ (aq) + 2H_3O^{+}\ (aq) + 2H_2SO_3\ (aq) \qquad (2\text{-}R9)$$

The silver is reduced and the sulfur is oxidized from an oxidation state of +2 to +4. Four electrons are transferred. The separate half-reactions are:

$$Ag(S_2O_3)_2^{3-}\ (aq) + e^- \rightleftarrows Ag^o(s) + 2S_2O_3^{=}\ (aq) \qquad (2\text{-R10a})$$

(reduction - $\varepsilon_1^o = 0.01$ v)

$$S_2O_3^{2-}\ (aq) + 5H_2O \rightleftarrows 2H_3O^+(aq) + 2H_2SO_3(aq) + 4e^- \qquad (2\text{-R10b})$$

(oxidation - $\varepsilon_2^o = -0.40$ v)

The standard redox potential is

$$\Delta\varepsilon^o = \varepsilon_1^o + \varepsilon_2^o = -0.39 \text{ v}$$

There is no evidence for the existence of the sulfurous acid molecule, H_2SO_3, in aqueous solution. <<Undissociated H_2SO_3 may be assumed as a short lived intermediate in acidification of sulfites at low temperatures in ethers but does not exist in detectable amounts in aqueous solutions of sulfur dioxide called sulfurous acid.>> [14] Consequently, H_2SO_3 (aq) will be replaced by SO_2 (aq). The electrochemical potential of the plating reaction, the forward reaction of 2-R9, is given by the standard Nernst equation.

$$\Delta\varepsilon = \Delta\varepsilon^o + 2.303\ \frac{RT}{Fn}\ \log\ \frac{[Ag(S_2O_3)_2^{3-}]^4}{[SO_2\ (aq)]^2\ [H_3O^+]^2[S_2O_3^{2-}]^7} \qquad (2\text{-}35a)$$

$$= -0.39 + 4.94 \times 10^{-5}\ T\ \log\ \frac{[Ag(S_2O_3)_2^{3-}]^4}{[SO_2\ (aq)]^2\ [H_3O^+]^2[S_2O_3^{2-}]^7} \qquad (2\text{-}35b)$$

$$< 0$$

14 Ref. 7, pg. 878.

The silver is recovered from the fixer by electrolysis. Thus, the potential of the plating reaction is negative.

Since the potential of the plating reaction is negative, one must supply an external opposing potential greater in magnitude than the plating potential. As the electroplating proceeds, the silver-thiosulfate complex ion activity decreases whereas the dissolved sulfur dioxide, thiosulfate anion and hydronium ion activities increase. As a result, the plating potential becomes increasingly more negative. Therefore, at a constant externally applied potential, the net driving potential decreases causing the plating rate to slow. The electroplating will stop when the two potentials are of equal magnitude.

The electroplating reaction produces acid and dissolved sulfur dioxide. During desilvering, the pH drops from 4.5 ± 0.1 to 3.4 ± 0.1. The fixer acquires a much deeper yellowish colour and an extremely acrid odor consistent with an increase in dissolved sulfur dioxide activity.

iv) Reconditioning of Desilvered Fixer

An extremely small percentage of thiosulfate anion is consumed during the fixing and subsequent desilvering processes. The used fixer has an $Ag(S_2O_3)_2^{3-}$ concentration of approximately 7.8×10^{-3} gmoles-L^{-1}. Therefore, only 1.56×10^{-2} gmoles-L^{-1} of thiosulfate anions are complexed during fixing, whereas in the horizontal case, their concentration in new fixer is 2.5 gmoles-L^{-1}. This indicates a 0.63% decrease in thiosulfate anion concentration during fixing. These thiosulfate anions are not destroyed. Instead, they are tied up as $Ag(S_2O_3)_2^{3-}$ complexes, each mole of silver cation tying up two moles of thiosulfate anion. In the subsequent desilvering redox reaction, 2-R9, seven moles of thiosulfate anion reappear for every four moles of $Ag(S_2O_3)_2^{3-}$ consumed. This results in a net consumption of one mole of thiosulfate anion for every four moles of silver dissolved during fixing and subsequently plated out of the fixer during desilvering. Since each liter of used fixer contains 7.8×10^{-3} gmoles of silver, only 1.95×10^{-3} gmoles-L^{-1} of thiosulfate anion are actually destroyed. Thus, the net thiosulfate anion consumption is only 0.078% and is therefore less than one tenth of one percent.

The consumed thiosulfate anions are converted to sulfurous acid which is actually dissolved sulfur dioxide. As previously mentioned, the pH drops from the required value of 4.5 to the more acidic value of 3.4 ± 0.1 since hydronium ion is produced in the plating reaction.

Since several equilibria must be simultaneously satisfied, some of the acid produced in the electroplating reaction must be consumed. If none of it were consumed, the pH of desilvered fixer would be 2.4. Since the acidity increases, the bisulfite anion activity must also increase to maintain the equilibrium of the decomposition reaction 2-R8 and thus prevent the decomposition of thiosulfate anions to elemental sulfur. The equilibrium for the second dissociation of sulfurous acid must also be satisfied, the reaction being

$$HSO_3^- (aq) + H_2O \rightleftarrows SO_3^= (aq) + H_3O^+ (aq) \qquad \text{(Ba-R5)}$$

for which the equilibrium constant, K_{a2}, is

$$K_{a2} = \frac{[SO_3^=]_e [H_3O^+]_e}{[HSO_3^-]_e} \qquad \text{(Ba-4)}$$

$$= 5.0 \times 10^{-6} \text{ gmoles-L}^{-1} \text{ @ } 25^oC$$

$$= 1.6 \times 10^{-7} \text{ gmoles-L}^{-1} \text{ @ } 7^oC$$

The enthalpy of reaction is 31381 cal./gmole. Production of hydronium ion causes Ba-R5 to shift to the left which produces bisulfite anion. Thus, some of the produced H_3O^+ is consumed. This production of HSO_3^- will cause Ba-R6 to shift to the left consuming some of the produced HSO_3^-, causing further consumption of produced H_3O^+ and production of dissolved SO_2.

The pH of the fixer depends upon the ratio of the activities of dissolved sulfur dioxide and bisulfite anion. This can be seen by re-arranging equation Ba-5, as follows.

$$[H_3O^+]_e = \frac{1}{K_{a1}} \frac{[SO_2\ (aq)]_e}{[HSO_3^-]_e} \qquad (2\text{-}37)$$

If the excess dissolved sulfur dioxide is removed in a controlled manner, the hydronium ion activity will decrease and the pH will increase back to the desired value of 4.5. The bisulfite anion activity is fixed by the addition of sodium metabisulfite and is not consumed in either the fixing or electroplating reactions although some excess is produced in the latter. Therefore, it should be possible to recondition and subsequently reuse desilvered fixer.

A reasonable design approach for removing the excess dissolved sulfur dioxide is to take advantage of the fact that it has a much higher vapor pressure at room temperature than at 7°C. In a closed vessel containing fixer, an equilibrium is established between dissolved and vaporized sulfur dioxide in accordance with the vaporization reaction

$$SO_2\ (aq) \rightleftarrows SO_2\ (g) \qquad (2\text{-}R11)$$

From Table IX, the standard Gibbs free energy of the reaction is 110 cal-gmole^{-1} at 25°C. The equilibrium constant can be calculated

from the thermodynamical relationship given by equation A-10 in Appendix A.

$$K_{eq} = \exp\{-\Delta G_r^o/RT\}$$

$$= 0.83 \text{ @ } 25^oC \qquad \text{(A-10)}$$

where

$$K_{eq} = \frac{[SO_2(g)]_e}{[SO_2(aq)]_e} \qquad \text{(2-38)}$$

Since this equilibrium constant is reasonably large, one could rapidly remove the excess dissolved sulfur dioxide by blowing air over a tank of well agitated desilvered fixer. Agitation would be necessary in order to maintain a homogeneous aqueous SO_2 concentration. Without proper agitation, concentration gradients would develop. The pH can be monitored until it has risen back to the correct value of 4.5 at which time the conditioning process can be stopped. The SO_2 vapor can be removed from the conditioning air by passing it through a water spray. The conditioning vessel must be covered and the system closed since a huge amount of sulfur dioxide escaping into a room would be a serious health hazard.

v) Corrosion of Developed Grains During Fixing

In high energy nuclear emulsion experiments, minimizing corrosion of developed grains is of utmost importance. The particle states are often extremely short-lived and highly relativistic. Thus, one is dealing with minimum ionizing particles which travel a very short distance in the laboratory reference frame. Particles travelling a distance of the order of ten microns can be detected with nuclear track emulsion. The detection limit obviously depends upon the minimum grain density, the track length and the fog density. If significant corrosion occurs during processing, the minimum detectable length of minimum tracks increases. This is undesirable.

Examination of the redox reaction, 2-R9, reveals that the forward reaction is the electroplating reaction whereas the reverse reaction is the corrosion reaction. Since an external potential must be applied to recover silver from used fixer, its corrosion potential must be positive. This indicates that the natural tendency is for the corrosion reaction to occur. In fresh fixer, which is essentially void of silver cations and silver-thiosulfate complex ions, the corrosion potential is extremely large. As a result, the most

dangerous period for corrosion occurs when the plates are transferred from the stop bath to fresh fixer since the corrosion potential is at maximum. At first glance, it would also seem that corrosion should occur continually through out the fixing stage since the corrosion potential of used fixer is still positive. Surprisingly, significant corrosion does not occur. There are two reasons for this.

Firstly, the fixing rate is diffusion controlled in nuclear emulsion processing. Because of this fact, there is a rapid build up of the silver-thiosulfate complex ion concentration in the gelatin network. The steady-state concentration is much larger than in either the bulk of the fixer or the used fixer. This concentration build up reduces the corrosion potential. If the build up is great enough to reduce the corrosion potential to zero, corrosion will cease.

Secondly, several fixing substages are used. An expression for estimating the minimum silver-thiosulfate complex ion activity required to prevent corrosion can be found by setting the plating potential, $\Delta\varepsilon$, equal to zero in equation 2-35. As a result,

$$\log \left[Ag(S_2O_3)_2^{3-}\right]_{min} = \frac{0.39 \left(\frac{Fn}{2.303\ RT}\right) + \log\{[SO_2(aq)]^2[H_3O^+]^2[S_2O_3^{=}]^7\}}{4} \qquad (2\text{-}39)$$

This expression reveals a very important fact concerning the corrosion

potential in the fixing substages 1, 2, and 3 (¼-strength, ½-strength and full-strength in the horizontal case). Recall that the pH and consequently hydronium ion activities are identical in all fixing substages since the fixer is a buffer solution. Also, recall equations 2-33 and 2-34

$$[HSO_3^-]_e = K_{eq}\,[S_2O_3^=]_e[H_3O^+]_e \qquad (2\text{-}33)$$

$$[SO_2\ (aq)]_e = \frac{1}{K_{a1}}\,[HSO_3^-]_e[H_3O^+]_e \qquad (2\text{-}34)$$

When full strength fixer is diluted, the thiosulfate anion activity decreases. Since the pH is constant, there is an identical decrease in HSO_3^- and SO_2 (aq) activities. Thus, as revealed by equation 2-40, there is also a decrease in the minimum silver-thiosulfate complex ion activity required to prevent corrosion. It will consequently be greatest in full-strength fixer and smallest in ¼-strength fixer. Similar arguments apply in the vertical case.

As previously mentioned, when the plates are first transferred from the stop bath, the corrosion potential is very large due to the lack of silver-thiosulfate complex ions in fresh fixer. For finite complex ion activity in the gelatin network, the corrosion potential will be less in ¼-strength than in full-strength fixer since the minimum activity required to prevent corrosion is less in the former than in the latter. Consequently, ¼-strength fixer is less corrosive than ½-

strength fixer which in turn is less corrosive than full-strength fixer. As a result, the risk of corrosion during the critical period of build up of complex ion activity in the gelatin network is reduced by transferring successively from stop bath to ¼-strength to ½-strength to full-strength fixer.

2.6 Stage 5 - Washing

After fixing and the two-step dilution process , the emulsion plates are washed in order to remove the ionic species from the gelatin network: silver-thiosulfate complex ions, thiosulfate anions, bromine anions, bisulfite anions, metabisulfite anions and free silver cations. Filtered tap water is sufficient. For the E-531 development, 5 micron rust removal filters were used. The horizontal plates were washed at $\leq 10^{\circ}C$ at a high flow rate for approximately six days whereas the vertical plates were washed at a lower flow rate for twenty hours at $5^{\circ}C$. The average wash water flow rate was approximately 10 liters per minute per washing tank in the horizontal case compared to 2.5 liters per minute per tank in the vertical case. The plates were washed at low temperature so that the gelatin would remain hard and consequently undergo minimal further swelling.

There were two reasons for washing the horizontal plates much longer and at a much higher flow rate than the vertical plates. Firstly, the horizontal plates were approximately twice as thick as the vertical plates. Because of this, it takes much longer to remove the final traces of ionic species since they must diffuse out of a thicker layer of the gelatin. Secondly, the horizontal plates were placed horizontally, the emulsion side up, in the washing tanks whereas the vertical plates were placed vertically. Thus, the ionic species had to diffuse upwards against the force of gravity in the horizontal case whereas, in the vertical case, the diffusion was not gravitationally hindered.

With nuclear track emulsion, it is important to wash very thoroughly in order to remove all traces of thiosulfate anion if the plates must be kept for a long time. If traces of thiosulfate anion remain in the emulsion, they will undergo slow oxidation by dissolved oxygen in the absorbed water and the processed plates will gradually turn yellowish. If washed sufficiently, they maintain their initial clear colourless transparency.

No significant chemical reactions occur during washing.

2.7 Stages 6, 7, 8 and 9 - Alcohol Drying

By the end of the washing stage, a large amount of water has been absorbed in the gelatin. The gelatin is swollen to several times its initial size. This excess absorbed water must now be removed at a controlled rate in order to control the rate of shrinkage. At the same time, a plasticiser, usually glycerin, is added so that the processed emulsion does not become brittle and thus break or tear. The glycerin, being hygroscopic, increases the equilibrium quantity of absorbed water in the processed plates. Consequently, the plates can be stored at lower relative himidity than would be possible if no glycerin were added and are also less susceptible to damage from changes in the humidity of the storage environment.

Ethyl alcohol is commonly used as the drying agent. The plates are successively placed in drying baths of increasing alcohol concentration . Four baths are commonly used. The alcohol weight percent concentrations were 10, 30, 50 and 80 in the horizontal case and 8, 25, 55 and 85 in the vertical case. The initial drying bath was maintained at the same temperature as the washing stage. The second bath was warmed up gradually to near room temperature. The final two drying stages were done at room temperature.

2.8 Stage 10 - Drying In Air

After the plates are removed from the final drying stage, the emulsion still contains excess absorbed water. At this point, the emulsion thickness is greater than its final thickness by a factor 2.3 ± 0.1 - see Table VIc. This is also evidenced by the fact that the base of the emulsion pellicles are a chalk white colour. For the E-531 development, the plates were left on the processing racks which were placed in air in a nearly air tight vessel where they were left for one and one-half to two days. Since the vessel was nearly air tight, the humidity built up inside. Thus, the remaining excess water desorbed very slowly and the plates gradually came to equilibrium with the external environment as the external and internal humidities gradually came to equilibrium. When the base of the pellicles became a brownish colour, the processing racks were removed from the vessel. The plates were then removed from the racks and stored.

2.9 Processing Solution, Processing and Thermodynamic Data

TABLE I. PROCESSING SOLUTION COMPOSITIONS FOR VERTICAL EMULSION

330μ thickness

a) PRESOAK

Component		Concentration	
Name	Formula	gm/L	Molarity
Deionized water	H_2O	10^3	55.5
Sodium Sulfate	Na_2SO_4	5	3.5×10^{-2}

b) DEVELOPER

Component		Concentration	
Name	Formula	gm/L	Molarity
Deionized water	H_2O	1000	55.5
Sodium Sulfite	Na_2SO_3	6.7	5.3×10^{-2}
Sodium Metubisulsite	Saturated Solt^n of $Na_2S_2O_5$	1.4 ml	
Amidol	$(NH_2)_2C_6H_3OH.2HCl$	3 gm	1.52×10^{-2}

c) STOP BATH

Component		Concentration	
Name	Formula	gm/L	Molarity
Deionized water	H_2O	1000	55.5
Acetic Acid	CH_3COOH	5	8.3×10^{-2}

d) 3/3 FIXER - FULL STRENGTH

Component		Concentration	
Name	Formula	Amount/L of Sol.	Molarity
Sodium Thiosulphate Pentahydrate (Hypo)	$Na_2S_2O_3.5H_2O$	300 gm	1.90 (anhydrous)
Sodium Metabisulfite	$Na_2S_2O_5$	27.3 gm	1.44×10^{-1}
Potassium Aluminum Sulfate	$KAl(SO_4)_2$	5	1.9×10^{-2}
Deionized water	H_2O	enough for 1 liter of solution	

e) 2/3 FIXER

Component		Concentration	
Name	Formula	Amount/L of Sol.	Molarity
Sodium Thiosulfate Pentahydrate (Hypo)	$Na_2S_2O_3 \cdot 5H_2O$	200 gm	1.26 (anhydrous)
Sodium Metabisulfite	$Na_2S_2O_5$	27.3 gm	1.44×10^{-1}
Potassium Aluminium Sulfate	$KAl(SO_4)_2$	5 gm	1.9×10^{-2}
Deionized water	H_2O	enough for 1 liter of solution	

f) 1/3 FIXER

Component		Concentration	
Name	Formula	Amount/L of sol.	Molarity
Sodium Thiosulfate Pentahydrate (Hypo)	$Na_2S_2O_3 \cdot 5H_2O$	100 gm	0.63 (anhydrous)
Sodium Metabisulfite	$Na_2S_2O_5$	27.3 gm	1.44×10^{-2}
Potassium Aluminum Sulfate	$KAl(SO_4)_2$	5 gm	1.9×10^{-2}
Deionized water	H_2O	enough for 1 liter of solution	

g) DRYING SOLUTIONS

Component / Stage	Ethyl Alcohol wt. %	Water wt. %	Glycerin wt. %
I	8	87	5
II	35	60	5
III	55	35	10
IV	85	5	10

TABLE II. PROCESSING SOLUTION COMPOSITIONS FOR HORIZONTAL EMULSION 600μ thickness

a) PRESOAK - deionized water

b) DEVELOPER

Component		Concentration	
Name	Formula	gm/L	Molarity
Deionized water	H_2O	1000	55.5
Sodium Sulfite	Na_2SO_3	7.2	5.7×10^{-2}
Sodium Metabisulfite	$Na_2S_2O_5$	0.91	4.8×10^{-3}
Potassium Bromide	KBr	0.87	3.7×10^{-3}
Amidol	$(NH_2)_2C_6H_3OH.2HCl$	3.25	1.65×10^{-2}

c) STOP BATH

Component		Concentration	
Name	Formula	gm/L	Molarity
Deionized water	H_2O	1000	55.5
Acetic Acid	CH_3COOH	5	8.3×10^{-2}

d) 4/4 FIXER - FULL STRENGTH

Component		Concentration	
Name	Formula	Amount/L of sol.	Molarity
Sodium Thiosulfate Pentahydrate (Hypo)	$Na_2S_2O_3.5H_2O$	500 gm	2.5 (anhydrous)
Sodium Metabisulfite	$Na_2S_2O_5$	27.3	1.44×10^{-1}
Deionized water	H_2O	enough for 1 liter of solution	

e) 1/2 FIXER - DILUTED FROM 4/4 FIXER

f) 1/4 FIXER - DILUTED FROM 4/4 FIXER

g) DRYING SOLUTIONS

Component			
Stage	Ethyl Alcohol wt. %	Water wt. %	Glycerin wt. %
I	10	80	10
II	30	70	10
III	50	40	10
IV	75	15	10

h) ESTIMATED ACTIVITY COEFFICIENTS OF USED FULL STRENGTH HORIZONTAL FIXER

Ionic species	Concentration (moles/L)	Effective Size[15] in Angstroms	Activity Coefficient
$S_2O_3^{=}$	2.5	4.5	0.078
H^+	pH = 4.5 ± 0.1	9.0	0.702
Ag^+	-	2.5	0.372
HSO_3^-	-	4.0	0.303
$SO_3^{=}$	-	4.5	0.078

Notes 1) Ionic strength = 7.5 moles/L. Calculated from equation A-13.

2) Activity coefficients calculated from extended Debye-Huckel equation A-14.

15. ref. 25

TABLE III · VERTICAL EMULSION PRESOAK SOLUTION PH TESTS

Component	pH ± 0.1	$T^{o}C$ ± 0.1
H_2O	6.8	5.8
Na_2SO_4	6.8	5.8

Note: components were added in order and the pH measured after the addition of each component

TABLE IV DEVELOPING SOLUTION PH TESTS

a) HORIZONTAL DEVELOPER

i) All components included

Component	pH ± 0.1	T°C ± 0.1
H_2O	6.8	7.0
Na_2SO_3	9.8	5.6
$Na_2S_2O_5$	7.4	5.6
KBr	7.4	5.6
Amidol	6.6	5.6

ii) Just Water and Amidol

Component	pH ± 0.1	T°C ± 0.1
H_2O	6.8	5.2
Amidol	2.8	5.2

Note: components were added in the order in which they appear and pH was measured after the addition of each component.

b) VERTICAL DEVELOPER

i) All components included

Component	pH ± 0.1	$T^{o}C$ ± 0.1
H_2O	6.8	5.2
Na_2SO_3	9.6	5.2
$Na_2S_2O_5$	7.4	5.6
Amidol	6.8	5.3

ii) Just Water and Amidol

Component	pH ± 0.1	$T^{o}C$ ± 0.1
H_2O	7.0	4.6
Amidol	2.9	5.0

c) SATURATED SODIUM METABISULFITE ($Na_2S_2O_5$)

pH = 2.9 ± 0.1 $\qquad$ $T = 22^{o}C$

Note: components were added in the order in which they appear and pH was measured after the addition of each component.

TABLE V HORIZONTAL FIXER PH TESTS

a) 4/4 FIXER - FULL-STRENGTH

Component	pH ± 0.1	T°C ± 0.1
Water	7.0	22.6°C
$Na_2S_2O_3.5H_2O$	6.4	8.5°C
$Na_2S_2O_5$	4.5	9.4, 12.5, 15
	4.6	17

b) 1/2 FIXER - DILUTED FROM FULL-STRENGTH

pH ± 0.1	T°C ± 0.1
4.5	16.0
4.5	8.5

Note: components were added in order and the pH measured after the addition of each component.

c) 1/4 FIXER - DILUTED FROM FULL-STRENGTH

pH ± 0.1	$T^{\circ}C$ ± 0.1
4.5	19.2
4.5	8.5

d) WATER AND SODIUM METABISULFITE AT SAME CONCENTRATION AS FULL STRENGTH FIXER

Component	pH ± 0.1	$T^{\circ}C$ ± 0.1
Water	6.8	20.8
$Na_2S_2O_3$	4.0	20.8

Note: components were added in order and the pH measured after the addition of each component.

TABLE VIA SUMMARY OF E-531 PROCESSING DATA FOR VERTICAL EMULSION - 29 MODULES, 15.3 L OF EMULSION, 70 PLATES/MODULE, 0.53 L/MODULE.

Temp ^{o}C/Time from beginning of stage ± 0.1^{o}C

STAGE	DURATION	MOD 12 & 26	MOD 10 & 11	MOD 3 & 4	MOD 14 & 21	MOD 13 & 22	MOD 16 & 17	MOD 20 & 28	MOD 18 & 14
Presoak	50 min.	5.0	5	5	4.5	4.5	5.5	5.5	5.0
Develop	4.5 hrs.	5.0/start 5.0/end	6.0/start 6.0/3½ hrs	6.0/start	4.5	5.0	5.5/start 5.0/2 hrs.	5.0	5.5
Stop	50 min	5.0	5.0	5.1	4.5	4.5	5.0	5.0	5.0
Fix 1/3	50 min.	4.0	5.0	5.0	4.0	4.0	5.0	5.0	5.5
Fix 2/3	50 min.	4.0	4.9	4.8	3.5	4.0	4.0	4.0	5.0
Fix 3/3	∿ 20 hrs.	5.0/start 5.0/12 hrs.	5.0	4.0	3.5/start 5.0/12 hrs.	3.5/start 5.0/11 hrs.	4.5/start 4.5/12 hrs.	4.5/start 4.5/12 hrs.	4.5/start 4.5/15 hrs.
Fix 2/3	50 min	5.0	4.0	4.0	5.0	5.0	5.0	5.0	5.0
Fix 1/3	50 min	4.5	5.0	5.0	5.0	5.0	5.0	5.0	5.2
Wash	∿ 19 hrs.	6.0/start 4.8/3.5 hrs. 4.0/12 hrs.	5.0	5.0	7.0/start 5.0/end	5.0/start 5.0/end	6.0	6.0	5.4
Dry I	50 min.	9.5	7.0 → 15.0	7 → 15	7.0 → 15.0	7.0 → 15.0	8.0 → 13.0	8.0 → 13.0	8.0 → 16.0
Dry II	50 min	13.5	19.0	19.0	15.0 → 20.0	15.0 → 20.0	15.0 → 20.0	15.0 → 20.0	16.0 → 18.0
Dry III	50 min	14.5	22.0	22.0	22.0	22.0	21.0	21.0	21.0
Dry IV	2 hrs.	15.0	22.0	22.0	22.0	22.0	21.0	21.0	21.0

Notes:

1. Washing Rate ∿ 2.5 to 3L/min
2. Clearing time ≤ ∿ 11 hrs.
3. Processing time ∿ 33 hrs./Two Modules

Temp ^{o}C/Time from beginning of stage ± 0.1^{o}C

STAGE	DURATION	MOD 27 & 29	MOD 6 & 7	MOD 15 & 27	MOD 2 & 5	MOD 8 & 25	MOD 1 & 9	MOD 23
Presoak	50 min	5.0	5.0	5.0	4.5	4.5	4.0	4.0
Develop	4.5 hrs.	5.5	5.5/start 5.1/3.25 hrs.	5.5/start 5.1/2 hrs.	4.8/start 4.9/3.5 hrs.	4.8/start 5.0/end	5.0	5.0
Stop	50 min.	5.0	5.0	5.0	3.5	3.5	3.0	3.0
Fix 1/3*	50 min.	5.5	5.0	5.0	4.5	4.5	5.0	5.0
Fix 2/3	50 min	4.5	4.0	4.5	4.5	4.5	4.5	4.5
Fix 3/3	∿ 20 hrs.	5.0/start 4.0/4 hrs.	5.0/start 4.5/15 hrs.	5.0/start 4.5/4 hrs.	5.0/start 4.5/15 hrs.	4.5/start 4.0/14 hrs.	4.5/start 4.0/15 hrs.	3.5/start 4.0/15 hrs.
Fix 2/3	50 min	5.0	4.0	4.0	5.0	5.0	3.5	3.5
Fix 1/3	50 min.	5.2	4.5	4.5	4.0	4.0	4.0	4.0
Wash	∿ 19 hrs.	5.4	5.5/start 5.4/end	5.5/start 5.4/end	4.5	4.5	5.2/start 5.4/end	5.2/start 5.4/end
Dry I	50 min	8.0 → 16.0	9.0 → 11.0	9.0 → 11.0	9.0 → 12.0	9.0 → 12.0	6.4 → 12.0	6.4 → 12.0
Dry II	50 min	16.0 → 18.0	11.0 → 18.0	11.0 → 18.0	12.0 → 15.0	12.0 → 15.0	11.0 → 16.0	12.0 → 16.0
Dry III	50 min.	21.0	21.0	21.0	21.0	21.0	21.0	21.0
Dry IV	2 hrs.	21.0	21.0	21.0	20.8	20.8	21.0	21.0

TABLE VIB SUMMARY OF HORIZONTAL PROCESSING DATA - 13 MODULES, 9.8 LITRES OF EMULSION, 1.5 MOD/RUN, 176 PELLICLES/MODULE, 0.76 L/MODULE, 600μ thick

Temp. °C/time from beginning of stage ± 0.1°C

STAGE	DURATION	RUN 1	RUN 2	RUN 3	RUN 4	RUN 5	RUN 6	RUN 7	RUN 8	RUN 9
Presoak	2 hrs.	6.5/start 6.5/end	5.0/start 5.5/end	7.0/end	6.0/start 7.0/end	7.5/start 7.8/end	6.5/start 7.0/end	7.2/start 7.0/end	6.5/start 6.9/end	7.5/start 7.5/end
Tank A		7.0/start 7.0./1 hr. 7.0/2 hrs. 7.0/3 hrs. 7.0/4.5 hrs. 7.0/6 hrs. 6.9/7.75 hrs. 7.0/8.25 hrs. 7.0/end	7.0/start 7.0/2 hrs. 7.0/4 hrs. 7.2/5 hrs. 7.5/6.5 hrs. 7.5/8 hrs. 7.5/10 hrs. 7.5/end	7.0/start 7.5/1.5 hrs. 7.0/2.5 hrs. 7.0/4 hrs. 7.0/5 hrs. 7.0/6.5 hrs. 7.0/8.5 hrs. 7.0/10 hrs. 7.0/end	6.5/start 6.9/1 hr. 7.0/2.5 hrs 7.0/4 hrs. 7.0/6.25 hrs. 7.0/7.5 hrs. 7.0/9.25 hrs. 7.0/11.25 hrs. 7.0/end	6.8/start 6.9/1.5 hrs. 7.0/3.5 hrs. 7.0/5 hrs. 7.0/7 hrs. 7.0/9 hrs. 7.0/end	6.8/start 7.0/2 hrs. 7.0/6.25 hrs. 7.2/9 hrs. 7.1/9.75 hrs. 6.9/end	7.0/start 7.0/1.75 hrs. 6.9/4.75 hrs. 6.6/6.5 hrs. 6.5/9.5 hrs. 6.5/end	6.7/start 6.5/3.5 hrs. 6.5/6.5 hrs. 6.6/8 hrs. 6.7/end	6.6/start 6.7/2.5 hrs. 6.9/4.5 hrs. 7.1/8 hrs. 7.0/10 hrs. 7.2/end
Develop	12 hrs.	7.0/start 6.8/1 hr. 7.0/2 hrs. 7.0/3 hrs. 7.0/4.5 hrs. 7.0/6 hrs. 6.9/7.75 hrs. 7.0/8.25 hrs 7.0/end	7.0/start 7.0/2 hrs. 7.0/4 hrs. 7.2/5 hrs. 7.5/6.5 hrs 7.5/8 hrs. 7.5/10 hrs. 7.5/end	7.0/start 7.5/1.5 hrs. 7.0/2.5 hrs. 6.8/4 hrs. 7.0/5 hrs. 7.0/6.5 hrs. 7.0/8.5 hrs. 7.0/10 hrs. 7.0/end	6.5/start 6.6/1 hr. 7.0/2.5 hrs. 7.0/4 hrs. 7.0/6.25 hrs. 7.0/7.5 hrs 7.0/9.25 hrs. 7.0/11.25 hrs. 7.0/end	6.8/start 8.0/1.5 hrs. 7.0/3.5 hrs. 7.0/5 hrs. 7.0/7 hrs. 7.0/9 hrs. 7.0/end	6.8/start 7.0/2 hrs. 7.0/6.25 hrs. 7.2/9 hrs. 7.1/9.75 hrs. 6.9/end	7.0/start 7.0/1.75 hrs. 6.4/4.75 hrs. 6.7/6.5 hrs. 6.5/9.5 hrs. 6.5/end	6.6/start 6.5/3.5 hrs. 6.5/6.5 hrs. 6.6/8 hrs. 6.7/end	6.7/start 6.7/2.5 hrs. 6.8/4.5 hrs. 7.0/8 hrs. 7.0/10 hrs. 7.0/end
Tank B										
Tank C		7.0/start 6.7/1 hr. 6.9/2 hrs. 7.0/3 hrs. 7.0/4.5 hrs. 7.0/6 hrs. 7.0/8.25 hrs. 7.0/end	7.2/start 7.0/2 hrs. 7.0/4 hrs. 7.2/5 hrs. 7.5/6.5 hrs. 7.5/8 hrs. 7.5/10 hrs. 7.5/end	7.0/start 7.5/1.5 hrs. 7.0/2.5 hrs 7.0/4 hrs. 7.0/5 hrs. 7.0/6.5 hrs. 7.0/8.5 hrs. 7.0/10 hrs. 7.0/end	6.5/start 6.6/1 hr. 7.0/2.5 hrs. 7.0/4 hrs. 7.0/6.25 hrs. 7.0/7.5 hrs. 7.0/9.25 hrs. 7.0/11.25 hrs. 7.0/end	6.8/start 6.9/1.5 hrs. 7.0/3.5 hrs. 7.0/5 hrs. 6.9/7 hrs. 7.0/9 hrs. 7.0/end	6.5/start 7.0/2 hrs. 7.0/6.25 hrs. 7.2/9 hrs. 7.1/9.75 hrs. 6.9/end	7.0/start 6.9/1.75 hrs. 6.7/4.75 hrs. 6.6/6.5 hrs. 6.5/9.5 hrs. 6.5/end	6.6/start 6.5/3.5 hrs. 6.5/6.5 hrs 6.6/8 hrs. 6.7/end	not used.
Stop	2 hrs.	7.0/start 7.0/end	7.4/start 8.0/end	7.0/start 7.0/end	7.0/start 7.0/end	7.5/start 7.0/end	5.5/start 6.5/end	7.0/start 7.0/end	6.5/end	6.5/start 7.6/end

Fix. 1/4	2 hrs.	7.0/start 7.5/end	7.5/start 6.5/end	7.0/start 7.0/end	7.0/start 7.0/end	7.2/start 7.0/end	7.0/start 6.5/end	6.6/start 6.5/end	6.7/start 6.7/end	7.3/start 7.1/end
Fix. 1/2	2 hrs.	7.0/start 7.0/end	7.0/start 7.0/end	7.5/start 7.3/end	7.0/start 7.0/end	7.5/start 7.5/end	6.5/start 7.2/end	7.0/start 6.5/end	7.2/start 7.5/end	7.1/start 7.0/end
Fix.	~4 days	7.0/start 7.6/14 hrs. 7.0/24 hrs. 7.0/26.5 hrs. 7.0/40 hrs. 7.0/43 hrs. 7.0/45 hrs. 7.5/63 hrs. 6.9/73 hrs. 7.2/96 hrs. (end)	9.0/start 7.5/2 hrs. 7.5/4.5 hrs. 7.0/18 hrs. 7.0/21 hrs. 7.0/23 hrs. 7.6/41 hrs. 7.0/51 hrs. 7.1/74 hrs. 7.7/96 hrs. (end)	7.7/start 7.0/19 hrs. 7.0/26 hrs. 7.0/44 hrs. 6.7/50 hrs. 7.0/67 hrs. 7.5/77 hrs. 7.4/88 hrs. 6.5/96 hrs. (end)	7.0/start 7.3/3 hrs. 7.5/21 hrs. 7.0/27 hrs. 7.0/44 hrs. 7.5/54 hrs. 7.6/67 hrs. 8.0/97 hrs. (end)	7.5/start 7.4/44 hrs. 7.0/69 hrs. 7.2/89 hrs. (end)	7.5/start 7.2/20 hrs. 7.5/45 hrs. 7.5/97.5 hrs. (end)	7.0/start 7.5/16.5 hrs. 7.5/46.5 hrs. 7.4/51 hrs. 7.6/65.5 hrs. 8.0/77 hrs. 7.5/96 hrs. (end)	7.4/start 7.6/24 hrs. 7.4/28.5 hrs. 7.6/43 hrs. 8.0/52.5 hrs. 8.0/92 hrs. (end)	8.0/start 7.7/17 hrs. 7.5/41 hrs. 7.1/71 hrs. 7.5/96 hrs. 7.5/96.5 hrs (end)
Fix. 1/2	2 hrs.	7.2/start 6.8/end	8.0	8.0/start 7.5/end	8.0/start 7.5/end	7.5/start 7.0/end	8.5/start 7.5/end	8.0/start 8.0/end	7.9/start 7.6/end	6.0/start 7.0/end
Fix 1/4		6.5/start 7.0/end	7.0	7.5/start	7.5/start 7.5/end	7.0/start 7.0/end	7.0/start 7.0/end	7.4/start 7.5/end	7.0/start 7.3/end	7.0/start 6.5/end
Wash	~6 days	6.0/start 6.0/30 hrs. 6.5/end	6.0/start 6.0/8 hrs.	6.5/start 10.0/end	8.8/start 8.8/end	9.0/start 10.0/end	9.0/start 9.6/end	10.0/start 10.0/end	9.6/start 10.5/end	2.5/start
Dry I	2 hrs.	9.0/start 9.0/end	9.5/start 9.0/end	9.0/start 9.0/end	8.5/start 9.0/end	11.0/start 10.0/end	9.6/start 10.0/end	8.0/start 9.0/end	9.0/start 8.5/end	9.0/end
Dry II	2 hrs.	10.5 → 14.0	11.5 → 16.8	8.5 → 16.0	9.9 → 16.5	11.0 → 16.7	10.8 → 15.0	9.0 → 16.0	12.0 → 15.5	
Dry III	2 hrs.	20.5/start 21.5/end	21.5/start 20.5/end	17.5/start 17.5/end	18.8/start 18.5/end	19.0/start 20.8/end	19.6/start 19.8/end	20.0/start 20.0/end	20.0/start 20.2/end	
Dry IV	6 hrs.	21.5/start 21.5/end	21.0/start	17.7/start 18.2/end	19.0/start	21.5/start 20.8/end	21.0/start 21.0/end	21.0/start 21.5/end	20.5/start 21.0/end	

TABLE VIC HORIZONTAL PELLICLE THICKNESS MEASUREMENTS

a) After Alcohol Drying - Measured One Pellicle Per Run

Run	Thickness in microns ± 1.0
1	753
2	715
3	745
4	769
5	781
6	734
7	789
8	816
Average	760 ± 23

b) Final Thickness @ 60% R.H. After Drying In Air

Note: each pellicle thickness is an average of six measurements.

Pellicle No.	Thickness in microns
1	320 ± 4.5
2	328 ± 3.7
3	338 ± 4.5
4	325 ± 7.3
5	310 ± 4.0
6	326 ± 8.0
Average	324 ± 2.7

Note: Uncertainties quoted are for the 95% confidence level

$$\text{mean} = \bar{t} = \frac{\sum_{i=1}^{n} t_i}{n} \quad ; \quad s = \sqrt{\frac{\sum_{i=1}^{n} (t_i - \bar{t})^2}{n-1}}$$

$$s_{\bar{t}} = \frac{s}{\sqrt{n}}$$

$$\bar{t}_{true} = \bar{t} \pm 2s_{\bar{t}} \quad \text{at 95\% confidence level.}$$

- distributions assumed to be Gaussian.

TABLE VIB

Notes:
1. Clearing time $\leq$ 42 hrs.
2. Washing Rate $\sim$ 15 L/min.
3. Run 9 was washed cold because of many small bubbles. Bubbles caused by insufficient drying after sticking.
4. Drying temperatures of Run 9 were not recorded.

TABLE VIIA SOLUBILITY OF KBr and AgBr IN WATER.

DATA IS TAKEN FROM THE INTERNATIONAL CRITICAL TABLES

a) KBr[16]

$T^{o}C$	Moles/L ± 1%	K_{sp} ± 2%
-10	3.98	15.84
0	4.49	20.16
10	4.97	24.70
20	5.24	27.45
30	5.88	34.54
40	6.31	39.82
100	8.84	78.14

Note: $K_{sp} = [K^{+}] [Br^{-}]$

16 Ref. 4 volume IV pg. 239.

b) $AgBr$[17]

$T^{o}C$	Moles/L	K_{sp}
19.6	4.2×10^{-7}	1.64×10^{-13}
21.1	5.4×10^{-7}	2.9×10^{-13}
25[18]	7.2×10^{-7}	5.2×10^{-13}
100	180×10^{-7}	3.24×10^{-10}

$$\Delta H_D^o = 20.1 \text{ kcal/gmole}$$

note: ΔH_D^o calculated using equation A-11.

17 Ref. 4 Volume VI pg. 256

18 Ref. 5 pg 173.

TABLE VIIB HEAT OF FORMATION OF SEVERAL IMPORTANT SPECIES IN EMULSION PROCESSING

Species	State	Heat of Formation[19] (KJ/gmole)	Enthalpy of Formation (KJ/gmole)
H^+	∞	0	0
H_2O	liquid	286.2	-286.2
$SO_3^=$	aq	468	-468
$SO_4^=$	aq	885.5	-885.5
HSO_4^-	aq	878	-878
HSO_3^-	aq	617.3	-617.3
Ag^+	∞	-104	104
AgBr	c	99.8	-99.8
Br^-	aq	119.7	-119.7
KBr	c		-392.17[19a]
K^+	∞	252.4	-252.4
O_2	(aq)	13.8	-13.8
$S_2O_3^=$	(aq)	590	-590
$S_2O_5^=$	(aq)	948.7	-948.7
SO_2	(g)		-296.7[19a]
H_2SO_3(aq)	n=200	607.2	-607.2
$Ag(S_2O_3)^{3-}$	aq	1159	-1159
SO_2(aq)		321	-321

aq - diluted aqueous solution

c - macrocrystalline

∞ - infinite dilution

$$n = \frac{\text{moles of solvent}}{\text{moles of solute}}$$

[19] Ref 4 Volume V

[19a] Ref 13

TABLE VIIC ACTIVITY COEFFICIENTS FOR $Na_2S_2O_3$ at 25°C.

Molality	Mean Activity
0.1	0.457
0.2	0.382
0.3	0.340
0.4	0.313
0.5	0.292
0.6	0.276
0.7	0.262
0.8	0.251
0.9	0.242
1.0	0.234
1.2	0.222
1.4	0.214
1.6	0.207
1.8	0.202
2.0	0.198
2.5	0.195
3.0	0.199
3.5	0.207

R.H. Stokes Trans Faraday Soc., 44, 295 (1948). This contribution contains a complete bibliography of original source of these results.

x Ref 12 pg. 739 and 40

TABLE VIII STANDARD GIBBS FREE ENERGY OF FORMATION [20] AT 25°C

Species	Free Energy (cal/gmole)
HSO_3^- (aq)	-123,920
$S_2O_3^=$ (aq)	-125,100
S(g)	30,240
H_2O (ℓ)	-56,560
H^+	0 (by convention)
S(s)	0
SO_2 (aq)	-69,770
Ag^+ (aq)	18,448

[20] Ref. 4 Volume V

TABLE IX STANDARD GIBBS FREE ENERGY OF REACTION [21] AT 25°C

Reaction	Free Energy (cal/gmole)
$HSO_3^-(aq) = H^+(aq) + SO_3^=(aq)$	7240
$SO_2(aq) = SO_2(g)$	110

[21] Ref. 4 Volume V.

CHAPTER 3. DESIGN OF A LARGE SCALE NUCLEAR EMULSION PROCESSING SYSTEM.

3.1 Description of the System

The emulsion processing system, designed to develop nuclear on a large scale, is shown schematically in process flow diagrams PF - 1, PF - 2 and PF - 3. All processing tanks, except for the washing tanks, were installed in large, insulated, polyethylene, jacket tanks. - see Drawings 5 and 7. The processing tanks were made from type-304 stainless steel. - see Drawings 1, 2 and 3. All jacket tanks were insulated with 1½" - thick, styrofoam S.M. The styrofoam was stuck to the polyethelene with panel adhesive. The styrofoam was covered with a protective cover of 1/8" thick polyvinyl chloride (PVC). The washing tanks were covered directly with the same styrofoam insulation as the jacket tanks and the styrofoam was covered with PVC. All processing and jackets tanks have lids in order to make them light tight and prevent the escape of vapors from the processing solutions. This is especially important for the fixing and drying solutions since fixer has a significant sulfur dioxide vapor pressure and the drying solutions have a high ethyl alcohol vapor pressure.

Temperature control is necessary since large temperature fluctuations produce distortion and non-uniform development in the processed emulsion plates. A suitable coolant is necessary for low temperature development. The 25 liter, E-531 emulsion stack was processed at temperatures from 5 to 7°C. The system was designed and

built specifically to process this stack. Fortunately, from an economic point of view, the stack was processed during the winter of 1979. In Ottawa the average, ambient, wintertime, water temperature is between one and three degrees centigrade. Due to this extremely low ambient water temperature, standard photopanel mixing valves were used to mix hot and cold water in the desired proportions in order to provide coolant at the desired processing temperature. Coolant water was supplied continually to each jacket tank at a rate of approximately 3 liters per minute. Each jacket inlet was provided with a hand-operated, needle control valve to regulate the flow of coolant. The steady flow of coolant water provided the necessary initial cooling and subsequent temperature control. The continual flow prevented the creation of undesirable vertical temperature gradients in the processing solutions.

As discussed in detail in chapter 2, the most critical stage of emulsion processing is the development stage. Precise temperature control is of utmost importance if one wishes to achieve uniform development. Consequently, four small developing tanks, 9" x 18" x 20", (Drawing 3') were built instead of one large tank, 34" x 18" x 20", (Drawings 1 and 2) of the same type as those which were built for the other processing stages. The four small developing tanks were installed in one jacket tank. This increased the heat transfer area by a factor of 1.85 and thus provided improved temperature control. A security

system consisting of a temperature sensing bulb, a mechanical controller and a solenoid valve was installed in the coolant inlet line of the jacket tank of the developing tanks. The security system was designed to shut-off the coolant supply in case of an accidental rise in the coolant temperature, the solenoid valve being deactivated by the controller in such a case - see PF - 1. A small by-pass flow of coolant, taken downstream of the temperature sensor, was continually run to the sink so that the controller would reactivate the solenoid valve when the coolant temperature had returned to its preset value.

A circulation system was incorporated into the fixing tanks to increase the speed and improve the homogenity of the fixing process. Perforated jackets - Drawings 1C and D - were spot welded to the inside of the ends and bottom of the fixing tanks. Accompanying valve and piping systems - Drawing 5 - were installed and small circulating pumps were connected outside the jacket tanks. The circulating pumps, Model: 17870-00 Jabsco centrifugal pumps, were chosen specifically because of their resistance to corrosion by photographic processing solutions. All pump parts in contact with the fixing solutions were made of chlorinated polyvinyl chloride (CPVC). These circulating pumps were low-head, high-capacity pumps which circulated the fixer continuously at 10 to 15 liters per minute. The perforated jackets served as baffles to distribute the circulating fixer uniformly. The accompanying exterior valves, adaptors and piping were made of

PVC.

The washing tanks have circulating systems similar to those of the fixing tanks, the circulating pumps being identical in both stages. Circulation was included to distribute the wash water flow inside the washing tanks as uniformly as possible, thereby increasing the homogeneity of the washing by eliminating dead spaces. Circulation was not incorporated into any of the other processing stages.

The horizontal processing racks - Diagram 3 - were made from plexiglass and stainless steel. The racks were designed with adjustable, perforated walls. The adjustable walls allow the racks to be used for different plate sizes. Thus, it is not necessary to build a new set of racks for each emulsion stack of different pellicle dimensions. The walls were perforated to improve circulation. Each rack has a capacity of ninty-five emulsion pellicles mounted on 16 cm x 7 cm x 2 mm support plates. Eighteen racks were built for the horizontal portion of the E-531 stack so that many runs could be processing simultaneously.

The vertical processing racks - Drawing 4 - were made from type 304 stainless steel. For the E-531 development, approximately seventy plates were loaded on each rack. Spacer bushing were made from polyethylene tubing and the ends of the rods were capped with

TABLE X. SUMMARY OF SYSTEM PROCESSING VESSELS

Item	Quantity	Drawing No.
Presoak Tanks	1	2 and 5
Developing Tanks	4	3 and 7
Stop Bath Tanks	1	2 and 5
Fixing Tanks	4	1 and 5
Washing Tanks	2	1 and 6
Drying Tanks	2	2 and 5
Jacket Tanks	9	5, 6 and 7

TABLE XI. SUMMARY OF AUXILIARY PROCESSING EQUIPMENT

Item	Quantity	Drawing No.
Horizontal Emulsion Processing Racks	18	3
Vertical Emulsion Processing Racks	8	4
Fixing and Washing Tank Circulating Pumps	5	PF - 1 and 2
Photopanel Mixing Valves and Accompanying Distribution System	2	PF - 1 and 2
Water Deionizing System	1	PF - 3
Agitators	5	-
Chemical Solution Mixers	1	-

tight-fitting, annular rings made from nylon rod. Eight racks were built to process the vertical portion of the E-531 stack.

3.2 Process Flow Charts

The processing system flow charts are presented in this section.

PF-1 PROCESS FLOW DIAGRAM
FOR NUCLEAR EMULSION DEVELOPING SYSTEM

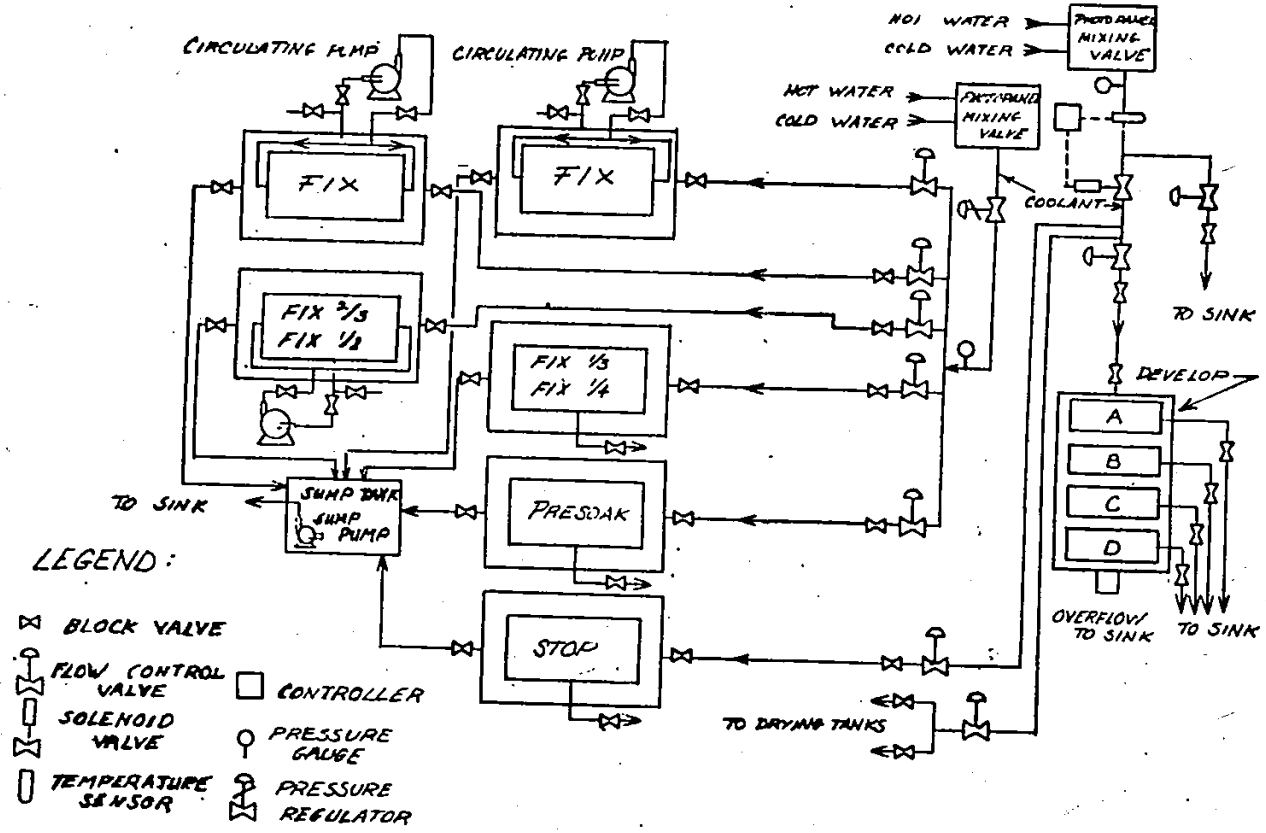

NOTES:

1. ALL EXTERIOR TANKS ARE POLYETHYLENE PLASTIC. THEY ARE INSULATED WITH STYROFOAM SM. THE STYROFOAM IS COVERED WITH PVC.
2. ALL INTERIOR TANKS ARE TYPE 304 STAINLESS STEEL.
3. CIRCULATING PUMPS ARE CPVC PLASTIC. ACCOMPANYING VALVES ARE PVC BALL VALVES.

PF-2 PROCESS FLOW DIAGRAM FOR NUCLEAR EMULSION WASHING AND DRYING SYSTEM

NOTES:

1. DRYING TANKS ARE IDENTICAL TO PRESOAK AND STOP BATH TANKS.
2. WASHING TANKS ARE TYPE 304 STAINLESS STEEL. THEY ARE COVERED DIRECTLY WITH STYROFOAM S.M. INSULATION. THE INSULATION IS COVERED WITH PVC.
3. CIRCULATING PUMPS ARE IDENTICAL TO FIXER CIRCULATING PUMPS.

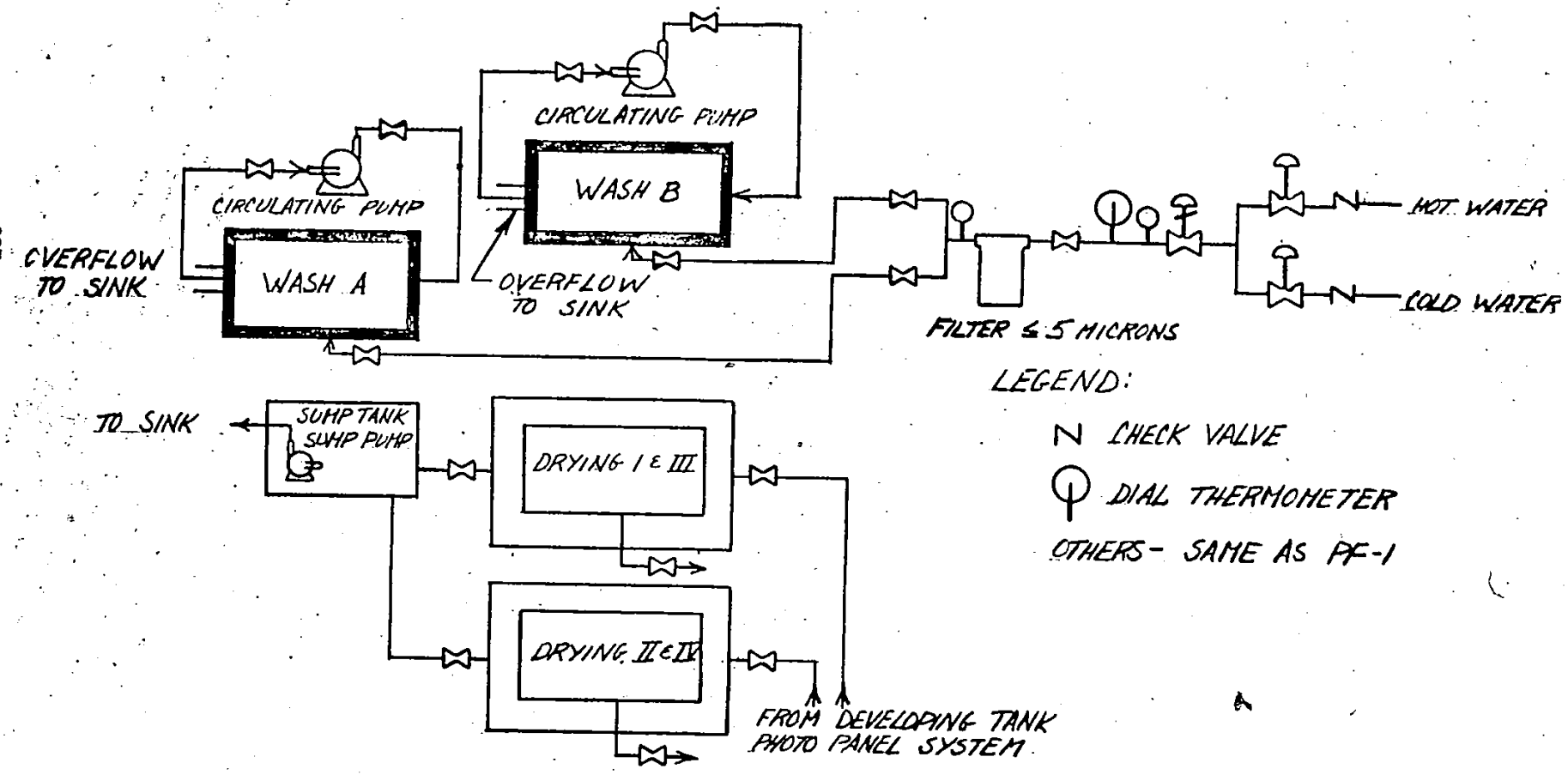

LEGEND:

N CHECK VALVE

DIAL THERMOMETER

OTHERS - SAME AS PF-1

PF-3 PROCESS FLOW DIAGRAM OF WATER FILTERING AND DEIONIZING SYSTEM

NOTES:

1. DEIONIZING UNIT IS A BARNSTEAD NANOPURE SYSTEM.
2. THIS SYSTEM IS INSTALLED IN THE DEVELOPING AND FIXING ROOM.

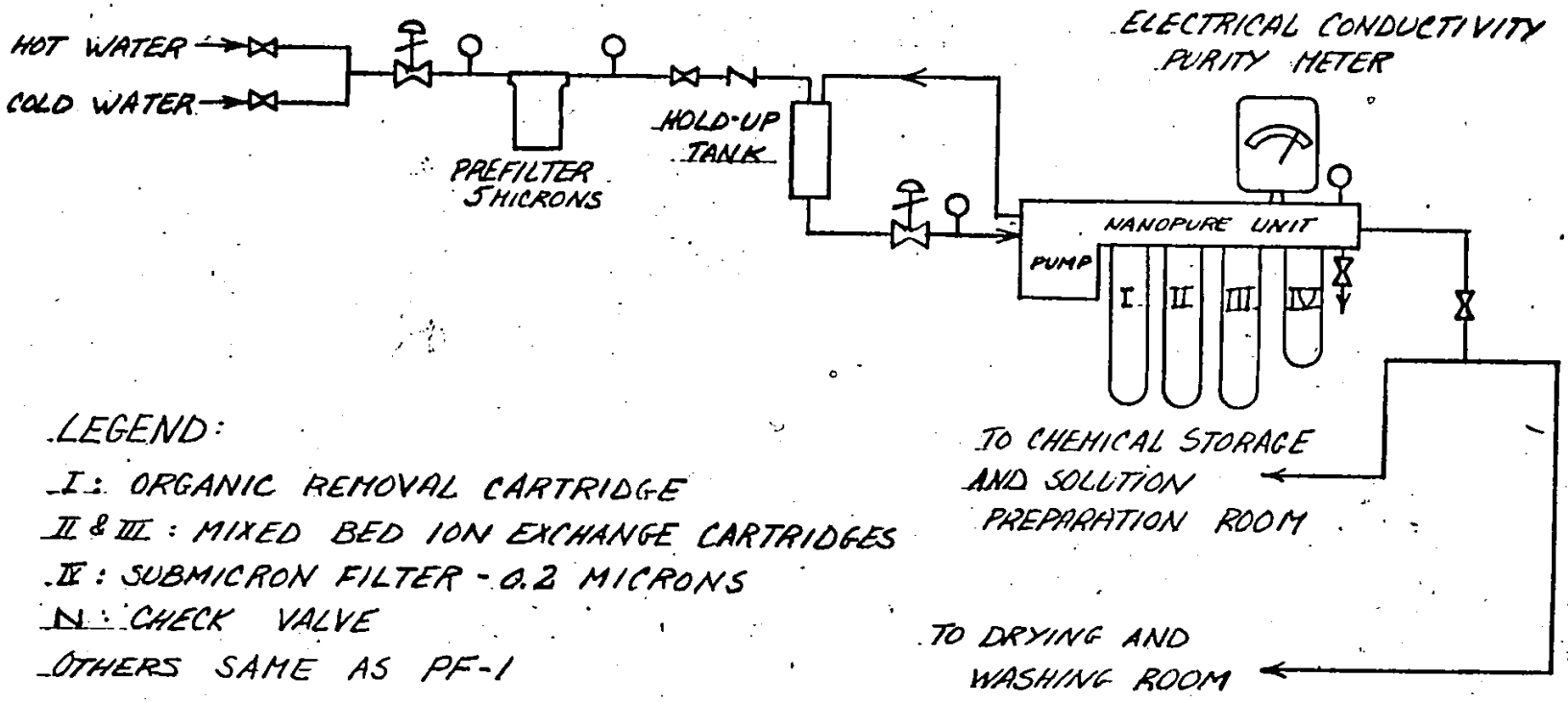

LEGEND:

I : ORGANIC REMOVAL CARTRIDGE
II & III : MIXED BED ION EXCHANGE CARTRIDGES
IV : SUBMICRON FILTER - 0.2 MICRONS
N : CHECK VALVE
OTHERS SAME AS PF-1

3.3 Design Drawings

In this section, equipment design drawings are presented.

DRAWING 1A - FIXING AND WASHING TANK DESIGN

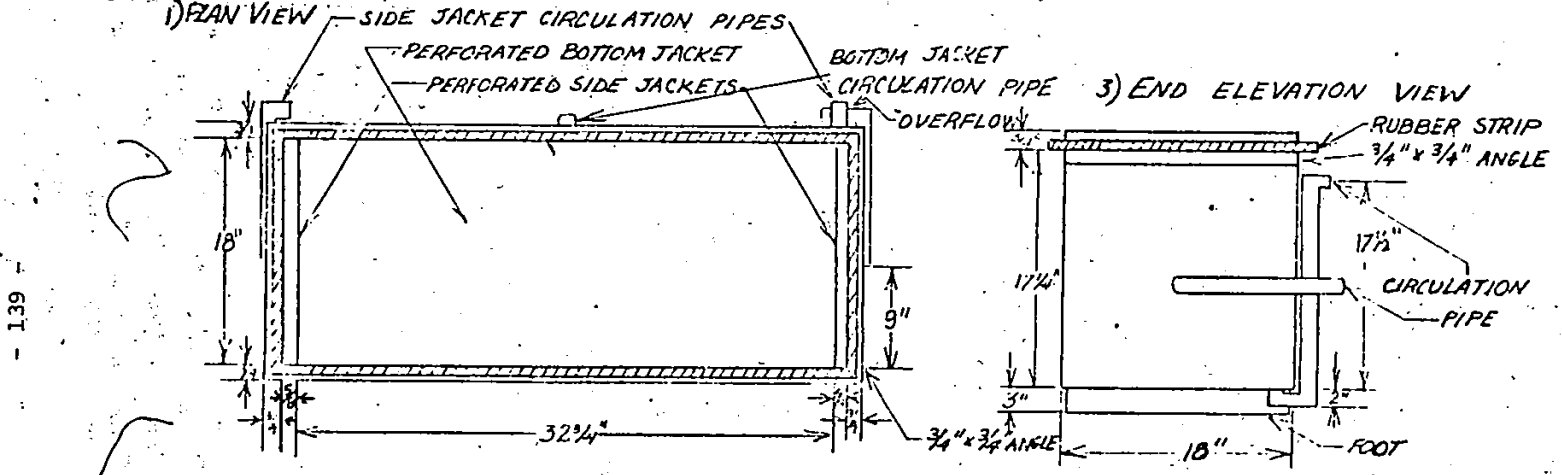

NOTES:

1. ALL CONSTRUCTION MATERIALS ARE TYPE 304 STAINLESS STEEL
2. JACKETS AND WALLS ARE 1/16" THICK (16 GAUGE)
3. CIRCULATION PIPES ARE ⅞" OD AND ½" NOMINAL ID
4. JACKETS ARE SPOT WELDED TO THE INTERIOR OF THE TANKS.
5. SUPPORT ANGLES ARE WELDED TO THE EXTERIOR
6. SEE DRAWINGS 1C AND 1D FOR DESIGN DETAILS OF JACKETS
7. QUANTITY: 5 TANKS

DRAWING 1B. PROCESSING TANK LID.

1. PLAN VIEW

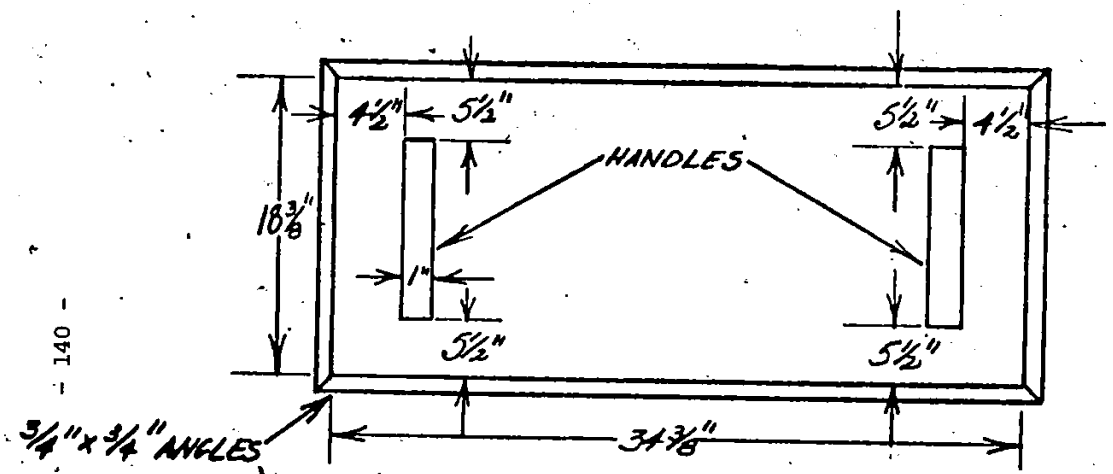

2. SIDE ELEVATION VIEW

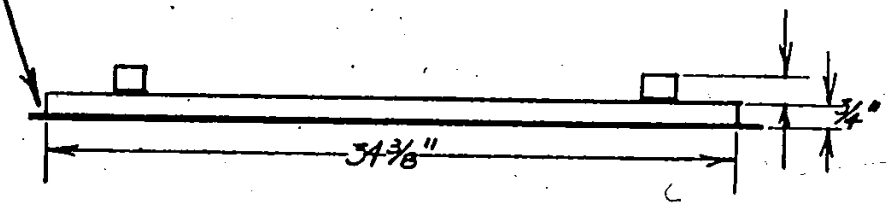

3. END ELEVATION VIEW

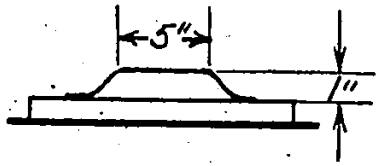

NOTES: 1. ALL CONSTRUCTION MATERIALS ARE TYPE 304 STAINLESS STEEL.

2. LIDS OF ALL PROCESSING TANKS ARE IDENTICAL EXCEPT FOR DEVELOPING TANKS.

DRAWING IC.- PERFORATED END JACKET OF FIXING AND WIISHING TANKS

1. END ELEVATION VIEW

2. SIDE ELEVATION VIEW

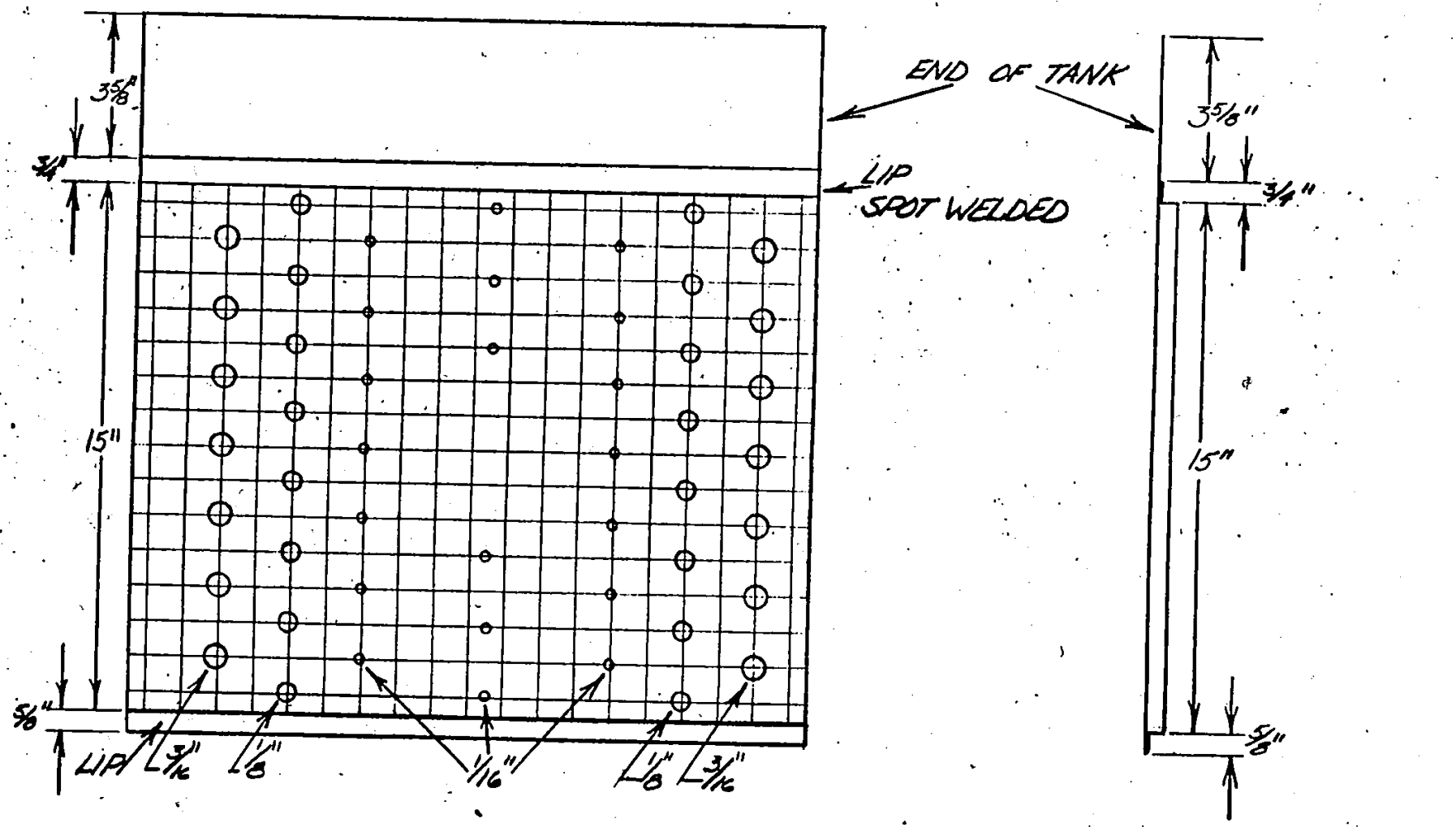

NOTES : 1. MATERIAL OF CONSTRUCTION IS 16 GAUGE TYPE 304 STAINLESS STEEL

2. SCALE : 1 SQUARE = 1" x 1"

DRAWING 10 - PERFORATED BOTTOM JACKET OF FIXING AND WASHING TANKS

1. PLAN VIEW

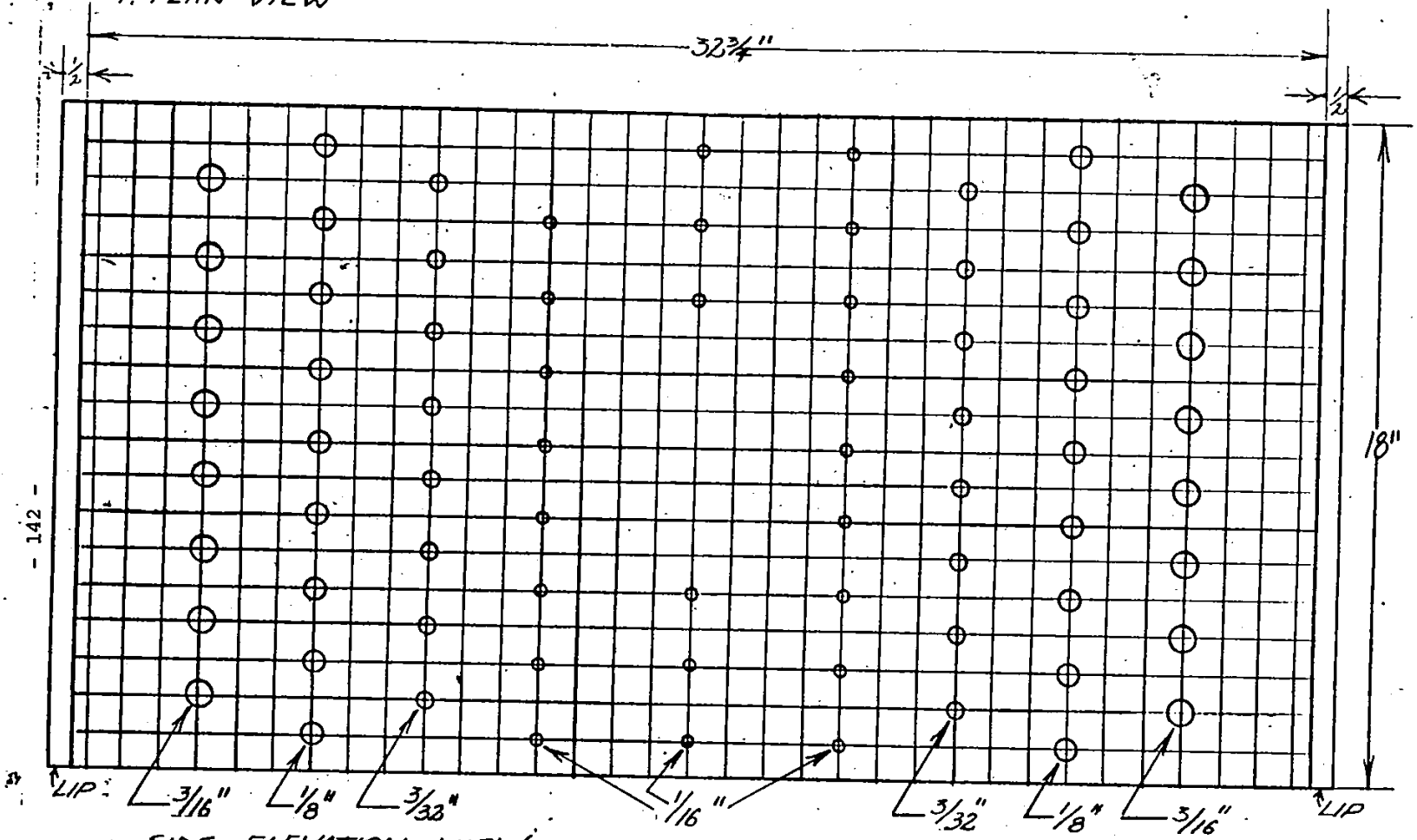

2. SIDE ELEVATION VIEW

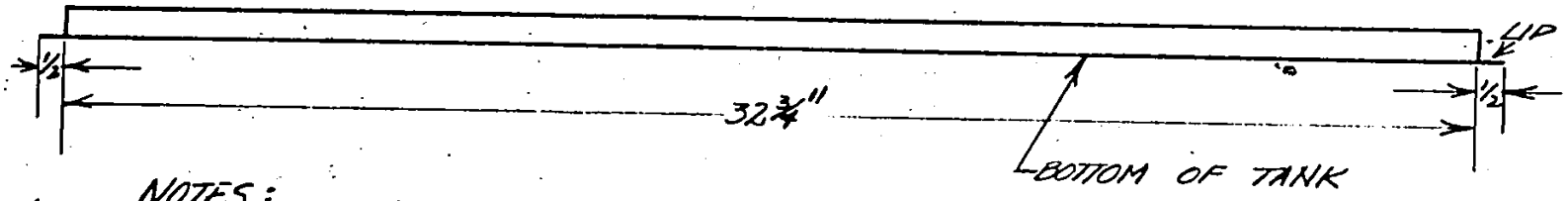

NOTES:

1. CONSTRUCTION MATERIAL IS 16 GAUGE TYPE 304 STAINLESS STEEL
2. SCALE : 1 SQUARE = 1" x 1"

DRAWING 2 - PRESOAK, STOP BATH AND DRYING TANK DESIGN

1. PLAN VIEW

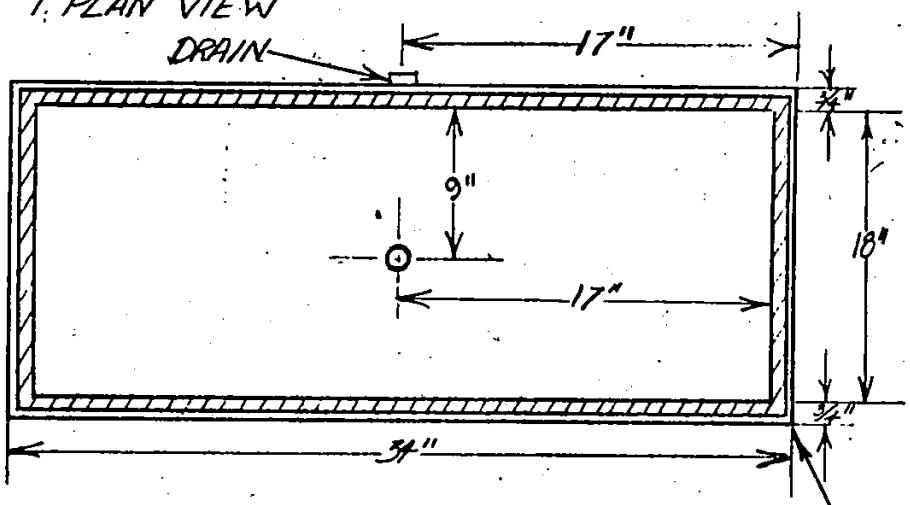

3. END ELEVATION VIEW

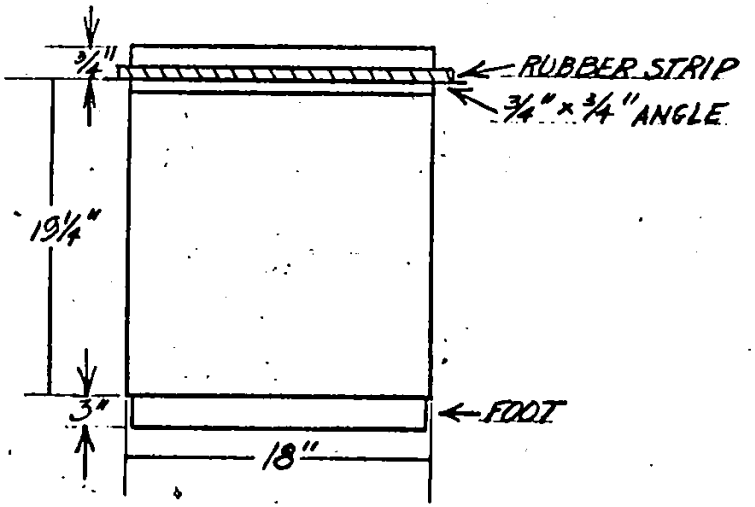

2. SIDE ELEVATION VIEW

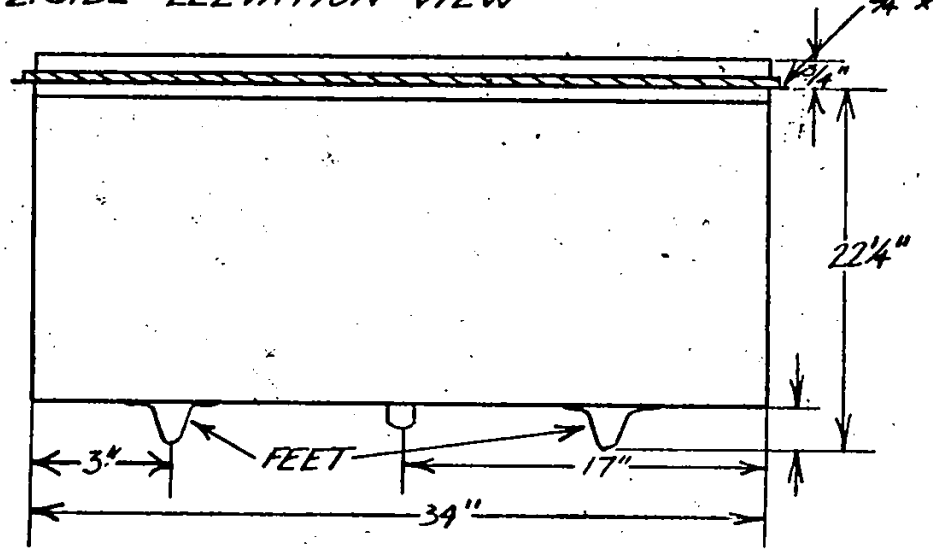

NOTES

1. ALL CONSTRUCTION MATERIALS ARE 16 GAUGE TYPE 304 STAINLESS STEEL.
2. DRAIN PIPE IS 7/8" O.D. AND 1/2 NOMINAL I.D.
3. QUANTITY: 5 TANKS

DRAWING 3' DEVELOPING TANK DESIGN

1. PLAN VIEW

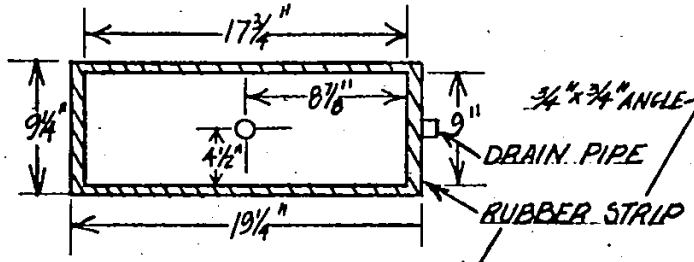

2. SIDE ELEVATION VIEW

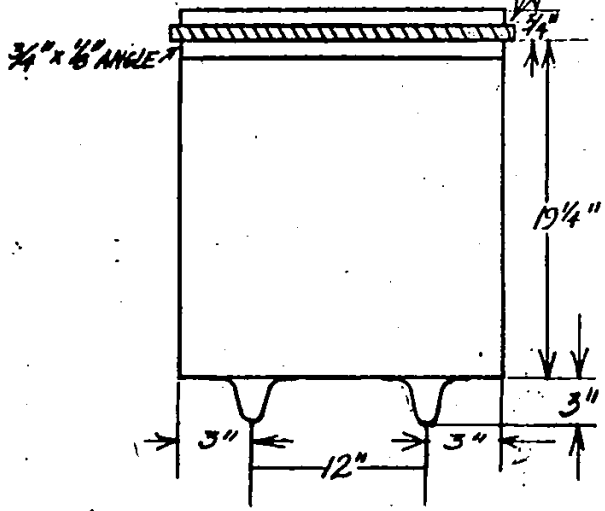

3. END ELEVATION VIEW

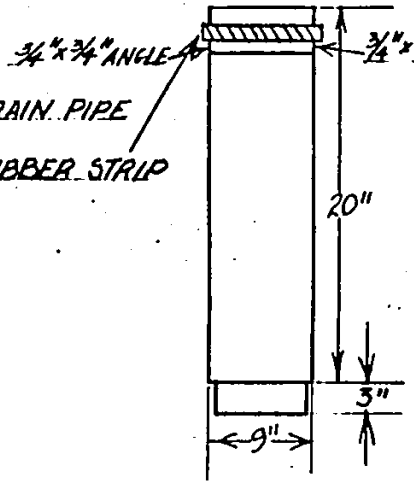

4. PLAN VIEW OF LID

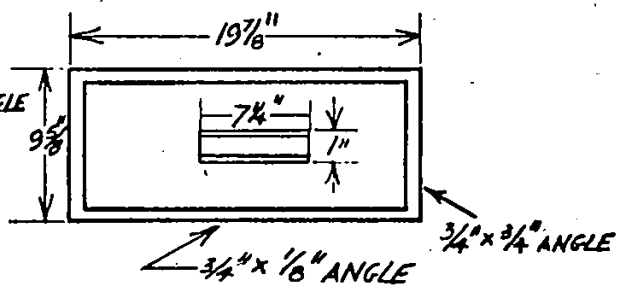

5. SIDE ELEVATION VIEW OF LID

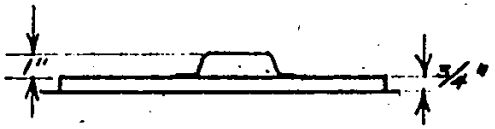

NOTES:

1. ALL CONSTRUCTION MATERIALS ARE TYPE 304 16 GAUGE STAINLESS STEEL.
2. DRAIN PIPE IS ⅞" O.D. AND ⅛" NOMINAL I.D.
3. QUANTITY: 4 TANKS

DRAWING 3A

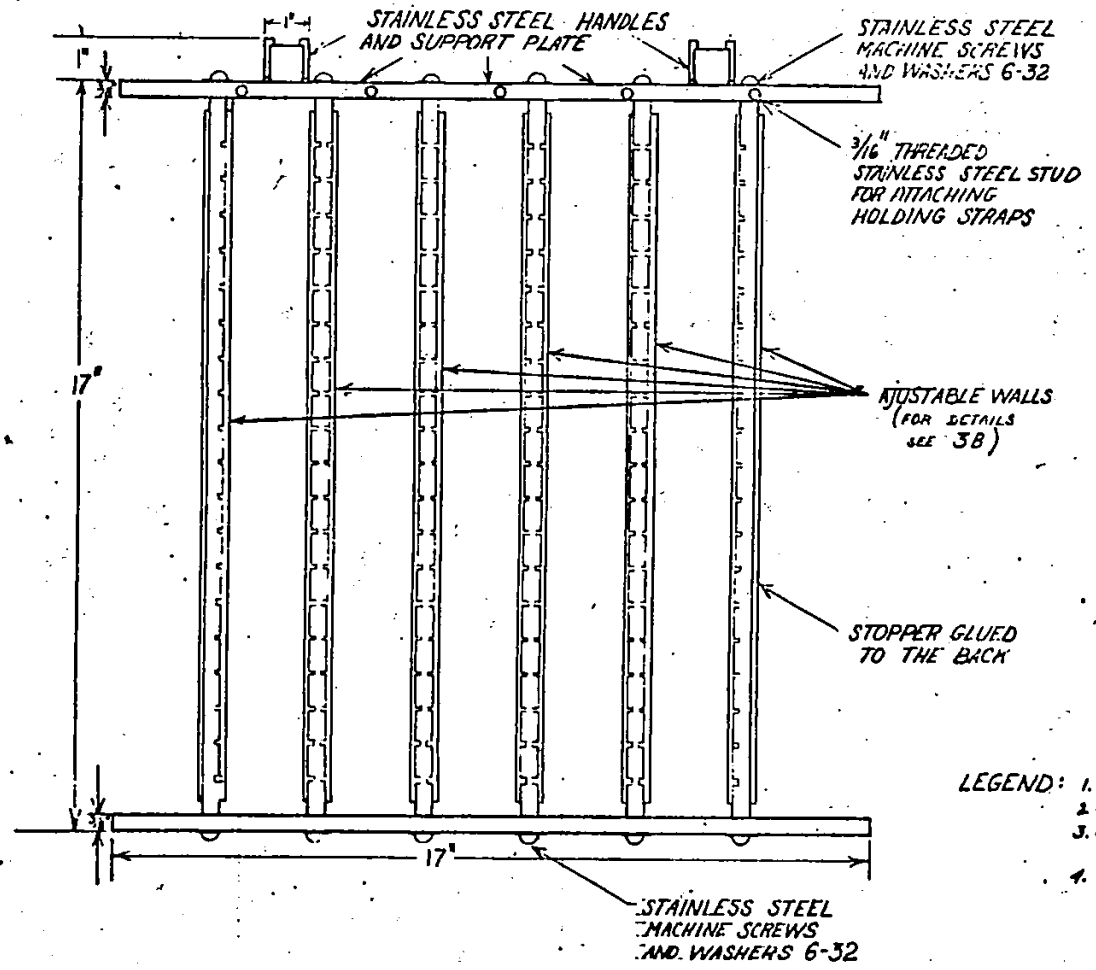

FRONT ELEVATION VIEW OF HORIZONTAL EMULSION PROCESSING RACK.

LEGEND: 1. MATERIAL OF CONSTRUCTION IS PLEXIGLASS
2. STAINLESS PLATES AND STRAPS ARE 1/16" TYPE 304
3. MACHINE SCREWS, WASHERS, NUTS AND STUDS ARE TYPE 6-18
4. QUANTITY : 18 RACKS

DRAWING 3B.- DETAILS OF AJUSTABLE WALLS OF HORIZONTAL EMULSION PROCESSING RACK.

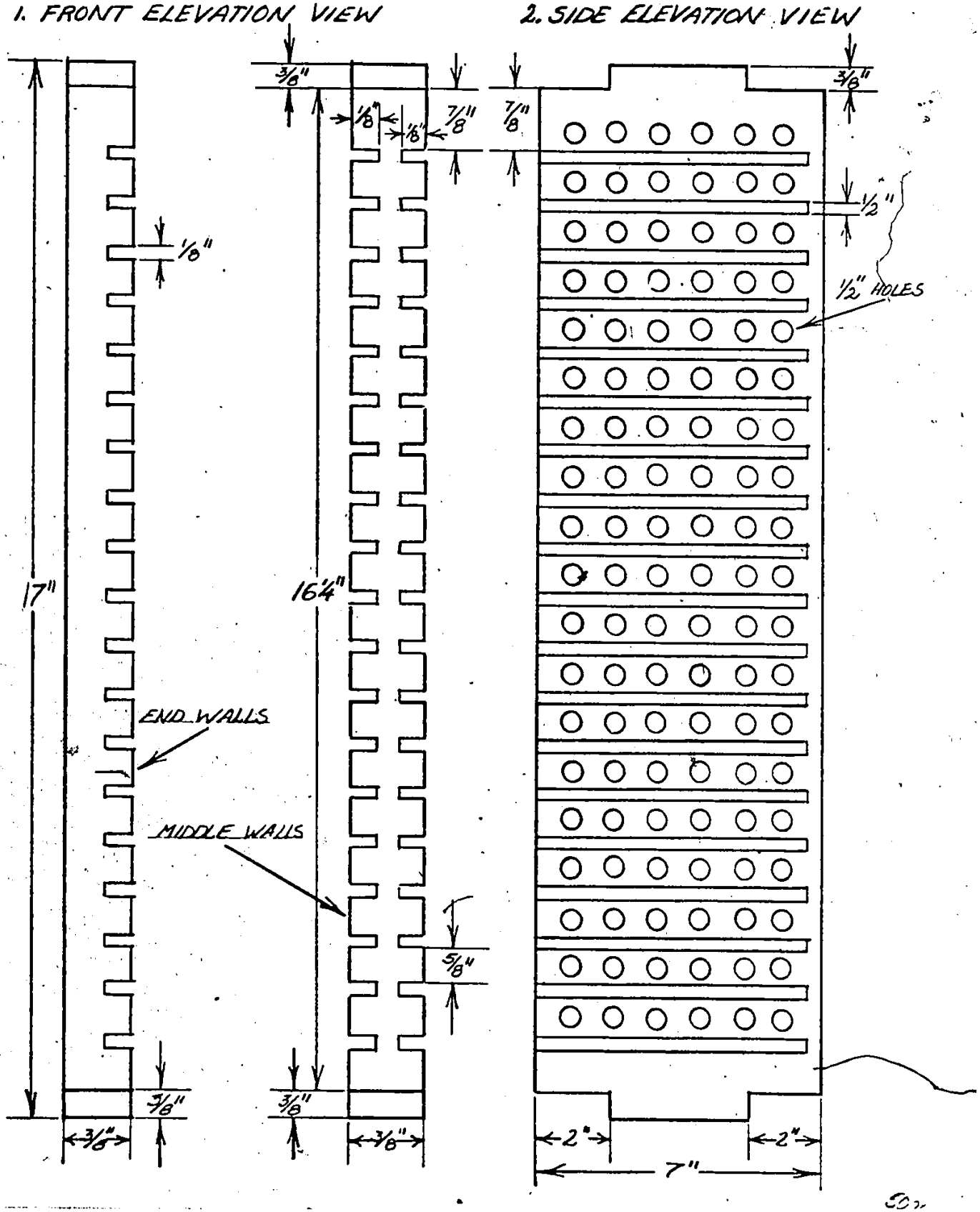

DRAWING 3C

PLAN VIEW OF HORIZONTAL EMULSION PROCESSING RACK.

1. TOP

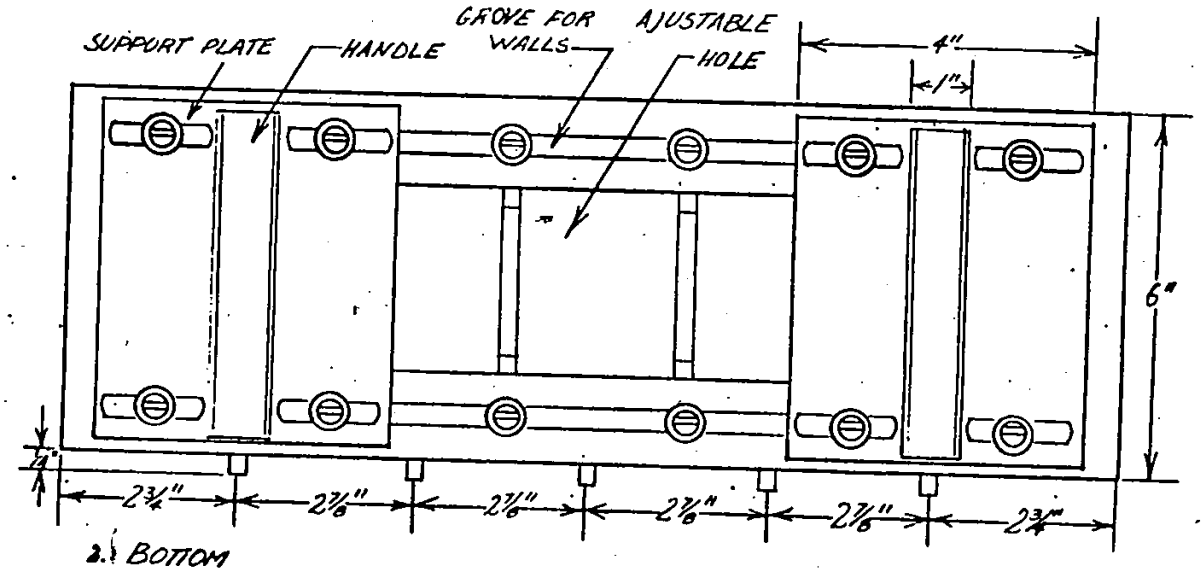

2. BOTTOM

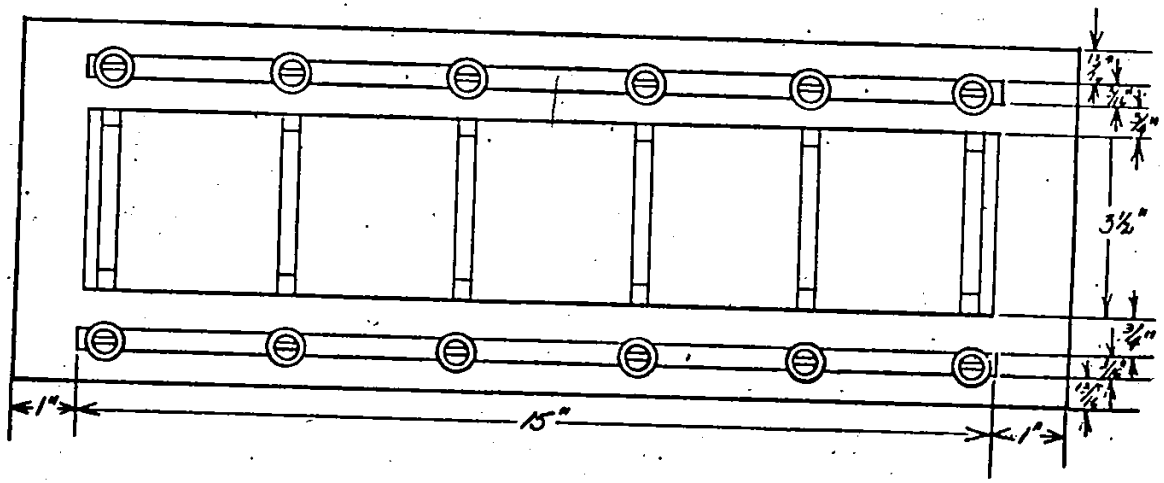

NOTE: TOP AND BOTTOM ARE THE SAME DIMENSIONS.

DRAWING 4A - FRONT ELEVATION VIEW OF

VERTICAL EMULSION
PROCESSING RACK

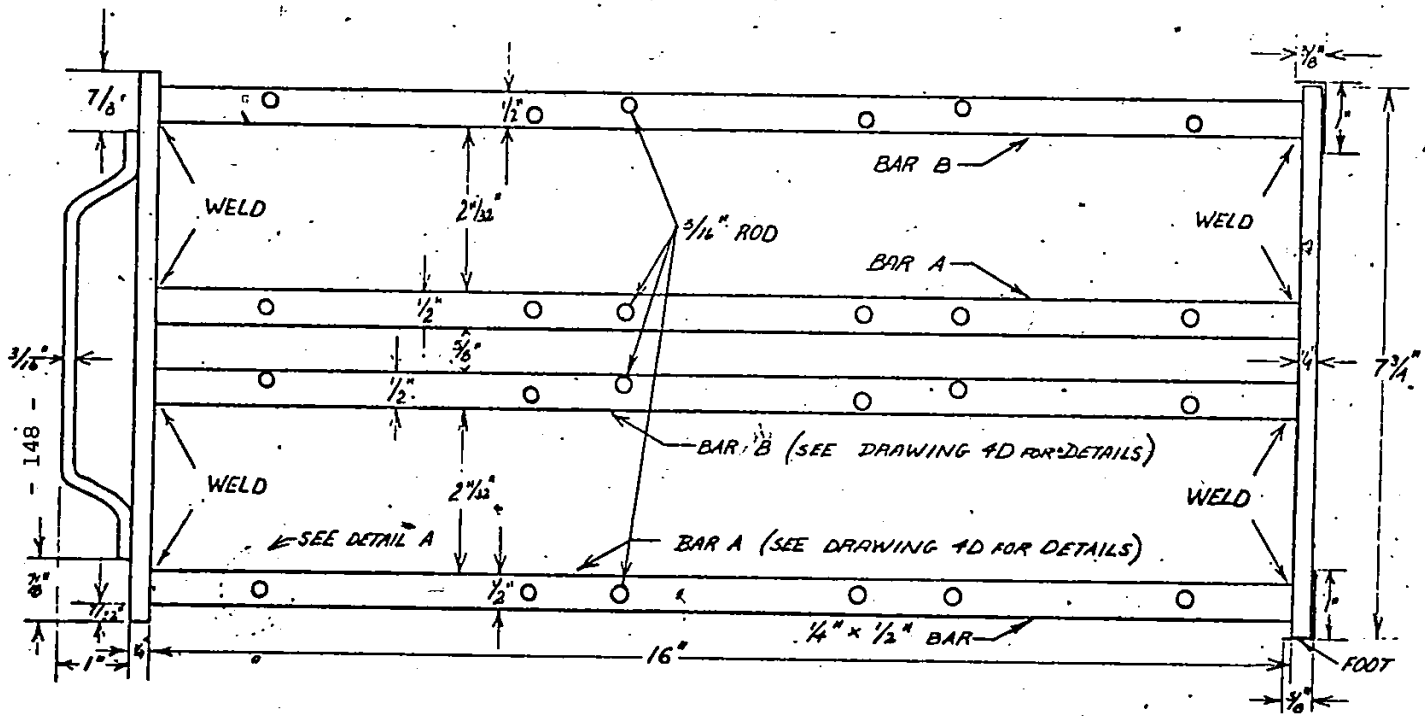

NOTES:

1. ALL CONSTRUCTION MATERIALS ARE TYPE 304 STAINLESS STEEL.
2. SUPPORT FRAME IS 1/4" x 1/2" BAR.
3. HORIZONTAL RODS ARE 3/16" DIAMETER.
4. FEET ARE MADE FROM 16 GAUGE SHEET.
5. QUANTITY: 8

DRAWING 4B - PLAN VIEW OF VERTICAL EMULSION PROCESSING RACK

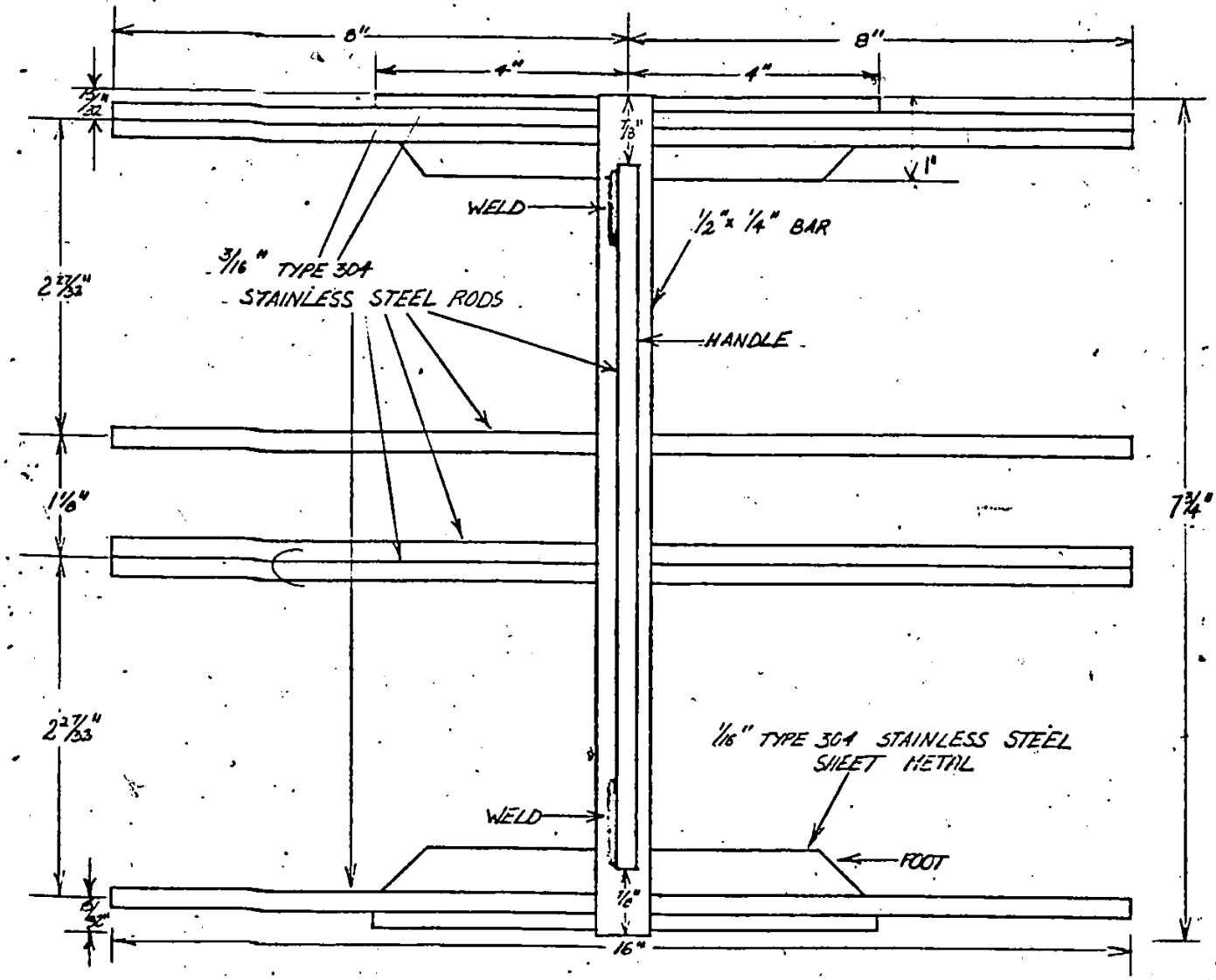

DRAWING-4D DETAILS OF BARS A AND B

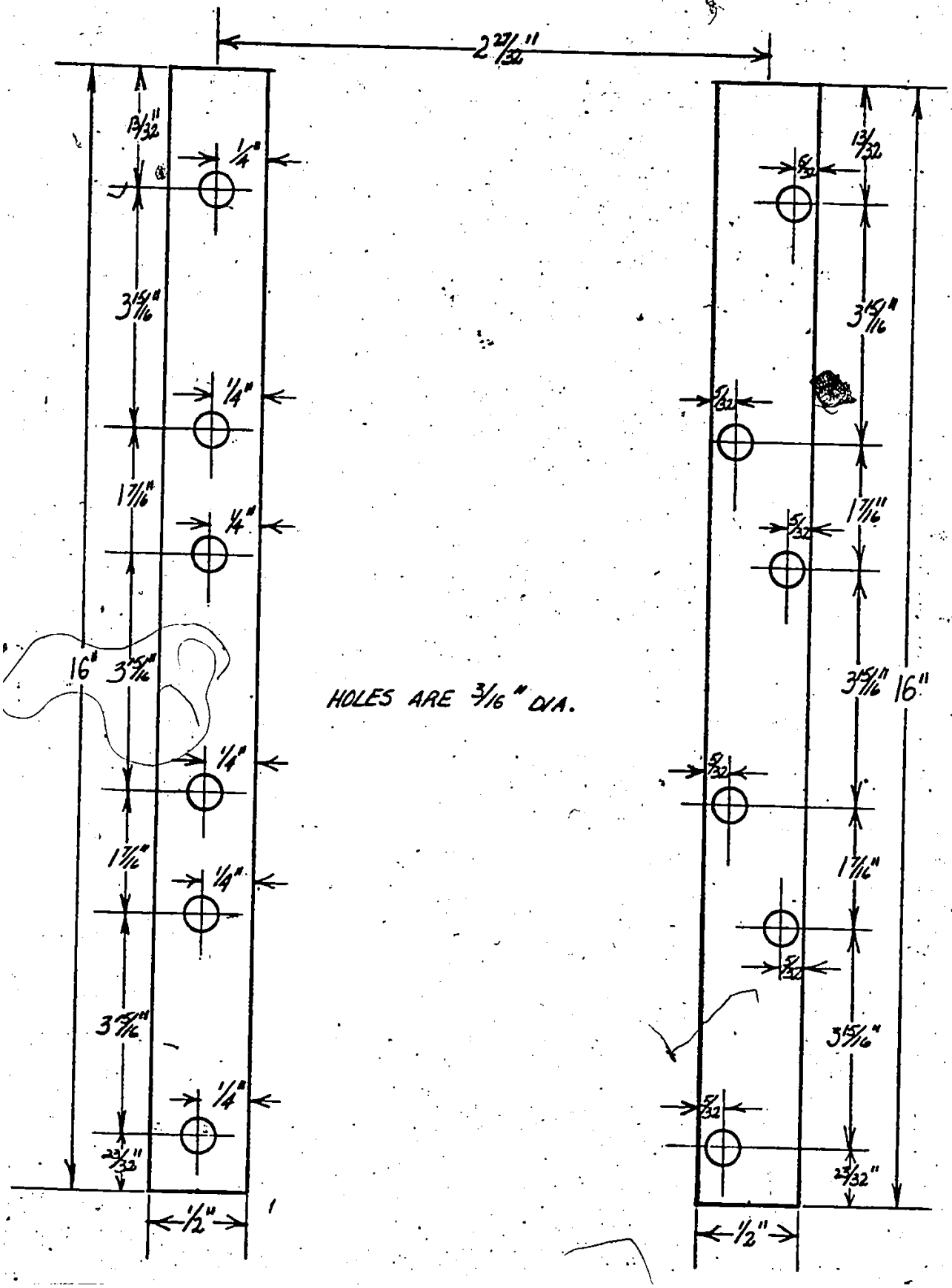

DRAWING 5A - PLAN VIEW OF FIXING JACKET TANK

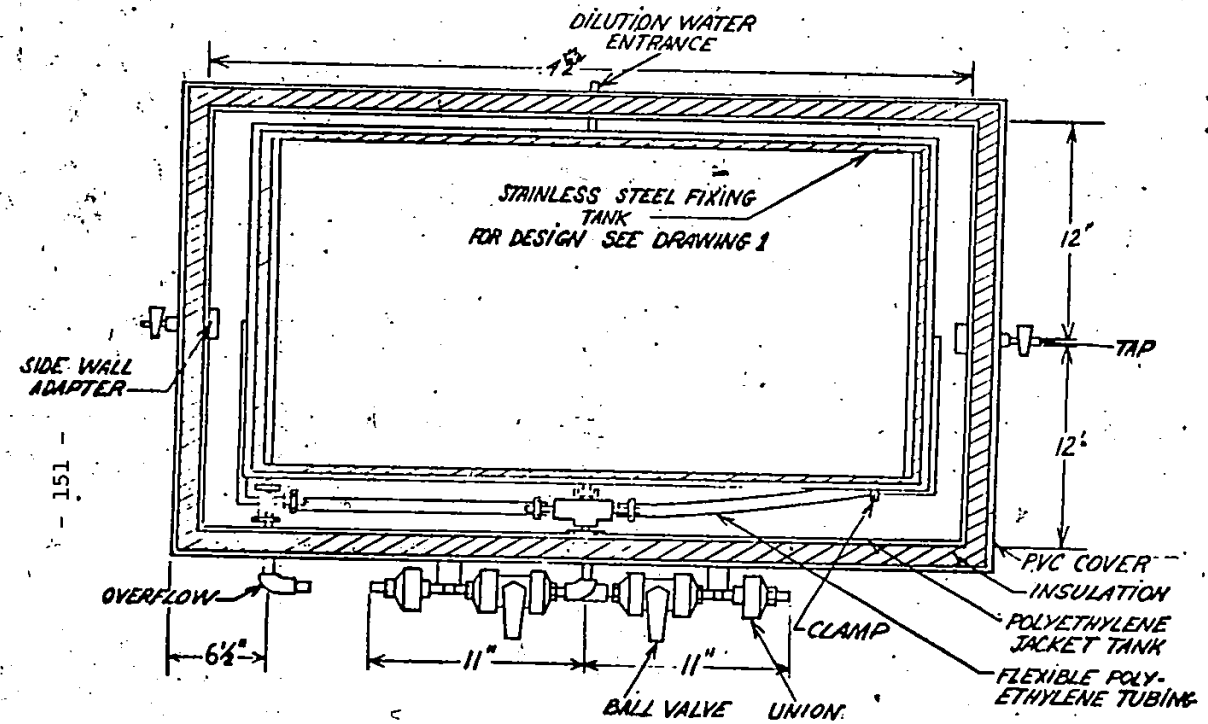

NOTES :,

1. JACKET TANKS ARE RECTANGULAR POLYETHYLENE 42" x 24" x 24" x 3/16".
2. INSULATION IS STYROFOAM S.M. 1½" THICK
3. PVC COVERING IS 1/8" THICK SHEET.
4. BALL VALVES, UNION, ELBOWS. TEES ARE ½" PV SIDE WALLS ADAPTERS ARE PVC.
5. EXTERIOR PIPING IS PVC. INTERIOR PIPING IS FLEXIBLE TUBING AND STAINLESS STEEL
6. JACKET TAPS ARE ¾" POLYETHYLENE.
7. STOP BATH, PRESOAK AND DRYING JACKET TANKS ARE IDENTICAL TO FIXING JACKET TANK EXCEPT THAT CIRCULATION, OVERFLOW AND DILUTION SYSTEMS ARE NOT INCLUDED.
8. QUANTITY: THREE FIXING JACKET TANKS. SIX NON-FIXING JACKET TANKS.

DRAWING 5B - SIDE ELEVATION VIEW OF FIXING JACKET TANK.

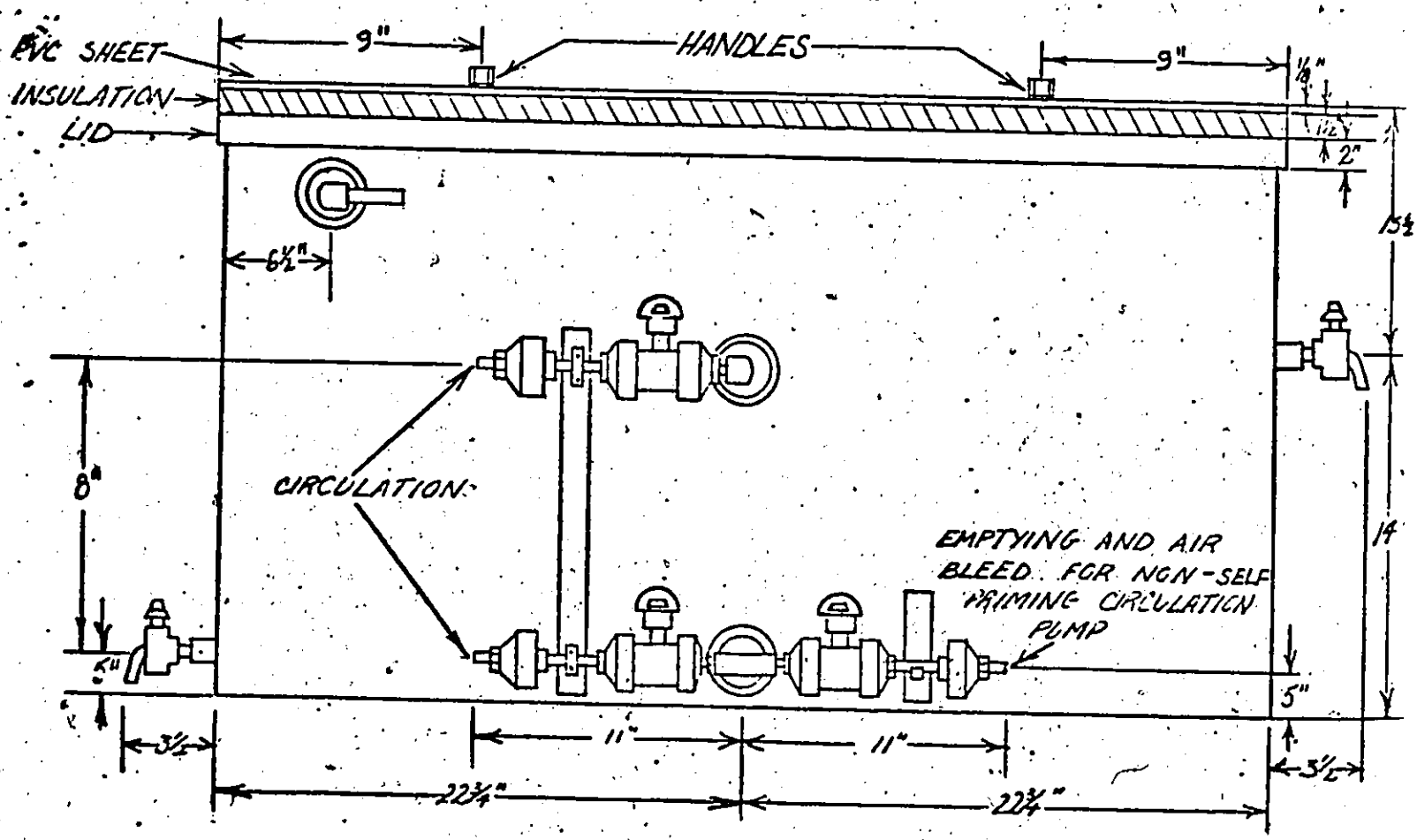

DRAWING 5C - END ELEVATION VIEW OF FIXING JACKET TANK.

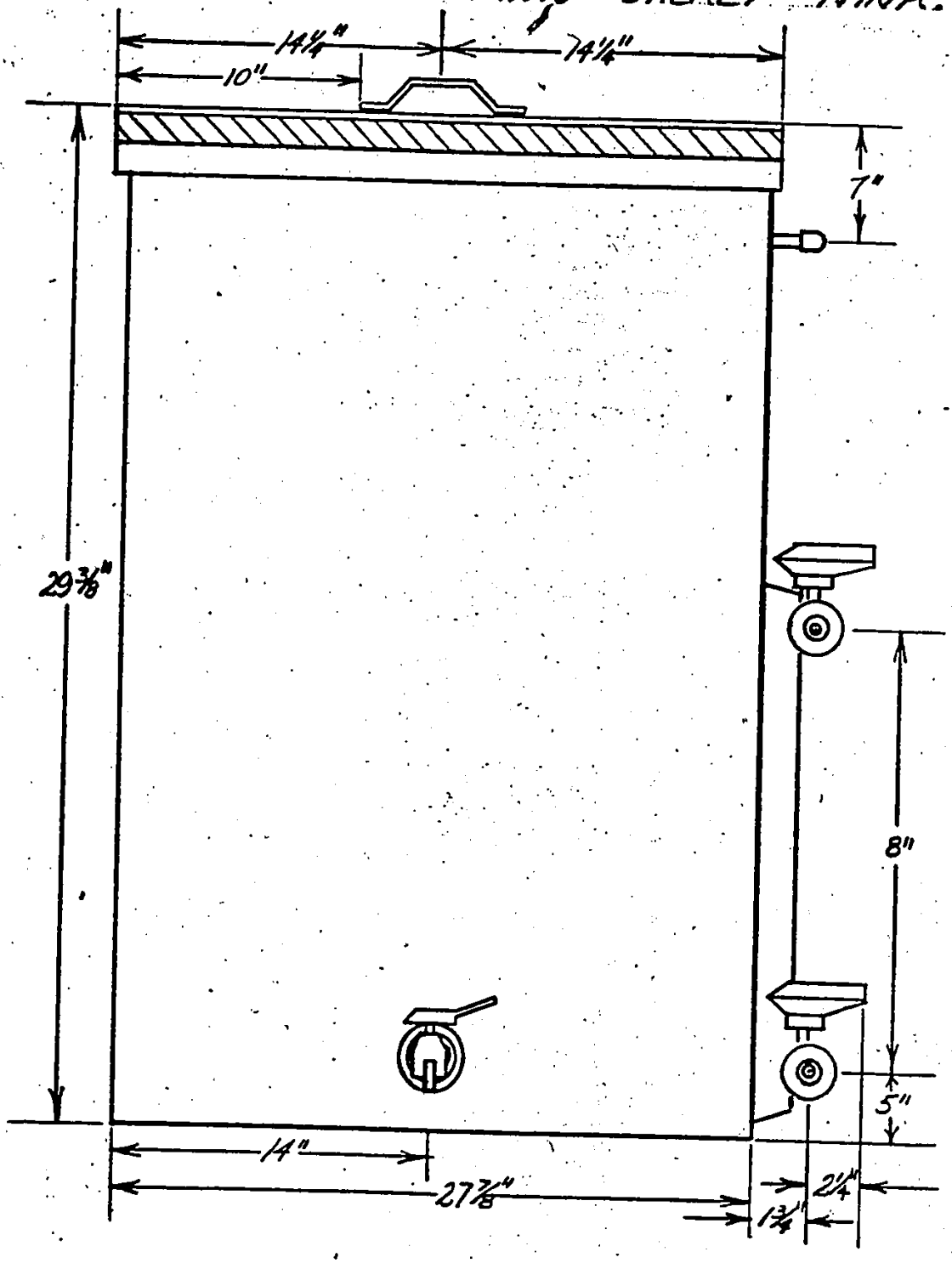

DRAWING 6A. PLAN VIEW OF WASHING TANK DESIGN.

NOTES: 1. VALVES, UNIONS, ELBOWS AND PIPING ARE ½" PVC.

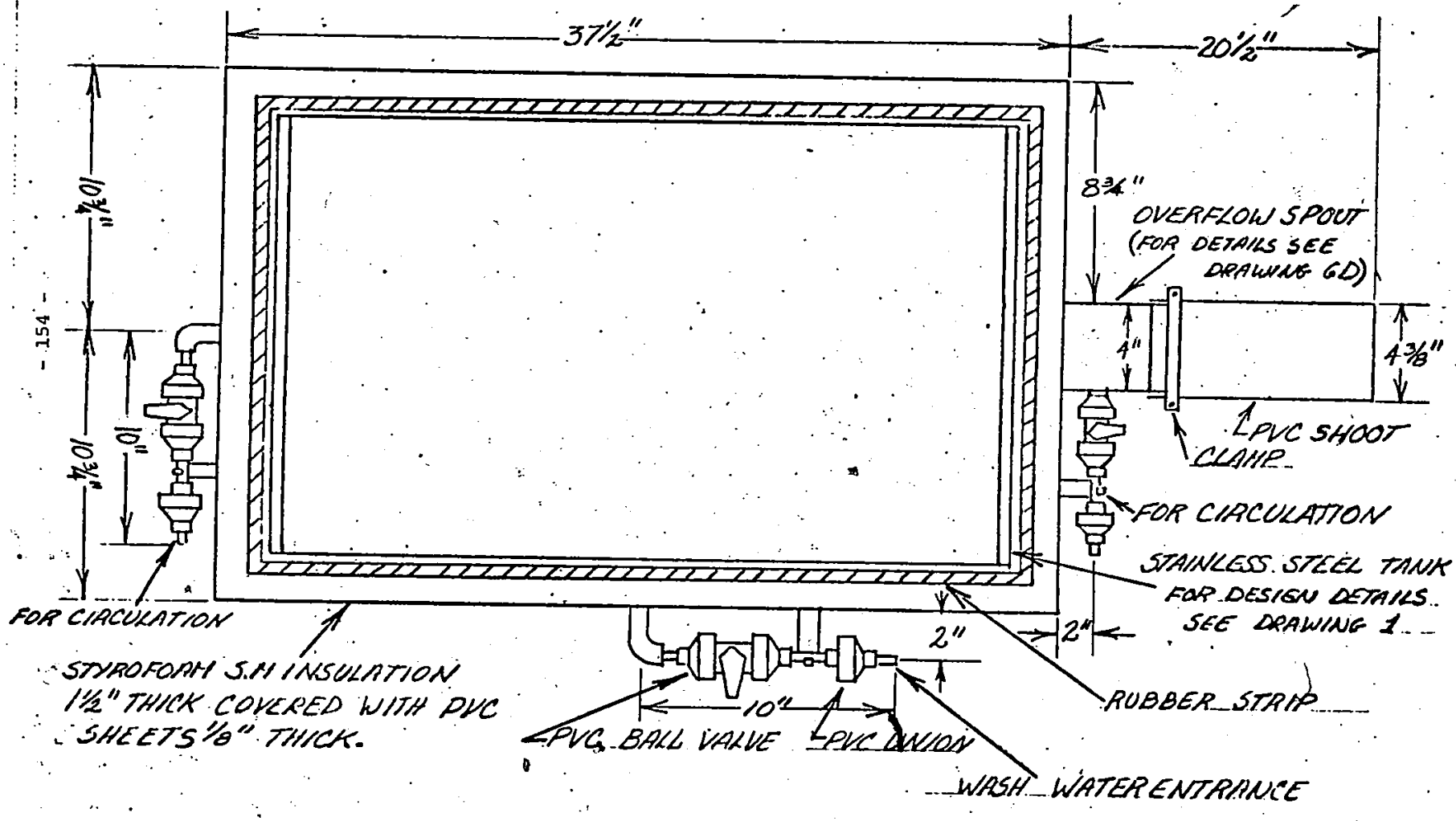

DRAWING 6B:- SIDE ELEVATION VIEW OF WASHING TANK

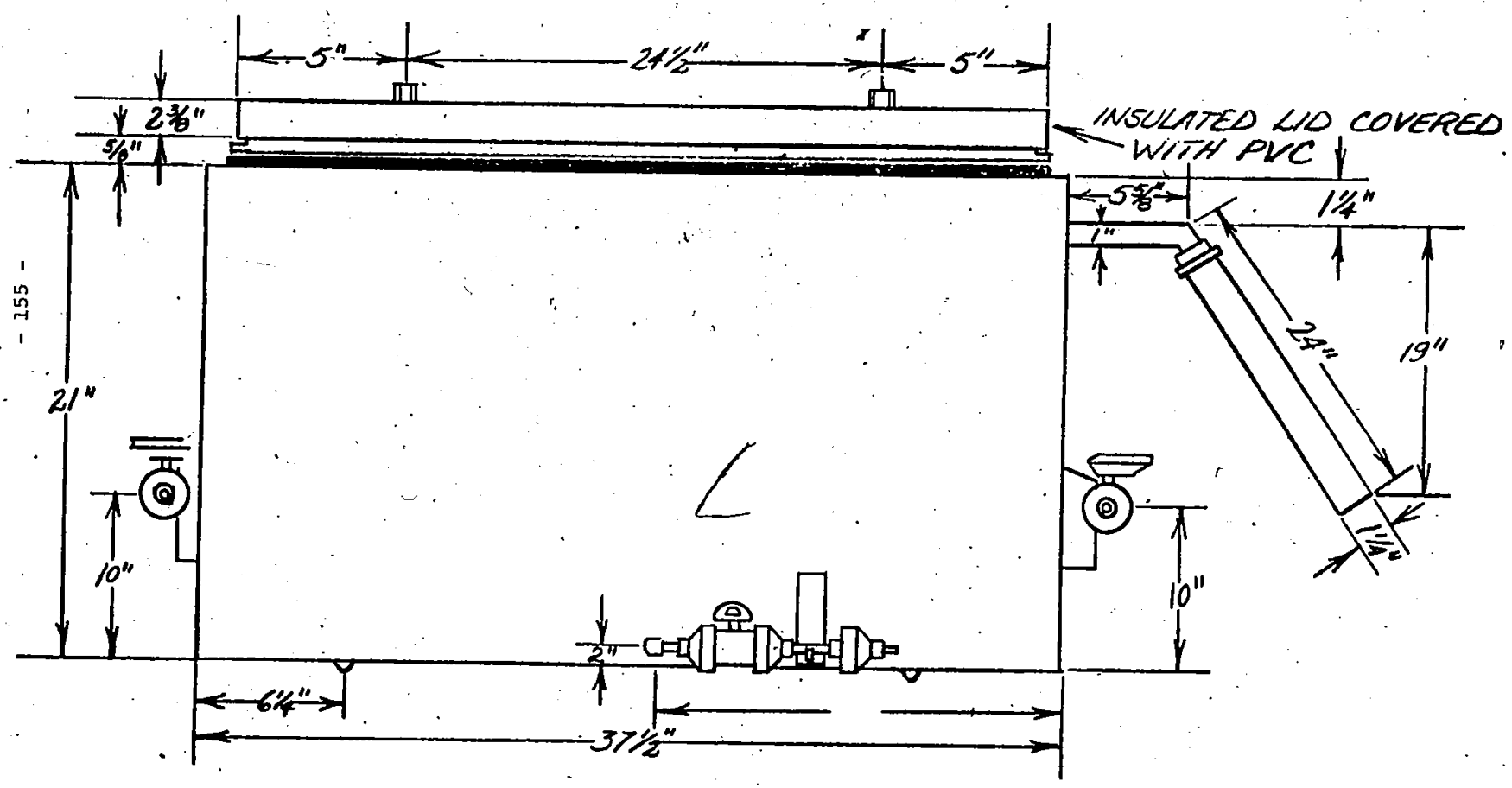

11

DRAWING 6C. - END ELEVATION VIEW OF WASHING TANK.

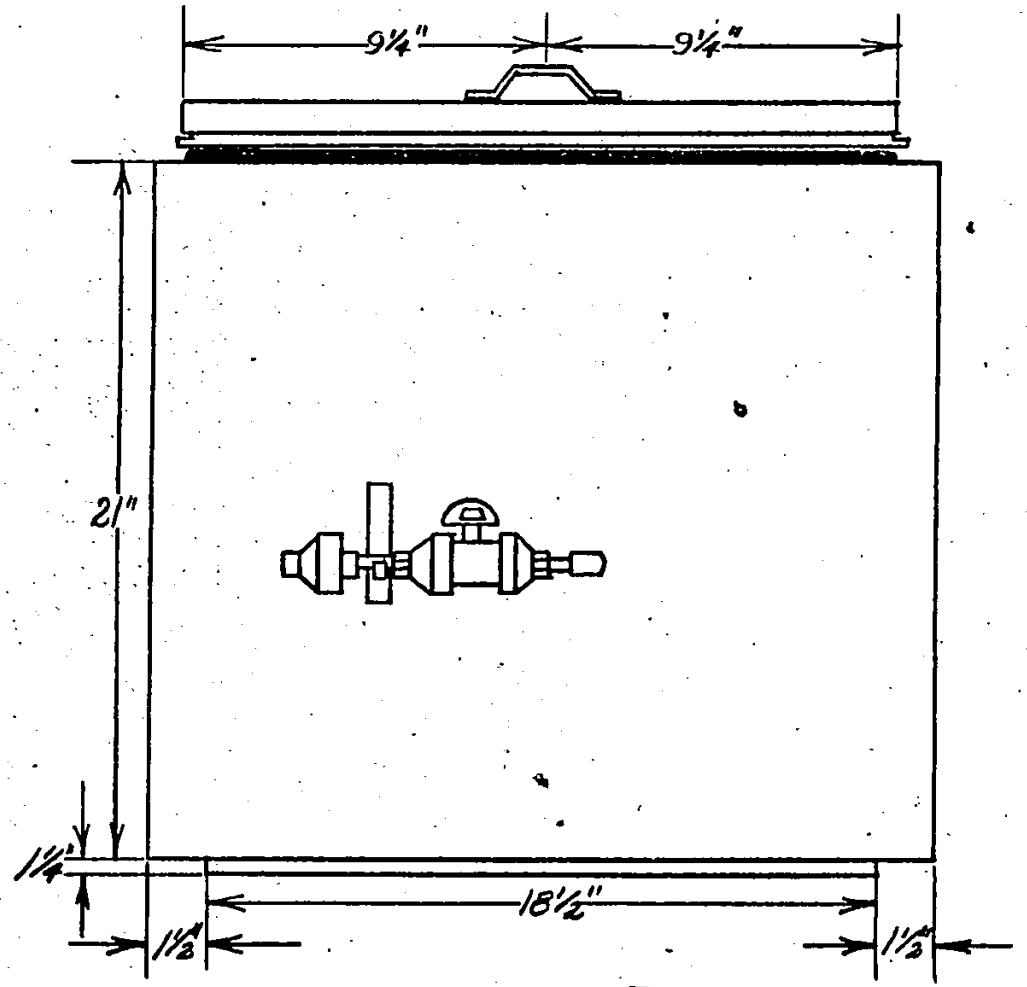

DRAWING 6D.- OVERFLOW SPOUT FOR WASHING TANK.

1. REAR ELEVATION

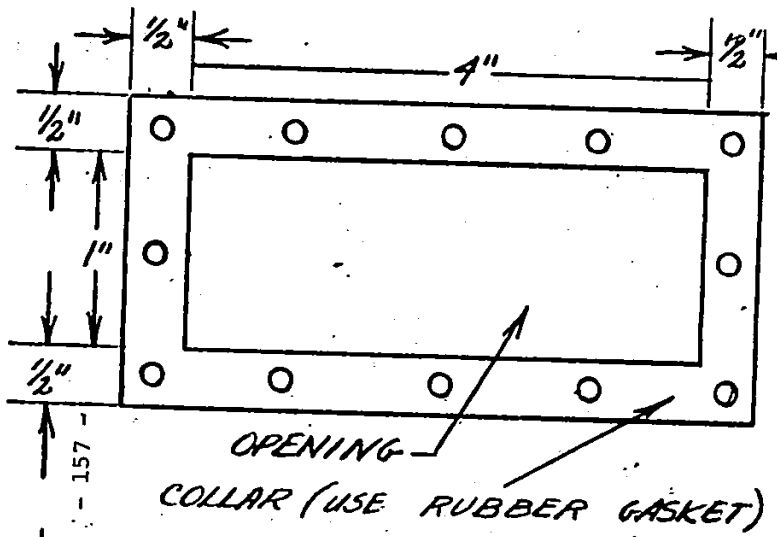

2. SIDE ELEVATION

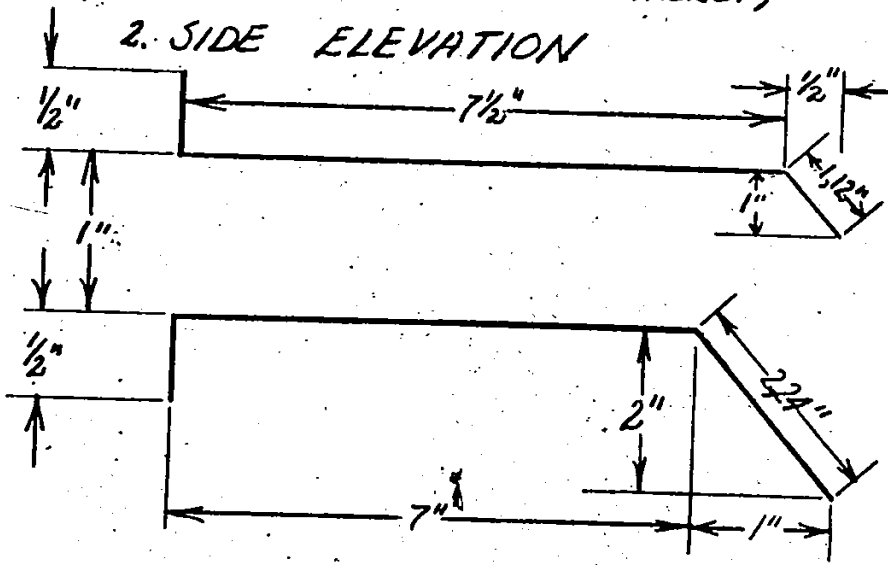

3. PLAN VIEW

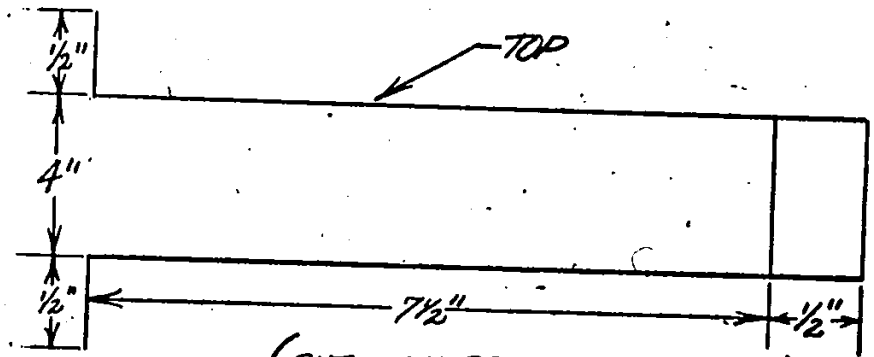

(PUT COVER ON THE TOP)

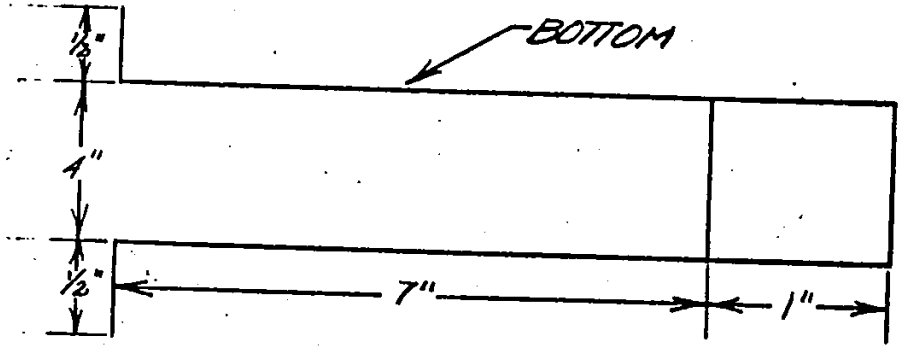

NOTES : ALL MATERIALS OF CONSTRUCTION TO BE TYPE 304 STAINLESS STEEL.

DRAWING 7A.- PLAN VIEW OF DEVELOPING JACKET TANK

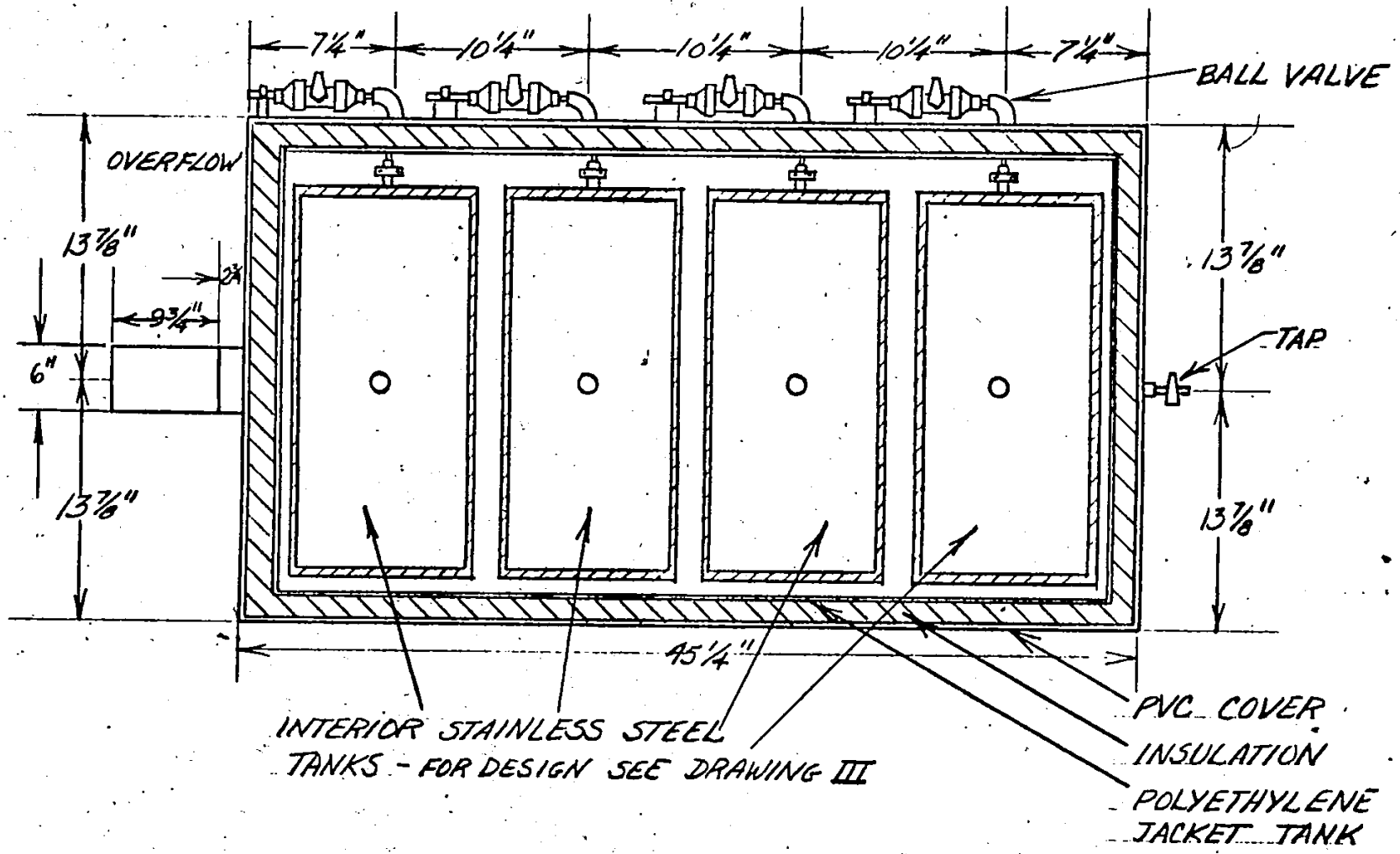

NOTES: 1 TO 5.- IDENTICAL TO THOSE IN DRAWING 5A
6. OVERFLOW IS MADE FROM TYPE 304 STAINLESS STEEL.
7. QUANTITY : 1 TANK.

DRAWING 7B.- SIDE ELEVATION VIEW OF DEVELOPING JACKET TANK.

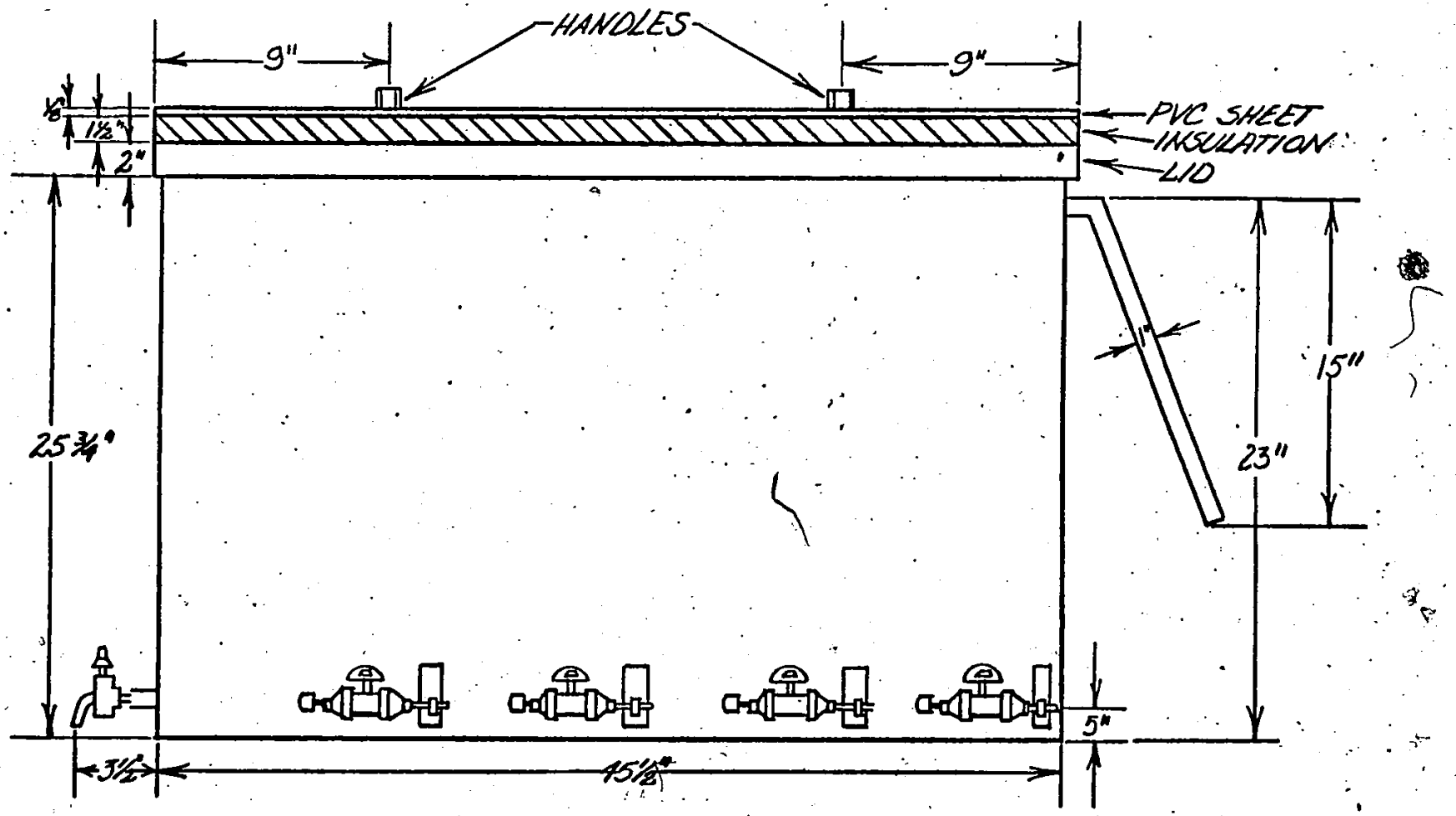

CONCLUSIONS

1) In the delta-ray energy distribution expression $N(E)\,dE = KE^{-2}\,dE$, K is a distribution parameter rather than a constant. This parameter is dependent upon the incident particle energy, varying with incident particle speed as $1/v^2$. Thus K's variation with incident particle speed is identical to the variation, with incident particle speed, of the average rate of energy loss of the incident particle.

2) The variation, with incident particle energy, of the number of latent image producing delta-rays is identical to the variation, with incident particle energy, of the delta-ray energy distribution parameter K and thus identical to the variation of the rate of incident particle energy loss.

3) In the developing stage, the silver grain growth rate varies exponentially with the development reaction redox potential. This growth rate is reduced to zero by lowering the pH until the redox potential is zero.

4) Developing stage, temperature control of $\pm 0.5^{\circ}C$ is adequate for low temperature development (5 - $7^{\circ}C$).

5) In the Bristol developing solution - Tables I and II - sodium sulfite and sodium metabisulfite combine to form a buffer, controlling the pH at 6.6 ± 0.1. Sodium sulfite also removes the dissolved oxygen but must be added before the other components since the hydrolysis of its anion provides the necessary alkalinity for the oxygen removal.

6) Temperature control of ± 1.0°C is adequate for low temperature fixing (5 - 7°C).

7) The fixing rate is diffusion controlled for nuclear track emulsion films.

8) The steady-state fixing rate is equal to the rate of discharge of $Ag(S_2O_3)_2^{3-}$ from the emulsion pellicles.

9) The differential steady-state fixing rate varies from zero at the base of a pellicle to a maximum at emulsion fixer interface, the differential fixing rate being a measure of the departure from chemical equilibrium of the reacting species. Thus the reacting species are in chemical equilibrium at the base.

10) Circulation in the fixing bath significantly increases the rate of fixing since it provides bulk mixing in the bulk fixer. This increases the rate discharge of $Ag(S_2O_3)_2^{3-}$ from the emulsion pellicles.

11) In the fixing solution, sodium metabisulfite acts as a buffer, maintaining the pH at 4.5 throughout the five fixing substages. It also prevents the dissociation of thiosulfate anion in acidic aqueous solution.

12) The Fuji emulsion used in experiment E-531 at Fermilab was manufactured using a cold lime hydrolysis process.

13) Fixing substages 1 and 2 ($\frac{1}{4}$ and $\frac{1}{2}$-strength fixer) reduce the risk of corrosion of developed grains during the initial phases of fixing.

14) Low temperature processing is much longer but much safer for large scale processing since it reduces the risk of bubble formation by minimizing the swelling, thereby keeping the emulsion relatively hard.

APPENDIX A

Standard Chemical Kinetic, Equilibria and Thermodynamic Relationships Employed

Consider an arbitrary binary reaction

$$aA + bB \rightleftarrows cC + dD \quad \ldots\ldots \qquad (A - R1)$$

The equilibrium constant, K_{eq}, is

$$K_{eq} = \frac{[C]_e^c \; [D]_e^d}{[A]_e^a \; [B]_e^b} \quad \ldots\ldots \qquad (A - 1)$$

where:

$[\;\;]_e$ is the equilibrium activity.

The forward reaction rate, R_f, is

$$R_f = k_1 \; [A]^n \; [B]^n \quad \ldots\ldots \qquad (A - 2)$$

where k_1 is the forward rate constant and n and m are the orders of the reaction with respect to A and B, respectively.

The reverse reaction rate, R_B, is

$$R_B = k_{-1} \; [C]^{n^1} \; [D]^{m^1}$$

where k_{-1} is the reverse reaction rate constant and n^1 and m^1 are the orders of the reaction with respect to C and D, respectively.

The net reaction rate, R_N, is the difference between the forward and reverse rates.

$$R_N = \text{Forward Rate} - \text{Reverse Rate}$$

$$= k_1 [A]^n [B]^m - k_{-1} [C]^{n^1} [D]^{m^1} \quad \ldots\ldots \quad (A - 4)$$

where

$$R_N = -\frac{1}{a}\frac{d[A]}{dt} = -\frac{1}{b}\frac{d[B]}{dt} = \frac{1}{c}\frac{d[C]}{dt}$$

$$= \frac{1}{d}\frac{d[D]}{dt} \quad \ldots\ldots \quad (A - 5)$$

n, m, n^1 and m^1, the orders of reaction, must generally be determined experimentally but are usually integers or half-integers. They are, respectively, equal to a, b, c, and d, the stoichiometric coefficients, only when the reaction is an elementary unimolecular, bimolecular or termolecular process in which case the stoichometric coefficients are equal and equal to unity. Equilibrium is reached when the forward and reverse reaction rates are equal. The equilibrium constant is given by the principle of detailed balancing which says that, at equilibrium, the forward and reverse reaction rates are equal for each elementary process in the reaction mechanism. Consequently, for a reaction with L steps in the mechanism

$$K_{eq} = \frac{k_1^1 \; k_2^1 \; k_3^1 \cdots k_L^1}{k_{-1}^1 \; k_{-2}^1 \; k_{-3}^1 \cdots k_{-L}^1} \quad \ldots\ldots \quad (A - 6)$$

where k_L^1 and k_{-L}^1 are the forward and reverse rate constants for the L-th step of the mechanism.

The standard Gibbs free energy change, ΔG_r°, of a reaction is

$$\Delta G_r^\circ = \Sigma \Delta G_f^\circ \text{ (products)} - \Sigma \Delta G_f^\circ \text{ (reactants)} \quad \ldots \quad (A - 7)$$

where ΔG_f° is the standard Gibbs free energy of formation of a chemical species. It is the free energy change when a reactant or a product is formed from its elements in their standard states, their standard states being defined as their states at 298°K and 1-atmosphere pressure. The Gibbs free energy is, by definition, the thermodynamic state function

$$G \equiv H - TS \quad \ldots\ldots \quad (A - 8)$$

where H is the enthalpy, S is the entropy and T is the absolute temperature. For an isothermic reaction,

$$\Delta G_r^\circ = \Delta H_r^\circ - T \Delta S_r^\circ \quad \ldots\ldots \quad (A - 9)$$

and

$$K_{eq} = \exp \{ - \frac{\Delta G_r^\circ}{RT} \} \quad \ldots\ldots \quad (A - 10)$$

where ΔH_r° is the standard enthalpy of reaction, ΔS_r° is the standard entropy of reaction and R is the ideal gas constant.

The standard enthalpy of reaction is

$$\Delta H_r^o = \Sigma \Delta H_f^o \text{ (products)} - \Sigma \Delta H_f^o \text{ (reactants)} \quad \ldots \quad (A - 11a)$$

and the standard entropy of reaction is

$$\Delta S_r^o = \Sigma S_f^o \text{ (products)} - \Sigma S_f^o \text{ (reactants)} \quad \ldots \quad (A - 11B)$$

where ΔH_f^o and S_f^o are the standard enthalpies and entropies of formation of reactants and products. They are defined in a manner identical to that of the standard Gibbs free energy of formation.

Over a limited temperature range, the variation of the equilibrium constant is approximated by

$$K_{eq}^1 = K_{eq} \exp \{ - \frac{\Delta H_r^o}{R} \left(\frac{1}{T^1} - \frac{1}{T} \right) \} \quad \ldots\ldots \quad (A - 12)$$

The temperature range must be such that the standard enthalpy and entropy of reaction are approximately constant over the range.

Activity coefficients are a quantitative measure of the non-ideality of solutions of electrolytes. They are a measure of the restricted mobility of ionic species, relating concentration to activity as follows

$$a = f c \quad \ldots\ldots \quad (A - 13)$$

where c is concentration, a is activity and f is the activity coefficient. f is dimensionless factor. The exact form of all chemical equilibria

and rate expressions requires that activities rather than concentrations be used. The ionic strength, I, of a solution is defined as

$$I = \frac{1}{2} \sum_i c_i Z_i^2 \qquad \ldots\ldots \qquad (A - 13)^{22}$$

where Z_i and c_i are respectively, the charge and concentration of ion i and the summation is over all ionic species in the solution. The extended form of the Debye-Hückel equation

$$\log f = \frac{- 0.509 Z^2 \sqrt{I}}{I + 0.328a \sqrt{I}} \qquad \ldots\ldots \qquad (A - 14)^{23}$$

can be used to calculate the activities of individual ions in solution at 25°C where a is the "effective" size of the ionic species in aqueous solution. The reliability of equation A - 14 has been experimentally verified up to concentrations of 0.1 molar << In more concentrated solutions, the activity coefficients depend on the natures of the individual ions. A general rule for all ions of one charge is not available. Experimental values can sometimes be found, but may be very different in mixtures of electrolytes. For this reason, only approximate calculations are possible for equilibrium calculations in solutions of high ionic strength.>>[24]

[22] Ref. 10, pg. 92

[23] Ref. 10, pg. 94

[24] Ref. 10, pg. 96

APPENDIX B

A Detailed Discussion of the Chemical Reactions Occuring During the Preparation of Developer and the Developing Stage

a) Addition of Sodium Sulfite and Metabisulfite to Pure Water.

As indicated in Table IV, pure water becomes alkaline when sodium sulfite is added. At a concentration of 5.7×10^{-2} molar, its concentration in the developing solution, the pH is 9.8 ± 0.1. This alkalinity can be attributed to the hydrolysis of sulfite anion since sodium sulfite is the salt of sulfurous acid, a weak acid. Therefore, by definition,

$$[H_3O^+] = 10^{-pH} = 1.6 \times 10^{-10} \text{ gmoles-L}^{-1} \text{ @ } 5^\circ C$$

$$K_w^{25} = [OH^-]_e \, [H_3O^+]_e = 1.85 \times 10^{-15} \text{ gmoles}^2\text{-L}^{-2} \text{ @ } 5^\circ C$$

$$[OH^-]_e = \frac{K_w}{[H_3O^+]_e} = 1.2 \times 10^{-5} \text{ gmoles-L}^{-1} \text{ @ } 5^\circ C$$

The following reactions occur.

i) Dissociation of the salt

Sodium sulfite completely dissociates in aqueous solution.

$$Na_2SO_3 \text{ (s)} \rightarrow 2Na^+ \text{ (aq)} + SO_3^= \text{ (aq)} \quad .... \quad \text{(Ba - R1)}$$

ii) Hydrolysis of $SO_3^=$

[25] Ref. 8, pg. D-92

The sulfite anion hydrolyzes - reacts with water - as follows

$$SO_3^{=}\ (aq) + H_2O \rightleftarrows HSO_3^{-}\ (aq) + OH^{-}\ (aq) \quad .... \quad (Ba - R2)$$

base 1 acid 2 acid 1 base 2

for which the hydrolysis constant, K_h, is

$$K_h = \frac{[HSO_3^-]_e\ [OH^-]_e}{[SO_3^=]_e} \quad .... \quad (Ba - 1)$$

$$= \frac{K_w}{K_{a_2}} = 2.0 \times 10^{-9}\ \text{gmoles-L}^{-1} \text{ @ } 25^oC$$

K_{a_2} is the second dissociation constant of sulfurous acid and K_w is the equilibrium constant for the acid base reaction of water with itself (see reaction 2-R2, chapter 2)

$$K_w = [H_3O^+]_e\ [OH^-]_e \quad .... \quad (Ba - 2)$$

iii) Bisulfite-Metabisulfite Anion Equilibrium.

<< All known hydrogen sulfites are easily soluble and cannot be isolated in substance because of the equilibrium

$$2HSO_3^-\ (aq) \rightleftarrows S_2O_5^=\ (aq) + H_2O \quad .... \quad (Ba - R3)$$

which goes to the right on increasing concentration.>> [26] The equilibrium expression for the reverse reaction is

$$K_e = \frac{[HSO_3^-]_e^2}{[S_2O_5^=]_e} \quad .... \quad (Ba - 3)$$

[26] Ref. 7, pg. 879

Thus, if the bisulfite anion activity increases by a factor of 2, the metabisulfite anion activity increases by a factor of 4 to re-establish the equilibrium.

Consider now the addition of sodium metabisulfite to pure water. As indicated in Tables II d and V d, at a concentration of 1.44×10^{-2} molar, its concentration in the developing solution, the pH is 4.0 ± 0.1. This indicates that the solution is acidic. The following reactions occur.

i) Dissociation of the salt.

Sodium metabisulfite completely dissociates in aqueous solution.

$$Na_2 S_2 O_5 (s) \rightarrow 2Na^+ (aq) + S_2 O_5^- (aq) \quad .... \quad (Ba - R4)$$

ii) Bisulfite-Metabisulfite Anion Equilibrium.

$$S_2 O_5^- (aq) + H_2O \rightleftarrows 2HSO_3^- (aq) \quad .... \quad (Ba - R3)$$

The equilibrium expression is given by equation Ba - 3.

iii) Bisulfite Anion Acid Dissociation.

The bisulfite anion partially dissociates in aqueous solution as follows

$$HSO_3^- (aq) + H_2O \rightleftarrows H_3O^+ (aq) + SO_3^- (aq) \quad .... \quad (Ba - R5)$$

The equilibrium expression is

$$K_{a_2} = \frac{[H_3O^+]_e \, [SO_3^=]_e}{[HSO_3^-]_e} \quad \ldots \quad \text{(Ba - 4)}$$

$$= 5 \times 10^{-6} \text{ gmoles-L}^{-1} \quad @ \ 25^\circ C^{27}$$

where K_{a_2} is the second dissociation constant of sulfurous acid. Thus, bisulfite anion is a weak acid.

iv) Formation of Dissolved Sulfur Dioxide

The bisulfite anion also reacts with water in order to establish the following equilibrium

$$SO_2 \ (aq) + 2H_2O \rightleftharpoons HSO_3^- \ (aq) + H_3O^+ \ (aq) \quad \ldots \quad \text{(Ba - R6)}$$

The equilibrium expression is

$$K_{a_1} = \frac{[HSO_3^-]_e \, [H_3O^+]_e}{[SO_2 \ (aq)]_e} \quad \ldots \quad \text{(Ba - 5)}$$

$$= 1.2 \times 10^{-2} \text{ gmoles-L}^{-1} \quad @ \ 25^\circ C$$

where K_{a_1} is the first dissociation constant of sulfurous acid.

At equilibrium in aqueous solution, expressions Ba - 2, Ba - 3, Ba - 4 and Ba - 5 must be simultaneously satisfied.

27 Ref. 4, Volume 7, p. 237

Consider now the addition of both sodium sulfite and sodium metabisulfite to water. They are added in the aforementioned order until their concentrations are the same as in developing solution. As has been seen, the solution becomes alkaline upon addition of sodium sulfite. The pH becomes 9.8 ± 0.1. If sodium metabisulfite is then added to a concentration of 5.7×10^{-2} molar, the pH drops to 7.4 ± 0.1 - see Table IVa. The drop in pH is due to the presence of the bisulfite anion, HSO_3^-, produced via Ba - R3 in order to satisfy the necessary equilibria.

Rearranging Ba - 4,

$$[H_3O^+]_e = K_{a_2} \frac{[HSO_3^-]_e}{[SO_3^=]_e} \quad \ldots\ldots \quad (Ba - 6)$$

The combined action of bisulfite and sulfite anion from their respective sodium salts forms a buffer since the pH depends upon the ratio of their activities. Sodium sulfite is the source of sulfite anion and sodium metabisulfite is the source of bisulfite anion.

This buffer solution is less sensitive to the addition of strong acid than is a conventional buffer solution. A conventional buffer is a solution of a weak acid and its sodium salt, an example being a solution of sodium acetate and acetic acid where

$$[H_3O^+]_e = K_a \frac{[HAOc]_e}{[AOc^-]_e} \simeq K_a \frac{[HAOc]_o}{[NaAOc]_o} \quad \ldots\ldots \quad (Ba - 7)$$

The subscript zero signifies the number of moles per liter added to the solution. In this case, hydrogen ion from the strong acid combines with acetate anion, AOc^-, to form undissociated acetic acid molecules. As a result, the HOAc activity increases, the OAc^- activity decreases and the pH increases. Thus, only a comparitively small amount of strong acid can be added if the pH is to remain reasonably constant. In the sodium sulfite-bisulfite buffer solution, addition of strong acid forces an increase in bisulfite anion activity and a decrease in $SO_3^=$ activity but equilibrium Ba - 3 must be simultaneously satisfied. Thus, some of the excess HSO_3^-, undissociated weak acid, formed is stored as metabisulfite anion, $S_2O_5^=$, since increasing the HSO_3^- activity by a factor of 2 will increase the $S_2O_5^=$ activity by a factor of 4. Consequently, the increase in the undissociated weak acid activity is less than in the more convential buffer and the corresponding increase in pH is reduced.

A considerable amount of strong acid can be added to the sodium bisulfite-metabisulfite buffer without causing a drastic reduction in pH. Amidol developer is highly acid since each molecule of amidol contains two molecules of hydrated hydrogen chloride, an extremely strong acid. As Table IVa indicates, the pH drops from 6.8 ± 0.1 to 2.8 ± 0.1 when amidol is added to pure water to a concentration of 1.65×10^{-2} molar, its concentration in the developing solution. With the buffer present, the pH drops from 7.4 ± 0.1 to 6.6 ± 0.1. Therefore,

the acidity increases by ten thousand fold with no buffer present whereas it increases by a factor of only 6.4 when the buffer is present.

b) Addition of Amidol Developer to Pure Water

As previously indicated, a 1.65×10^{-2} molar aqueous solution of amidol has a pH of 2.8 ± 0.1. The molecular structure of undissolved amidol (2, 4-diaminophenol dihydrochloride) is shown in Fig. 2.1. Each molecule of amidol contains two molecules of hydrated hydrogen chloride. Upon dissolution, the hydrated HCl will separate from the diaminophenol and undergo complete ionic dissociation. Thus, a 1.65×10^{-2} molar solution of amidol will contain 3.3×10^{-2} gmoles-L^{-1} of hydrochloric acid which should result in a pH of 1.48 instead of the measured value of 2.8 ± 0.1. This indicates that the H_3O^+ activity is actually $(1.6 \pm 0.4) \times 10^{-3}$ gmoles-L^{-1} rather than 3.3×10^{-2} gmoles-L^{-1}, indicating that the hydronium ion activity is less than expected by a factor of approximately twenty. This suggests the presence of a strong base which neutralizes most of the hydrochloric acid.

Diaminophenol will act as a strong base in aqueous solution. Consider first the behaviour of ammonia in pure deionized water. It acts as a base, undergoing the hydrolysis reaction

$$\underset{\text{base 1}}{NH_3\ (aq)} + \underset{\text{acid 2}}{H_2O} \rightleftarrows \underset{\text{acid 1}}{NH_4^+\ (aq)} + \underset{\text{base 2}}{OH^-\ (aq)} \quad \ldots\ldots \quad (Bb - Rl)$$

with equilibrium constant

$$K_b = \frac{[NH_4^+]_e\,[OH^-]_e}{[NH_3]_e} \qquad \ldots \quad (Bb - 1)$$

$$= 1.8 \times 10^{-5}\,\text{gmoles-L}^{-1} \quad @ \quad 25^oC^{28}$$

Since ammonia only hydrolyzes weakly, it acts as a weak base. Similarly, diaminophenol will act as a base, neutralizing hydronium ions via the reaction

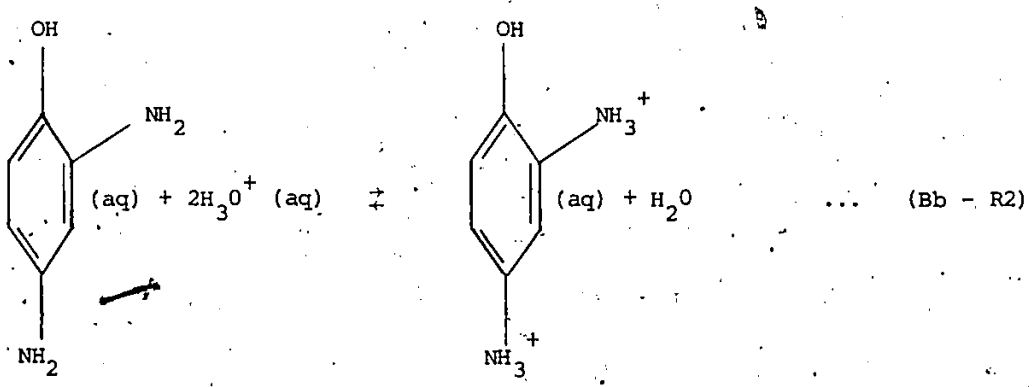

... (Bb - R2)

base 1 acid 2 acid 1 base 2

At equilibrium:

z - x 2(z - x) x

where z is the number of gmoles-L^{-1} of amidol which was dissolved, 2(z - x) is the concentration of hydronium ion and x is the concentration of the charged cation of diaminophenol. The factor 2 arises from the fact that each molecule of amidol contributes 2 molecules of hydrochloric acid. As in chapter 2, the diaminophenol will be symbolized as DAP. Its charged cation will be symbolized as DAP^{2+}. The equilibrium expression is

Ref. 5, pg. 194

$$K_b^1 = \frac{[DAP^{2+}]_e}{[DAP]_e \ [H_3O^+]_e^2} \qquad \ldots\ldots \quad (Bb - 2)$$

$$\simeq \frac{x}{4\ (z - x)^3}$$

but, $2\ (z - x) = 1.58 \times 10^{-3}$ gmoles-L^{-1} @ 5^oC

$$z = 1.65 \times 10^{-2} \text{ gmoles-}L^{-1}$$

$$x = z - 7.9 \times 10^{-4} \simeq z$$

Thus,

$$K_b^1 \simeq \frac{1.65 \times 10^{-2}}{4(7.9 \times 10^{-4})^3}$$

$$= 8.4 \times 10^6 \quad @ \quad 5^oC, \text{ gmoles}^{-2}\text{-}L^2$$

This large equilibrium constant indicates that diaminophenol acts as a very strong base in contrast to ammonia which acts as a weak base. Thus, diaminophenol has a much greater ability to accept protons than does ammonia. This can be attributed to extra charge stabalization produced by resonance on the benzene ring.

This large equilibrium constant also indicates that an overwhelmingly large proportion of the dissolved amidol exists as the doubly charged cation of diaminophenol in a highly acidic solution. As the pH

is raised and the solution consequently becomes less acidic, the equilibrium of Ba - R2 shifts to the left, producing diaminophenol from its cation. By rearranging equation Ba - 2, one can estimate the ratio of the cation to diaminophenol at neutral Ph.

$$\frac{[DAP^{2+}]_e}{[DAP]_e} = K_b [H_3O^+]_e^2 \quad \text{.... (Ba - 3)}$$

$$= 8.4 \times 10^6 \times (10^{-7})^2$$

$$= 8.4 \times 10^{-8}$$

Thus, an overwhelming proportion of the amidol exists as diaminophenol at neutral pH. Since the development is carried out at pH $\simeq$ 6.6 $\pm$ 0.1, near neutral conditions, the diaminophenol rather than its doubly charged cation must be the active species in the development reaction.

c) Proposed Development Reaction

For amidol developer, the overall development reaction and the mechanism via which it proceeds are not well known, although it is known to be a redox reaction. A reaction and its mechanism are suggested here.

It is well known that amidol develops satisfactorily only under neutral or near neutral conditions. The reaction can be stopped by increasing the acidity. Since the activity of diaminophenol decreases

rapidly whereas the activity of its doubly charged cation increase rapidly as the acidity is increased, the diaminophenol rather than its cation must be the reducing agent.

It is also known that latent image carrying silver bromide crystals develop much more rapidly than those which do not possess a latent image. << The study of the photolysis of silver halides falls into two categories; one in which after a relatively short exposure with actinic light the latent image is processed in a specific reducing solution, and one in which the exposure is so long that a visible density appears (print-out effect). The former is observed in photographic emulsions which consist of very small crystals suspended in a protective colloid such as gelatin. During development, the effect of the light reaction is amplified some 10^5 to 10^9 times. >>[29] Furthermore, it is known that latent images are due to aggregates of silver atoms on the surface of the silver bromide crystals and that they act as reaction sites. According to the free electron model of metallic crystals, valence electrons behave as free electrons confined to a box or potential well. Such metals are capable of accepting electrons since they can fall into this well and consequently lower their energy states. It is suggested that the latent image acts as a microcrystal of metallic silver. It can thus accept an electron from the OH radical of the diaminophenol which will consequently lose a proton. The negatively charged latent image will attract local free silver cations which will become attached

29. Ref. 11, pg. 1052

to its surface and consequently neutralized. This process will cause the latent image to grow into a grain of silver and the corresponding silver bromide crystal to disappear since it dissociates due to the local consumption of free silver cations.

The dissociation reaction of latent image carrying silver bromide crystals is

$$AgBr^{*} \rightleftarrows Ag^{+}\ (aq) + Br^{-}\ (aq) \quad .... \quad (Bc - R1)$$

where the symbol * indicates the presence of a latent image. The redox half reactions are proposed to be

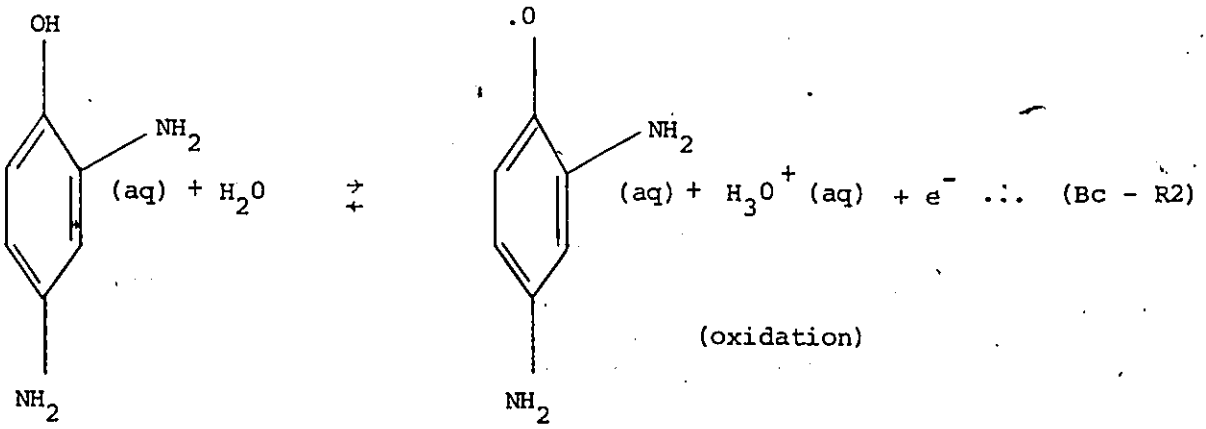

and

$$Ag^{+}\ (aq) + e^{-} \rightleftarrows Ag^{o}\ (s) \quad .... \quad (Bc - R3)$$

The redox reaction, found by adding the individual half-reactions, is

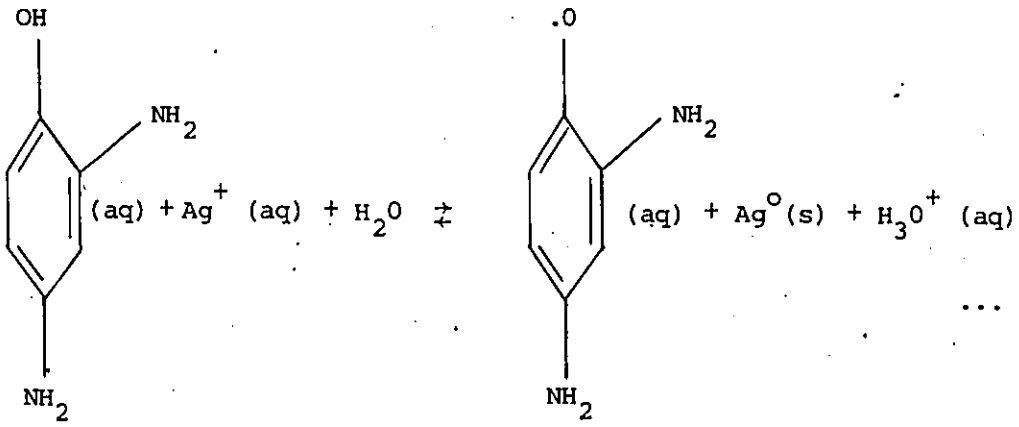

... (Bc - R4)

The resulting oxidized diaminophenol, symbolized here, as in chapter 2, as DAPOx, will be highly reactive since the oxygen now contains only five electrons in the 2p sub-shell. It may be partially stabalized by resonance on the benzene ring.

The overall development reaction, found by adding Bc - R1 and Bc - R4, is suggested to be

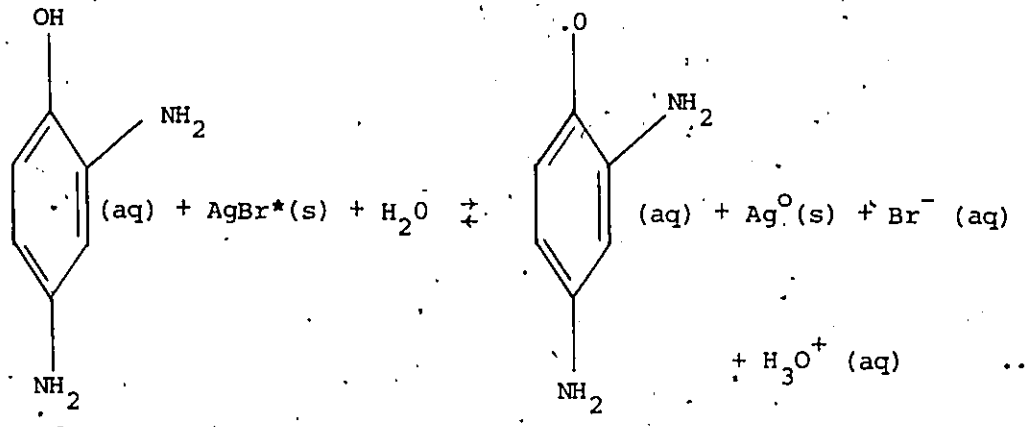

... (Bc - R5)

The redox potential, given by the standard Nernst equation, is

$$\Delta\varepsilon = \Delta\varepsilon^{o} + 2.3\,\frac{RT}{nF}\,\log\,\frac{[DAP]\,[Ag^{+}]}{[DAPOx][H_3O^{+}]} \qquad \text{(Bc-1)}$$

where $\Delta\varepsilon^{o}$ is the standard redox potential, R is the ideal gas constant, T is the absolute temperature, F is the faraday and n is the number of electrons transferred. In this case, n is equal to one. As the pH is lowered, the H_3O^+ activity increases whereas the diaminophenol activity decreases. Thus, the redox potential will decrease. When this potential is lowered to zero, the net redox reaction rate will become zero, indicating that the development has been stopped by increasing the acidity.

APPENDIX C

Emulsion Pellicle Material Balance

a) Unsteady-State Material Balance on an Emulsion Pellicle During Fixing.

Fig. AC - 1 Elevation View of a Horizontal Emulsion Plate Immersed in Fixer

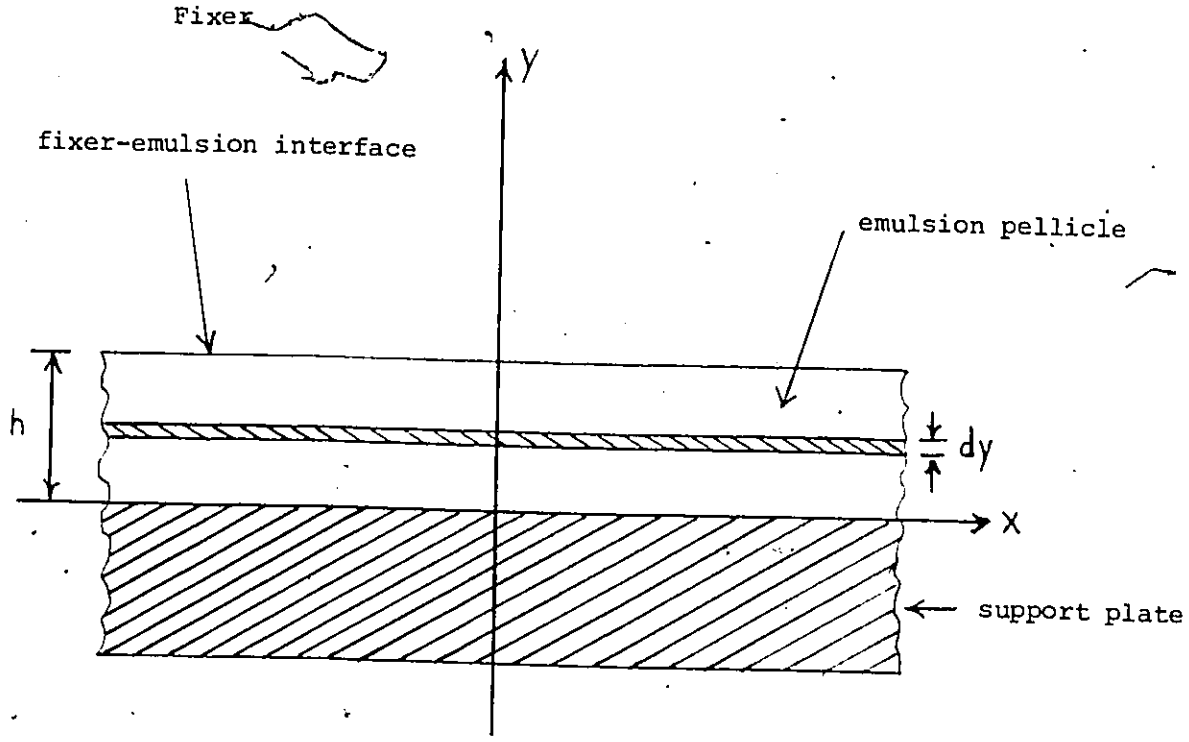

Consider a pellicle of length L, width W and thickness h. Generally, L and W are much greater than h, as explained during the discussion of the fixing stage in chapter 2. To a good approximation, this can thus be treated as a case of undirectional diffusion in the y direction, the thickness coordinate.

i) A Component Produced by the Fixing Reaction

Consider first a species, component A, which is produced by the fixing reaction and diffuses out of the emulsion. Let R_A be the net differential rate of production of A in units gmoles-cm^{-3} - s^{-1}. Under unsteady-state conditions, R_A is a function of both position and time. Thus,

$$R_A = R_A\ (y,\ t) \qquad \ldots\ (C - 1)$$

The flux, N_A, of component A in gmoles-cm^{-2} - s^{-1} toward the interface and its concentration, C_A, in gmoles-cm^{-3}, are also functions of position and time. Consequently,

$$C_A = C_A\ (y,\ t) \qquad \ldots\ (C - 2)$$

$$N_A\ (y,\ t) = - D_A \frac{\partial C_A\ (y,\ t)}{\partial y} \qquad \ldots\ (C - 3)$$

where D_A is the diffusivity of component A. In liquid phase diffusion, the diffusivity is a function of temperature and often a function of concentration at high concentrations. Thus, at constant temperature D_A may in general be a function of both time and position.

Consider a material balance across a thin strip of emulsion of infinitessmal thickness dy and area, A^1, equal to the surface area

of the pellicle (Fig. AC - 1).

$$\text{Accumulation Rate} = \text{Input Rate} - \text{Output Rate} + \text{Rate of Production} \quad \ldots \quad (C - 4)$$

$$\text{Input Rate} = A^1 N (y, t) \quad \ldots \quad (C - 5)$$

$$\text{Output Rate} = A^1 N (y + dy, t)$$

$$= A^1 \{ N (y, t) + \frac{\partial N (y, t)}{\partial y} dy \} \quad \ldots \quad (C - 6)$$

$$\text{Rate of Production} = R_A (y, t) A^1 dy \quad \ldots \quad (C - 7)$$

$$\text{Accumulation Rate} = A^1 dy \frac{\partial C_A (y, t)}{\partial t} \quad \ldots \quad (C - 8)$$

where the number of moles, N_A^1, contained in the strip is

$$N_A^1 (y, t) = A^1 dy C_A (y, t) \quad \ldots \quad (C - 9)$$

Substituting equations C - 5, C - 6, C - 7 and C - 8 into C - 4,

$$A^1 dy \frac{\partial C_A (y, t)}{\partial t} = A^1 \{ N_A (y, t) - N_A (y, t) - \frac{\partial N_A (y, t)}{\partial y} dy \}$$

$$+ R_A (y, t) A^1 dy \quad \ldots \quad (C - 10)$$

which reduces to the unsteady-state law of diffusion

$$\frac{\partial C_A (y, t)}{\partial t} = - \frac{\partial N_A (y, t)}{\partial y} + R_A (y, t) \quad \ldots \quad (C - 11)$$

If one considers a simplified situation of constant diffusivity, then, from equation C - 3, one obtains

$$\frac{\partial N_A (y, t)}{\partial y} = - D_A \frac{\partial^2 C_A (y, t)}{\partial y^2} \quad \ldots \quad (C - 12)$$

Thus, the unsteady-state law of diffusion, equation C - 11, becomes

$$\frac{\partial C_A (y, t)}{\partial t} = D_A \frac{\partial^2 C_A (y, t)}{\partial y^2} + R_A (y, t) \quad \ldots \quad (C - 13)$$

In the more general situation where the diffusivity is a function of both time and position, one obtains, upon differentiation of equation C - 3,

$$\frac{\partial N_A (y, t)}{\partial y} = - D_A (y, t) \frac{\partial^2 C_A (y, t)}{\partial y^2} - \frac{\partial D_A (y, t)}{\partial y} \frac{\partial C_A (y, t)}{\partial y} \quad \ldots \quad (C - 14)$$

and the unsteady-state law of diffusion, equation C - 11, becomes

$$\frac{\partial C_A (y, t)}{\partial t} = D_A (y, t) \frac{\partial^2 C_A (y, t)}{\partial y^2} + \frac{\partial D_A (y, t)}{\partial y} \frac{\partial C_A (y, t)}{\partial y}$$

$$+ R_A (y, t) \quad \ldots \quad (C - 15)$$

which is its most general form if diffusion at the edges of the pellicle is neglected.

ii) A Component Consumed by the Fixing Reaction

Consider now a species, component C, diffusing into the emulsion and consumed by the fixing reaction. The flux, N_C, of C into the emulsion is

$$N_C (y, t) = - D_C \frac{\partial C_C (y, t)}{\partial y} \quad .... \quad (C - 16)$$

A similar material balance yields the unsteady-state law of diffusion

$$\frac{\partial C_C (y, t)}{\partial t} = \frac{\partial N_C (y, t)}{\partial y} - R_C (y, t) \quad .... \quad (C - 17)$$

where R_C is the rate of consumption of C. For the assumption of constant diffusivity, C - 17 becomes

$$\frac{\partial C_C (y, t)}{\partial t} = - D_C \frac{\partial^2 C_C (y, t)}{\partial y^2} - R_C (y, t) \quad .... \quad (C - 18)$$

If D_C is both time and position dependent, equation C - 17 becomes

$$\frac{\partial C_C (y, t)}{\partial t} = - D_C (y, t) \frac{\partial^2 C_C (y, t)}{\partial y^2} - \frac{\partial D_C (y, t)}{\partial y} \frac{\partial C_C (y, t)}{\partial y}$$

$$- R_C (y, t) \quad .... \quad (C - 19)$$

b) Steady-State Material Balance

At steady-state, all concentrations of reactants and products

become time independent. Since the net differential reaction rates are functions of concentrations of reactants and products they are also time-independent. The diffusivities, which are concentration dependent, are likewise time-independent as are the fluxes. The analogus steady-state relationships for reaction product A are from C - 3,

$$N_A(y) = -D_A(y)\frac{dC_A(y)}{dy} \quad \ldots\ldots \quad (C-20)$$

and from C - 11,

$$\frac{dN_A(y)}{dy} = R_A(y) \quad \ldots\ldots \quad (C-21)$$

since

$$\frac{\partial C_A(y)}{\partial t} = 0$$

If no net chemical reaction is occurring - for example outside the pellicle or in a layer which is already clear -, the flux gradient, $\frac{dN_A(y)}{dy}$, is zero. Thus, the flux is constant. In the simplified situation of constant diffusivity, the flux, equation C - 20, becomes

$$N_A(y) = -D_A\frac{\Delta C_A}{\Delta y} \quad \ldots\ldots \quad (C-22)$$

where $\frac{\Delta C_A}{\Delta y}$ is a constant concentration gradient.

The relations for reaction product B are analogous to those of A.

LIST OF REFERENCES

1. IONOGRAPHIE - LES EMULSIONS NUCLEAIRES, Principes et Application; Pierre Demers; Les Presses Universitaire de Montréal; 1955.

2. THE STUDY OF ELEMENTARY PARTICLES BY THE PHOTOGRAPHIC METHOD; C.F. Powell, P.H. Fowler, D.H. Perkins; Pergamon Press, London, New York, Paris, Los Angeles; 1959.

3. NUCLEI AND PARTICLES - An Introduction to Nuclear and Subnuclear Physics; Second Edition; Emilio Segrè; W.A. Benjamin, Inc., Reading, Massachusetts; 1977.

4. INTERNATIONAL CRITICAL TABLES OF NUMERICAL DATA, PHYSICS, CHEMISTRY AND TECHNOLOGY; National Research Council of the United States; McGraw-Hill Book Company, Inc., New York and London; 1933.

5. UNIVERSITY CHEMISTRY; B.H. Mahan; Addison-Wesley Publishing Company, Reading Massachusetts; 1967.

6. PHOTOGRAPHY - Its Materials and Processes; Sixth Edition; C.B. Neblette; D. Van Nostrand Company, Inc., Princeton, New Jersey; 1962.

7. COMPREHENSIVE INORGANIC CHEMISTRY, Volume 2; First Edition; Editorial Board - J.C. Bailar Jr., H.J. Emeléus, Sir Ronald Nyholm, A.F. Trotmun-Dickenson; Pergamon Press, London; 1973.

8. HANDBOOK OF CHEMISTRY AND PHYSICS; 49th Edition; Editor, Robert C. Weast; The Chemical Rubber Co., 18901 Cramwood Parkway, Cleveland, Ohio; 1968.

9. INTRODUCTION TO HIGH ENERGY PHYSICS; D.H. Perkins; Addison-Wesley Publishing Company, Reading, Massachusetts; 1972.

10. QUANTITATIVE CHEMISTRY: Measurements and Equilibrium; W.B. Guenther; Addison-Wesley Publishing Company, Reading, Massachusetts; 1968.

11. PHYSICS OF ELECTROLYTES, Volume 2; J. Hladik; Academic Press, London, New York; 1972.

12. THE PHYSICAL CHEMISTRY OF ELECTROLITIC SOLUTIONS: Harned and Owen; Third Edition, Reinhold Publishing Corporation, New York, Chapman and Hall, Ltd., London; 1958.

13. JANAF THERMOCHEMICAL TABLES, The Thermal Research Laboratory Dow Chemical Company Midland Michigan. Technically Assisted by the Joint Army-Navy-Air Force-ARPA-NASA Thermochemical Working Group.

14. Keith and Mitchell; Phil. Mag. 44, 877 (1953).

15. Forty; Advances in Phys. 3, 1 (1954).

16. Evans, Hedges and Mitchell; Brit. J. Photo Sci., 3, 73 (1955).

17. Mitchell; Z. Phys. 138, 381 (1954); see also Rep. Prog. Phys. 20, 433 (1957); and Sci. & Industr. Phot. 29, 1 (1958).

18. Evans and Mitchell; Report on Conference of Defects in Crystalline Solids, p. 409 (1955)

19. Mitchell; Brit. J. Phot. Sci. 1, 110 (1953) and 6, 33 (1958).

20. Gurney and Mott; Proc. Roy. Soc. (A) 164, 151 (1938).

21. Clark and Mitchell; Brit. J. Photo. Sci. 4, 1 (1956).

22. Berg; Reports on Progress in Physics 11, 248 (1947).

23. Demers; Ionographie, Montreal, pg. 30.

24. Mees; The Theory of the Photographic Process, New York 1942.

25. J. Kielland; J. Am. Chem. Soc. 59, 1675 (1937).